

From Neo-Tethys rifting to Alpine convergence in restored 2D seismics: NW Negev, Levant basin

Thesis for the Degree of Master of Science

Submitted by

Inga Boianju

Under the supervision of

Prof. Amotz Agnon

August 2018

Department of Geology

Institute of Earth Sciences

Faculty of Mathematics and Natural Sciences

The Hebrew University of Jerusalem

Abstract

The northern Negev terrain has been shaped by deformational events since the early Mesozoic and can be regarded as an evolution model for much of the Levant. A simple basin inversion model, from Triassic Neo-Tethyan rifting to Cenomanian Alpine-related convergence, was proposed to explain lateral thickness and facies variations on a regional scale. However, subsurface data has challenged this inversion model for some of the structures in the Northern Negev. Moreover, spatiotemporal distribution of deformation is poorly resolved, along with timing the onset of Alpine related shortening. A dense network of 2D seismic lines and check-shot surveys in Qeren and Agur area in the northern Negev offers an opportunity to restore the deformation on both Qeren and Agur structures. In this study, structural sequential restoration is carried out on two interpreted seismic sections in the northern Negev. Effects of sediment compaction, isostatic adjustment, fault related folding and fault slip are accounted for in order to restore each seismic section for its deposition time. A total of ten horizons are restored, timed from base Triassic to Coniacian in upper Cretaceous. The restoration confirms regional tilt from SE to NW in the early Jurassic and supports the basin inversion concept. The study reveals middle Jurassic reverse faulting that cut across the Qeren and Agur fault structures. Indication for possible Cenomanian strike slip activity is also detected. The use of structural restoration in an area with tectonic constraints appears to be effective in shedding light on various phases of deformation on complex faults and can now be used as a validation technique in poorly constrained geological structures elsewhere.

Acknowledgments

I would like to express my deepest gratitude to my supervisor Amotz Agnon, for the long process I went through during this work. For the uncountable opportunities to meet experts and introduce myself to various research methods and equipment. For the independence, patience, guidance, and willingness to help

I also want to thank Dr. John Hall for all the ‘Neev Center’ facilities and equipment I used. For the professional contribution and the useful advice

I want to thank Midland ValleyTM for the use of the MoveTM Software Suite granted by the Academic Software Initiative. For the great support and company at the training course in Glasgow 10.2016

Bernard Blasband, for the great advice and the practical help with the software, thank you for the meetings and the skype talks

Neevers, my research group and family: Osnat Barnea and Yaniv Darvasi, for the support at any given moment, Ron Algon, Nadav Navon and Guy Tzarfati

To my good friends David Giguzin, Nicole Behar, Evyatar Cohen, Jonathan Keinan, Natalie Neagu, Ortal Sava, Roie Dann, Koko (Moshe) Armon, Ido Sirota and Lior Suchoy for the motivation throughout the years

To my family and most importantly my mother, for making sure I’m making my own choices

And to Nitzan, who colors each moment in HDR.

Table of contents

1	Background.....	1
1.1	General introduction.....	1
1.2	Structural framework.....	3
1.2.1	Neotethys extension.....	6
1.2.2	Syrian arc convergence phase.....	8
1.2.3	Basin inversion.....	9
1.3	Structural restoration.....	11
2	Research objective.....	13
3	Methodology.....	14
3.1	Workflow.....	14
3.2	Digitization.....	15
3.3	Depth conversion.....	16
3.3.1	Velocity surveys.....	16
3.3.2	3D structure.....	16
3.4	The stratigraphic column.....	18
3.5	Restoration.....	19
3.5.1	Faulting.....	19
3.5.2	Folding.....	19
3.5.3	Compaction.....	21
3.5.4	Flexural Isostasy.....	21
4	Results.....	23
4.1	Section EM-7748.....	25
4.2	Section EM-7726.....	26
4.3	Restoration results.....	27
4.3.1	Determination of detection limit.....	27
4.3.2	Lower to middle Triassic (251-240 Myr).....	27
4.3.3	Middle to late Triassic (240-220 Myr).....	28
4.3.4	Late Triassic to early Jurassic (220-176 Myr).....	29
4.3.5	Early to middle Jurassic (176-168 Myr).....	29
4.3.6	Middle to late Jurassic (168-159 Myr).....	30
4.3.7	Oxfordian to Tithonian in the late Jurassic (159-150 Myr).....	31
4.3.8	Late Jurassic to Albian in lower cretaceous (150-112 Myr).....	32
4.3.9	Albian in lower Cretaceous to Cenomanian in Upper Cretaceous (112-99 Myr).....	33
4.3.10	Cenomanian to Coniacian in Upper Cretaceous (99-89 Myr).....	33
4.4	Restoration synthesis.....	34
4.4.1	EM-7726.....	35
4.4.2	EM-7748.....	36
5	Discussion.....	37
5.1	Timing the shortening periods in the Qeren-Agur area.....	37

5.2	Evidence for strike-slip in the Cenomanian.....	39
5.3	Thickness variations in the middle Jurassic.....	41
5.4	From SE regional trend in the Triassic to NW in following periods.....	42
6	Conclusions.....	44
7	References.....	46
8	Appendix.....	53
8.1	Depth conversion.....	53
8.2	Compaction calculation.....	53
8.3	Stratigraphic interpretation.....	53
8.3.1	EM-7748.....	53
8.3.2	EM-7726.....	53
8.4	Restoration procedure.....	53
8.4.1	EM-7748.....	53
8.4.2	EM-772.....	67

List of figures

Figure 1: Geological map of the study area.....	1
Figure 2: Stratigraphic table of the Formations exposed in the Qeren-Agur area.....	2
Figure 3: Generalized stratigraphic table of the Mesozoic section	3
Figure 4: General location of study area, on top of DEM	4
Figure 5: Cross section A-A' from Agur to Boqer	4
Figure 6: Top Judea Group structural map.....	5
Figure 7: Neo-Tethyan extension and Paleo-Tethys subduction.....	6
Figure 8: Main tectonic elements of the Eastern Mediterranean region.....	7
Figure 9: Distribution of axes in the syrian arc fold belt.....	8
Figure 10: Santonian configuration of part of the Neo-Tethys Ocean	9
Figure 11: Schematic diagram showing a basin inversion	10
Figure 12: simplified Schematic stratigraphic column.....	11
Figure 13: Restoration of a cross section.....	12
Figure 14: Flowchart of restoration process	15
Figure 15: From structural scanned map to a 3D structure	15
Figure 16: A simplified check-shot velocity survey.....	16
Figure 17: 3D structure of study area that is cut vertically by faults.....	17
Figure 18: 3D fault structure of study area along with location map.....	17
Figure 19: Stratigraphic column used in the restoration process.....	18
Figure 20: Before and after unfauling of horizon C4	19
Figure 21: Folded horizon restoration using vertical simple shear unfolding tool.....	20
Figure 22: Restoration by oblique simple shear	21
Figure 23: Schematic figure showing the deflection applied	22
Figure 24: Locations of faults, seismic sections and velocity surveys.....	24
Figure 25: Seismic section EM-7748.	25
Figure 26: Seismic section EM-7726.	26
Figure 27: Detection limit determination based of reflector spacing	27
Figure 28: Restoration of lower to middle Triassic.....	28
Figure 29: Restoration middle to late Triassic	28
Figure 30: Restoration of late Triassic to early Jurassic.....	29
Figure 31: Restoration of early to middle Jurassic	30

Figure 32: Restoration of middle to late Jurassic	31
Figure 33: Restoration of late Jurassic	32
Figure 34: Restoration of late Jurassic to lower Cretaceous	32
Figure 35: Restoration lower Cretaceous to upper Cretaceous	33
Figure 36: Restoration Cenomanian to Coniacian in upper Cretaceous.....	34
Figure 37: Restoration synthesis of section EM-7726..	35
Figure 38: Restoration synthesis of section EM-7748.	36
Figure 39: Left- Flower structure scheme	40
Figure 40: Top Daya horizon surface (168 Myr) along with locations of seismic sections and surveys	41
Figure 41: Thickness variations in both sections EM-7726 and EM-7748	43

1 Background

1.1 *General introduction*

The Qeren area (Figure 1) has been marked by the Israel Electricity Company as a possible area for the location of a nuclear power plant in the 1980s. This has brought extensive research to the area. Most of the rocks exposed on the Qeren-Agur area belong to the Avdat group (Braun, 1964) of Eocene age, and more specifically to the Nizzana formation (Zilberman, 1980) (Figure 2). Eocene limestones crop out on anticlines throughout the area whereas the synclines are lined by Quaternary, Pleistocene and Holocene sand dunes that overlie continental Neogene sediments (Zilberman, 1980). The study area of this work is 25km x 45km wide and it comprises the complex fault structures of Qeren and Agur in the sub-surface. This area has been a site of platform deposition during all of its post Precambrian history. The section comprises mainly carbonates with some sandstones and shales and an episode of gypsum deposition in the late Triassic (Druckman et al., 1995) (Figure 3). Reflectors ranging from base Triassic to upper Cretaceous were affected by the Qeren and Agur fault structures (Figure 25, Figure 26) and are analyzed and discussed in this work.

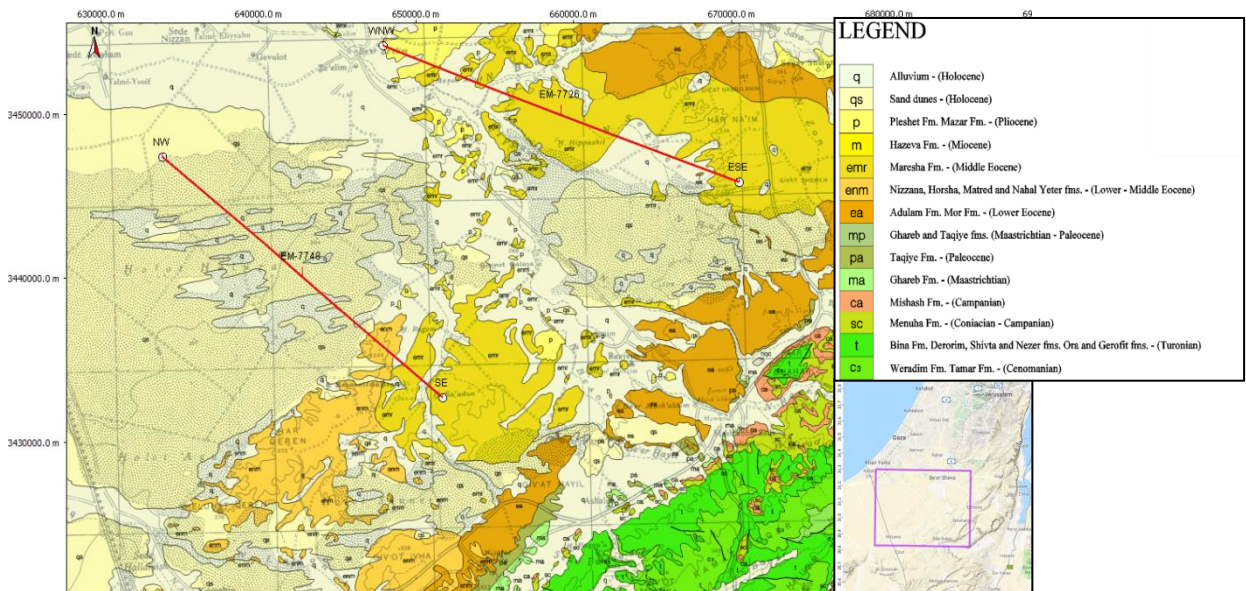


Figure 1: Geological map of the study area, along with Geographic location. 2D seismic sections discussed in this work are marked in red.

Due to the complexity of the fault structures, the Qeren-Rogem-Hazerim faults will be referred as the Qeren structure, and the Agur-Haluza faults will be referred as the Agur fault structure. In both structures, the amount of displacement on the main faults varies on most of the stratigraphic markers throughout the entire sedimentary sequence, indicating a complex displacement history.

STRATIGRAPHY סטרטיגרפיה

SYSTEM תקופה	SERIES - STAGE סדרה - דרגה	SYMBOL סימן	THICK. מ' עובי	LITHOLOGY מסלע	LITHOSTRATIGRAPHY ליתוסטרטיגרפיה			
					MAPPING UNITS יחידות מיפוי	GROUP חבורה		
QUATERNARY קוורטר	HOLOCENE הולוקן	Al	2+		Alluvium, colluvium, soil אלובים קלובים סרטע			
	PLEISTOCENE-HOLOCENE פלייסטוקן-הולוקן	Qs Qsd	0-10		Sand cover כיסוי חול		Dunes דינות	
TERTIARY טרצייר	PLIOCENE פליוקן	NQa NQc	1-5		Ahuzam Conglomerate קונגלומרט אחוזם	Cgl. & Loess קונגלומרט ולס	SAQIYE סקייה	
	MIOCENE מיוקן	Nh	5+		Hazeva Formation תצורת חצבה		AVEDAT עבדת	
	MIDDLE EOCENE איאוקן תיכון	Emr	25+		Maresha Formation תצורת מרשה			
	LOWER EOCENE איאוקן תחתון	Ea	60		Adulam Formation תצורת עדולם			
	PALEOCENE פלאוקן	Thr	0-35		Taqiye Formation תצורת טקייה		MOUNT SCOPUS הר הצופים	
CRETACEOUS קרטיקון	SENONIAN סטון	MAASTRICHTIAN מאסטריוכט	Kug	10-50		Ghareb Formation תצורת ערב		
	CAMPANIAN קמפן	Kumi	20		Mishash Formation תצורת מישאש			
	SANTONIAN סנטון	Kum	5-30		Menuha Formation תצורת מנוחה			
	TURONIAN טורון		Kun	10-40		Nezer Formation תצורת נצר	JUDEA יהודה	
			Kush	20-30		Shivta Formation תצורת שבטה		
			Kud	0-15		Derorim Formation תצורת דרורים		
CENOMANIAN קנומן		Kut2	35		Tamar Formation תצורת תמר פרט עליון			
	Kut1	20		Tamar Formation תצורת תמר פרט תחתון				

Limestone
גיר

Dolomite
דולמיט

Chalk
קרטון

Marl
חורר

Chert
צור

Clay
חריטית

Loess
לס

Sand
חול

Sandstone
אבן חול

Gravel
חלקים

Conglomerate
קונגלומרט

Fossils
מאובנים

Figure 2: Stratigraphic table of the Formations exposed in the Qeren-Agur area (Sneh and Avni, 2011)

ERA	SYS.	SERIE	STAGE	Gr.	Formation		Lithology N. Negev S.	Thick. [m]	
MESOZOIC	CRET.	E. CRET.	Albian - L. Ceno.	KURNUB	Uza	Hatira		60-80	200
			Albian		Malhata			80-100	
			L. Albian - U. Aptian		Dragot			30-240	500
			U. Aptian - Neocom.		Zeweira			90-240	
	JURASSIC	Malm	Kimmer - Tithon.	A R A D	Haluzza	Amir		40-300	2-66
			Oxfordian		Beer Sheva		100-230		
			L. Oxford. - Callov.		Kidod		0-120		
		Dogger	Callov. - U. Batho.		Zohar		108-182		
			U. - M. Batho.		Sherif		238-338		
			Bajocian		Daya		38-308		
		Lias	Aalenian		Inmar		181-576		
			Hattangian		Ardon		12-541		
			Mishhor			4-31			
		TRIASSIC	Tr 3		Carni. - Norian	RAMON	Mohilla		46-211
					Ladin. - Carnian		Saharonim		172-290
			Anisian		Gevanim			55-287	
	Tr 1		Anis. - U. Spath	Ra'af			66-128		
			Spathian	NEGEV	Zafir			174-357	

	Granite		Dolomite		Arkosic SS
	Shale		Conglomerate		Sandstone
	Limestone		Gypsum		

Figure 3: Generalized stratigraphic table of the Mesozoic section in the subsurface of the Negev region (modified after Calvo and Gvirzman 2013)

1.2 Structural framework

The study area spans the north-western hills of the northern Negev desert (Figure 1). The northern Negev lies on the southern margins of the Levant basin (Kempler and Garfunkel, 1994). A regional subsidence of this area between the early Mesozoic and the Neogene made room for accumulation of a sedimentary wedge up to a few kilometers thick (Freund et al., 1975). The Qeren structure consists of the Qeren anticline; its trend is NE-SW and it is underlain by Qeren faults in the subsurface (Figure 6). The anticline forms a low ridge, 15 km long, 3 km wide and rising about 100m above its surroundings (Begin, 1981) (Figure 4).

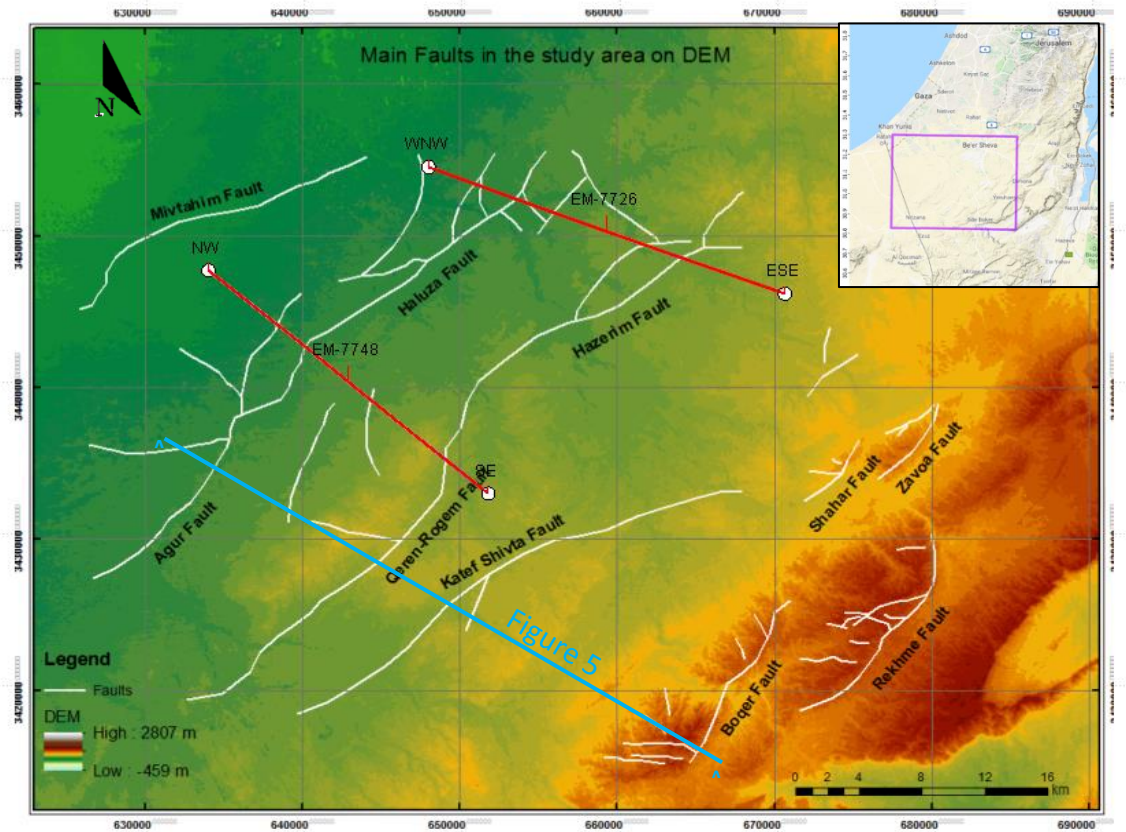


Figure 4: General location of study area, along with DEM. 2D seismic sections relevant for this work are marked in red

The Agur structure consists of the Agur anticline revealed in the upper 300m of the subsurface and is underlain by Agur faults (Figure 5). The structural framework of the study area at any late Mesozoic datum is dominated by roughly parallel chains of monoclines, as confirmed by seismic surveys and boreholes (Figure 5).

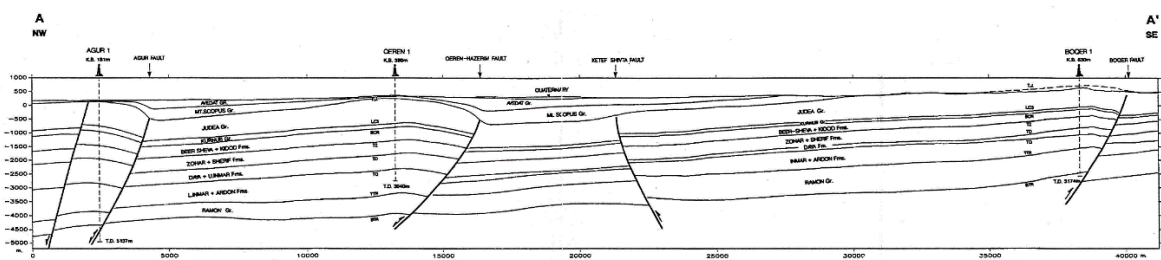


Figure 5: Cross section A-A' from Agur to Boqer, showing the stratigraphic and structural relations of the sedimentary sequence to base (druckman et al, 1995). Section location is shown on figure 4

The structural axes are oriented NE-SW (Bruner, 1991; Druckman et al., 1994). From west to east these are the Agur-Haluza, Qeren/Rogem-Hazerim, Boqer-Zavoia, and

Rehme chains (Figure 4). The monoclines are strongly asymmetric, each with a rather steep southeastern flank and a gently inclined northwestern flank (Druckman et al., 1995) (Figure 6). Within each monoclinical chain, the amplitude of each individual structure decreases towards the northeast. At the top Judea level, the monoclinical chains are separated by the flanks of the next chain, and the overall structural pattern corresponds to an arrangement of subparallel tilted blocks (Freund, 1979; Reches et al., 1981; Druckman et al., 1995; Shamir and Eyal, 1995) (Figure 6).

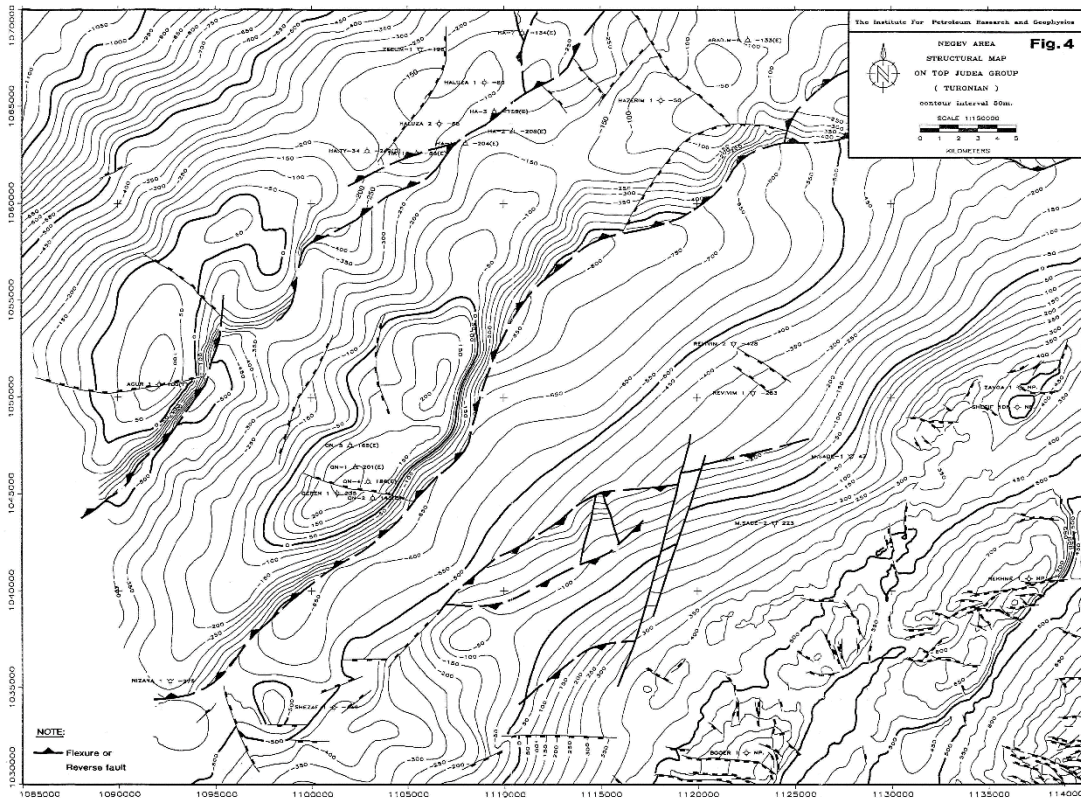


Figure 6: Top Judea Group structural map showing four roughly parallel chains of monoclines, whose axes are oriented in a NE-SW direction (Druckman et al, 1995)

Deeper Mesozoic levels are offset by normal and reverse faults. Some of the faults initiated with normal slip during the early Mesozoic and re-activated in a reverse direction (Freund et al., 1975; Reches et al., 1981; Bruner, 1991; Druckman et al., 1994), a process referred as a 'basin inversion' (Williams et al., 1989; Lowell, 1995; Guiraud, 1998).

1.2.1 Neotethys extension

During the early Triassic, rifting initiated on the northern edge of the Gondwana supercontinent, splitting the edge of the future African Plate. The Paleo-Tethyan continental margin was pulled North making space for the expanding Neo-Tethys Ocean and the construction of a new continental margin (Figure 7) (Stampfli, 2000). According to onshore geologic observations from around the eastern Mediterranean, this margin was first deformed by a multi-step Middle Triassic to Early Jurassic (Garfunkel and Derin, 1984) or Late Triassic-Early Jurassic (Ben-Avraham, 1989) extension. According to recent magnetic anomaly mapping, rifting initiated already in the Permian (Granot, 2016). This complex rifting phase separated Turkey from the Levant basin and Africa (Figure 7) along the eastern Mediterranean margin. The separation of Turkey from the Levant led to the opening of the Levant Basin and to the formation of an oceanic crust (Granot, 2016). It is suggested that the early Mesozoic orogenic deformation and magmatism in Iran, Turkey and Greece occurred in island arcs on the western side of the Tethys Ocean, behind which the eastern Mediterranean expanded as a marginal basin (Garfunkel, 2004; Stampfli, 2000; Stampfli et al., 2013). It is now located in a region where the major Arabian, African, and Eurasian plates interact (Figure 8).

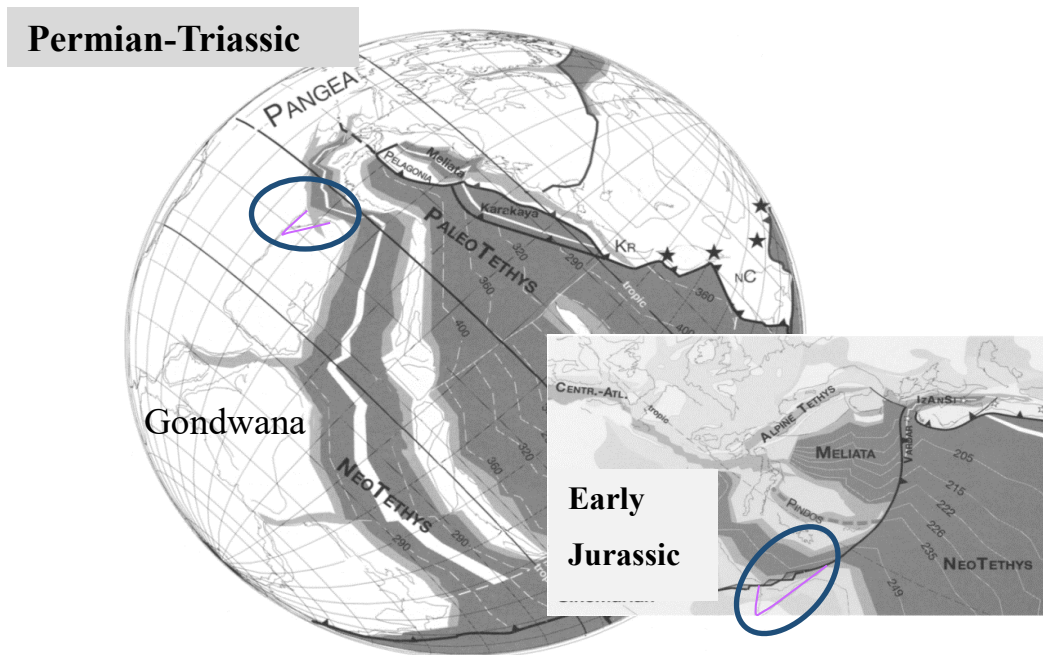


Figure 7: Neo-Tethyan extension and Paleo-Tethys subduction in Permian-Triassic and Early Jurassic. Location of the Levantine basin and the Sinai plate is circled and marked (modified after Stampfli, 2000).

Part of the eastern Mediterranean basin, a relic of the Neo-Tethys ocean, is now encountered in the northern Negev (Sengor et al., 1984; Garfunkel and Derin, 1984; Garfunkel, 1998; Stampfli, 2000; Garfunkel, 2004; Granot, 2016).

A thin sequence of platform sediments covers the area in the Paleozoic (Freund et al., 1975). In the early Mesozoic, The dominant stratigraphic features observed in the northern Negev are rapid subsidence and accumulation of thick marine sequences northwest of the central Negev. Evidence collected from Israel, northern Sinai and Syria show that the rifting phase was accompanied by the formation of extensive horst and graben systems (Garfunkel and Derin, 1984; Druckman et al., 1995; Garfunkel, 1998) and block tilting (Bosworth et al., 1999; Guiraud et al., 2005). The early Mesozoic extension phase evident in Israel is contemporaneous with orogenic deformation and magmatism in Turkey and Iran (Freund et al., 1975; Stampfli, 2000).

The main phase of igneous activity in Israel, consisting of alkaline, high-K intermediate and basic intrusives and volcanics, apparently occurred later than the vertical movements mentioned above, namely in late Triassic and early Cretaceous (Freund et al., 1975; Katzir, 1998). Following the rifting phase, from the Late Triassic and onwards, passive margin drift conditions were established with prolonged post-rift subsidence (Freund et al., 1975; Garfunkel and Derin, 1984; Stampfli, 2000) that continued until the Late Eocene, when the continental margin was reactivated along with the Africa–Arabia breakup (Steinberg et al., 2008; Gvirtzman and Steinberg, 2012).

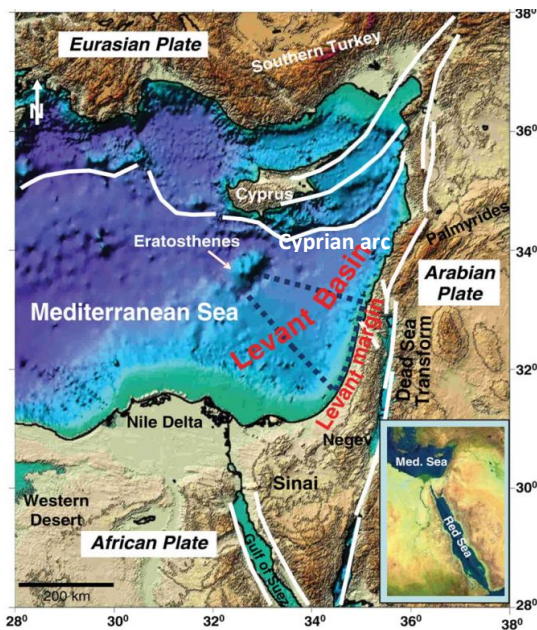


Figure 8: Main tectonic elements of the Eastern Mediterranean region shown on a shaded relief map. The Levant Basin is located on the north-eastern edge of the African plate, south of the Cyprian Arc (marked by thick white lines) (Gardosh et al., 2010)

1.2.2 Syrian arc convergence phase

Evidences exist for an anticlockwise rotation of Africa in the upper Cretaceous (Bosworth et al., 1999). This, progressively generated collision between Europe and Africa, giving birth to the Alps (Jolivet and Faccenna, 2000) and, in its local margin, to the Syrian arc fold belt (Shahar, 1994; Stampfli, 2000). Evidence of shortening during the Cenomanian and throughout the upper Cretaceous appear across the eastern Mediterranean (Freund et al., 1975; Stampfli, 2000). This deformation period was expressed in the formation of extensive anticlines and synclines known as the Syrian Arc fold belt (Krenkel, 1924; Freund et al., 1975; Eyal and Reches, 1983; Eyal, 1996; Walley, 1998; Bosworth et al., 1999). The trends of the Syrian Arc axes vary systematically from an E–W in northern Sinai, to an almost N–S in central Israel, and to NE–SW in the Palmyra fold and thrust belt in Syria, forming a lateral distribution of a 1000 km long S shaped feature (Figure 9). In Israel, the folds are exposed inland and are buried by younger sediments in the coastal plain and continental shelf (Bruner, 1991; Druckman et al., 1995). The fold amplitudes range from a few hundred meters to a kilometer and their crests are in places complicated by secondary domal culminations and saddles (Picard, 1943; Shamir and Eyal, 1995).

Thickness variations related to the nucleation of the Syrian Arc structures indicate that the Syrian Arc deformation in the area started in the Cenomanian (Freund and Zak, 1973; Freund et al., 1975) and continued through the Tertiary (Freund, 1970; Ron and Eyal, 1985; summary by Eyal, 1996; Walley, 1998). Thicknesses also vary on several anticlines in the Late Eocene–Oligocene sections, indicating two main pulses of tectonic activity separated by a relatively long and quiet period lasting about 35 Myr (Eyal, 1996; Walley, 1998; Guiraud et al., 2005).



Figure 9: Distribution of axes in the syrian arc fold belt, from Palmyra in the north' through the northern Negev to Sinai in the south (modified after Garfunkel, 1998)

1.2.3 Basin inversion

A change in the configuration of the North Atlantic–Eurasian–African plates during late Santonian (late Cretaceous) occurred simultaneously with the onset of collision of the African plate with Eurasia (Stampfli, 2000; Garfunkel, 2004). Progressively, the Tethyan oceanic domain south of the Eurasian margin closed from 65 to 35 Ma (Le Pichon, 1982; Jolivet and Faccenna, 2000).

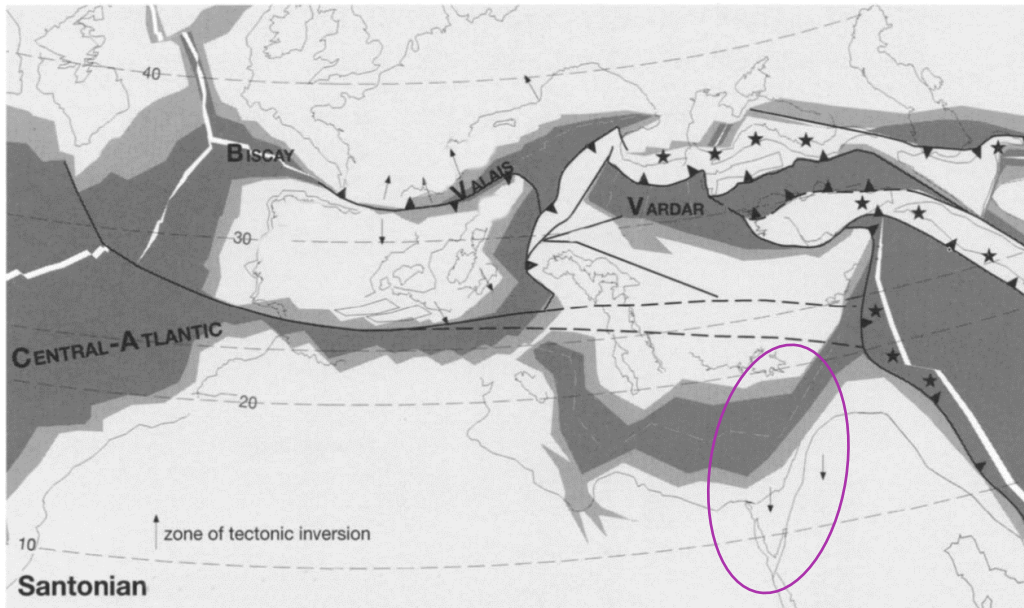


Figure 10: Santonian configuration of part of the Neo-Tethys Ocean. Levantine area is circled, arrows represent areas with evident basin inversion (modified after Stampfli, 2000).

The collision led to high-pressure metamorphism in the Alps and transpressive inversion of E-W trending basins, such as the West Netherlands Basin (Bodenhausen and Ott, 1981), along the southwest Bohemian Border zone (Ziegler, 1990) and the eastern Levantine basin (Guiraud et al., 2005) (Figure 10).

The term inversion refers to a reversal of the sedimentary basin record in its sense of motion during different stages of basin evolution (Mitra, 1993; Coward, 1994). Basin inversion can be defined as the process of shortening of extensional basins which is accommodated by compressional reactivation of pre-existing normal faults (Williams et al., 1989). As a result, a fault may accommodate net extension at deeper levels with net contraction associated with an anticline in the upper portion of the faulted rocks (Lowell, 1995; Williams et al., 1989). Thus, initially subsiding areas become subsequently uplifted.

Basin inversion can occur at different scales and is widely documented in different tectonic settings. The driving force to the inversion process can be far-field stresses transmitted within tectonic plates. Basins can be inverted by compression, strike-slip or combination of both (Coward 1994, Lowell 1995). An example of tectonic inversion caused by compression are the Atlas Mountains in Morocco, where the ENE-WSW Triassic-Jurassic Atlas Rift inverted due to NNW-SSE compression caused by Miocene convergence of Africa and Iberia. The compression resulted into the formation of low-angle thrusts on both sides of the Atlas (Beauchamp et al., 1999; Brede et al., 1992; Guiraud and Bosworth, 1997). Strike slip related inversion has been identified in the western Barents Sea (Norwegian shelf) and dated to Late Paleozoic, Mesozoic and Cenozoic (Gabrielsen et al. 2011). Inversion structures including reverse faults, deformation of footwall blocks and deformed fault planes were reported from Turonian throughout Late Cretaceous and into Early Cenozoic in particular (Gabrielsen et al. 1997). A common way to detect a basin inversion structure is by the characterization of three stratigraphic sequences (Figure 11). Pre-rift sequence can be recognized by equal thickness of strata on hanging walls and footwalls, syn-rift sequence is characterized with growth faulting, and post-rift sequence that can also be deposited on top of a marked break-up unconformity, reflecting erosion or non-deposition (Figure 11). A perfect reversal of net fault slip is unlikely and most inversion structures probably result from superimposed oblique slip movements (Williams et al., 1989).

An analysis of thickness variations of the Late Triassic and Early Jurassic formations in the northern Negev by Freund et al. (1975) revealed that in several areas thick accumulations of these strata are present underneath present-day monoclines (Figure 12). This observation, and the recognition that the monoclines are underlain by high-angle reverse faults, have led the authors to propose what has become known as the 'structure inversion model' for the development of the Syrian Arc anticlines in the eastern Levantine basin (Freund et al., 1975a; Reches et al., 1981; Bruner, 1991; Jolivet and

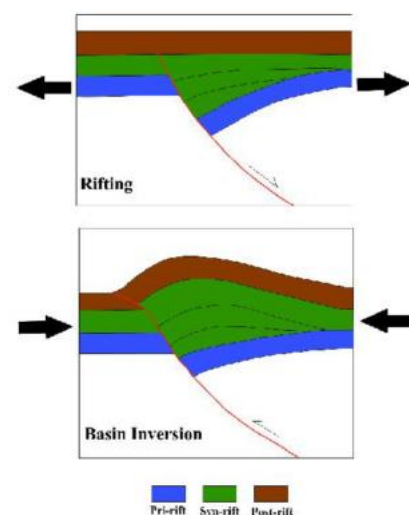


Figure 11: Schematic diagram showing a basin inversion (modified after Williams et al., 1989). Colors represent stratigraphic sequences

Faccenna, 2000). According to this hypothesis, slip occurred along reverse faults at depth and led to the development of monoclines or folds in the upper part of the stratigraphic column (Reches et al., 1981; Eyal and Reches, 1983). Some of the folds are associated with reactivation of Early Mesozoic normal faults in a reverse motion (Freund et al., 1975; Druckman et al., 1995).

Reverse faults that underlie the Syrian arc anticlines have been observed in outcrop only at the Ramon crater in the Negev desert (Freund et al., 1975). Evidence for reverse faults was also encountered in a few boreholes with apparent section doubling around the study area of this work: Rehme 1, Zavoa 1 and Sherif 1 (Bruner, 1991; Freund et al., 1975a; Druckman et al., 1995). It has been shown that essentially the same model also applies very well to the structural evolution of the south-western Palmyride fold belt in Syria (Chaimov et al, 1993). Whole-basin scale inversion, documented across the African-Arabian continental plate (Bosworth et al., 1999), is a manifestation of the Wilson cycle (Wilson, 1963).

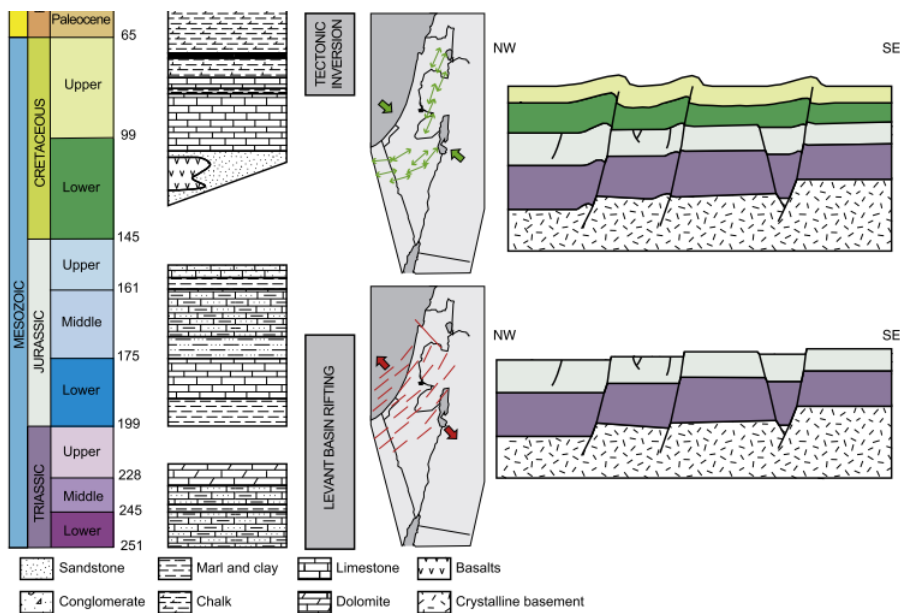


Fig. 2. Simplified stratigraphic column and synthesis of the three main tectonic events recognized in Israel. See text for details.

Figure 12: simplified Schematic stratigraphic column and synthesis of the main tectonic events recognized in Israel (Hardy et al., 2010)

1.3 Structural restoration

Structural restoration is the process of removal of the effects of sediment compaction, isostatic adjustment, fault-related folding and fault slip that have altered the present day section since deposition. Restoration is a tool used for defining the amounts of shortening

or extension in a region (Griffiths et al., 2002; Cukur et al., 2011), assessment of the timing of hydrocarbon trap development (Baur et al., 2009; Durand-Riard et al., 2013) unraveling structural and stratigraphic history (Beauchamp et al., 1999), and revealing tectonically masked features (Tanner et al., 2003).

Restoration of cross-sections (Dahlstrom, 1969), maps (Rouby et al., 2002), or volumes (Santi et al., 2002; Durand-Riard et al., 2013) has been successfully applied to complex thrust or normal fault systems. Restoration techniques were also tested through models for restoration of inverted basins in the lab (Bulnes and McClay, 1999). This lead to improved understanding of the spatial and temporal development of geological structures, constraining the kinematics of structural growth (Dahlstrom, 1969; Griffiths et al., 2002; Cukur et al., 2011).

A seismic section can be restored by inverse modeling (Figure 13). A restored section is then restored to the time of deposition of the designated reference horizon. Because sections are restored from the top down, the shape of a restored horizon depends not only on the deformed structure of the event and the reference horizon, but also on the shape and the slip of any faults that lie above it in the restored section.

As structural restoration is a kinematic modeling tool, the techniques for the restoration of a structure are necessarily based on models for the evolution of the geometry. Structures with complex fault geometries can be restored by making geological assumptions on the timing of faults and testing various scenarios. The scenario that is preferred should be geologically viable (Tobergte and Curtis, 2006).

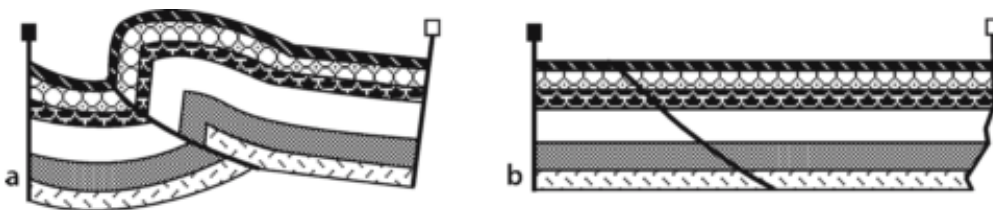


Figure 13: Restoration of a cross section. a- Deformed state section; b- Restored section (Tobergte and Curtis, 2006)

Structural restoration of seismic data starts with the available interpreted seismic sections. An interpreted seismic section in depth across a sedimentary basin contains implicit information about the tectono-stratigraphic evolution of the basin. This information can be extracted by producing a series of structurally restored seismic sections that illustrate the subsurface geology for various times in the past. The structural restoration can

validate the interpreted geometry in cross section, providing information on the processes of progressive deformation in the region.

The data for the present work were acquired using 2D seismic surveys for hydrocarbon exploration ween the years 1986-1987. The data were interpreted by Elvira Gelbermann from the Geophysical Institute of Israel (Gelbermann and Grossovicz, 1990; Fleischer et al., 1993; Gelbermann, 1995)

2 Research objective

The main objective of this study is to examine the temporal evolution of the Qeren and Agur structures.

These structures consist of two buried anticlines, Qeren-Rogem and Agur-Haluza, and associated re-activated faults. The area was chosen because its broad geological story is rather constrained, thus leaving space for high resolution examination and validation of the suggested evolution model.

Additional questions that arise from the main objective are:

1. Are there masked tectonic phases of deformation other than the Triassic-early Jurassic extension and Syrian arc shortening in the upper Cretaceous?
2. When does the Syrian arc shortening initiate in the Agur and Qeren structures, accepting the lateral migration of the Syrian arc system? (Freund and Zak, 1973)
3. Is there a difference between the northern and southern segments of the Qeren and Agur structures?

This study extends previous studies and uses the available 2D seismic sections, 3D structural maps and borehole data to test known tectonic concepts. Sequential structural restoration enables us to shed light on second or third order tectonic phenomena that have eluded the overall plate tectonic framework until now.

3 Methodology

This study took advantage of various software packages. The seismic data was georeferenced using Arcmap GIS and Blue Marble Geographics Global Mapper, depth-converted using Schlumberger software package Petrel, digitized using Able Software Corp. R2V. The seismic data was then kinematically analyzed and sequentially restored using Midland valley Move™.

Move™ is a software package that offers a full range of tools for geometrically constrained model building and kinematic analysis in 2D and 3D space.

3.1 *Workflow*

The loading history of a basin can be modeled by sequential back-stripping and decompaction of balanced geological cross-sections (Griffiths et al., 2002; Tobergte and Curtis, 2006). Restoration of seismic sections accounts for plastic long-scale geological processes that determine structure. This allows one to assess the amounts, rates, and periods of deformation that affected the Negev.

Before starting the restoration process per se, the seismic sections had to be digitized and depth-converted. The depth-conversion process made use of seismic velocity surveys from the study area. The sections were digitized using the Move™ digitization tools. The depth-converted digitized sections were then imported to the 2D Move™ module for cross-section restoration. The depth-converted sections were balanced and restored by accounting for compaction, faulting, folding and isostasy for each stratigraphic layer. The integrity of each layer in the digitized seismic section (e.g., horizon termination, attachment of horizons to faults and boundaries, and complete closure of polygons) was checked before restoring each layer.

A complete flowchart of the restoration process is presented in Figure 14.

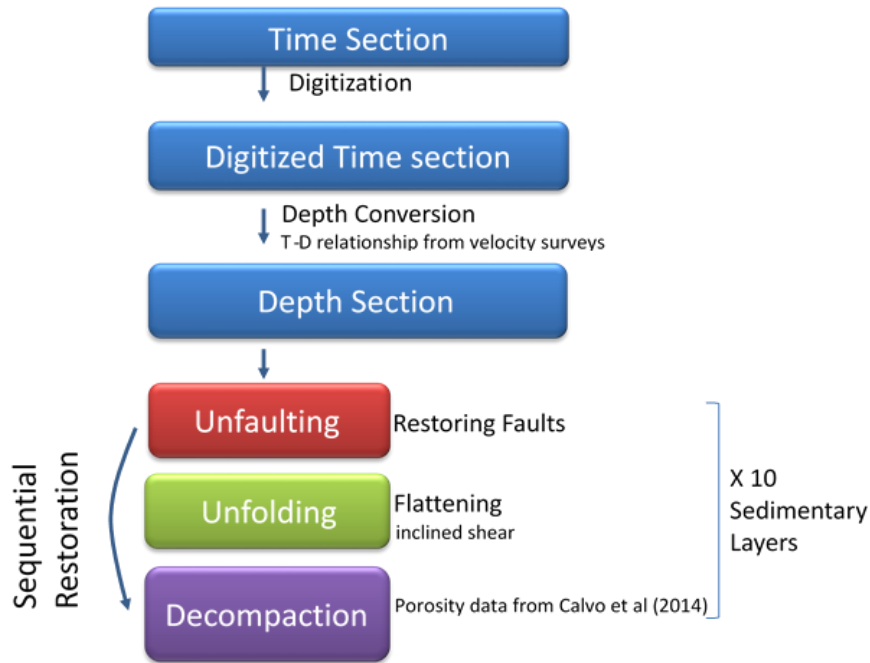


Figure 14: Flowchart of restoration process

3.2 Digitization

Eight seismic horizons were digitized using the Able Software Corp. R2V and Blue Marble Geographics Global Mapper software packages. Surfaces were interpolated using the Delaunay TIN triangulation method (Delaunay, 1934; Lee and Schachter, 1980) (Figure 15). 2D seismic and velocity surveys were digitized and integrated into the model using Move™ digitization tools.

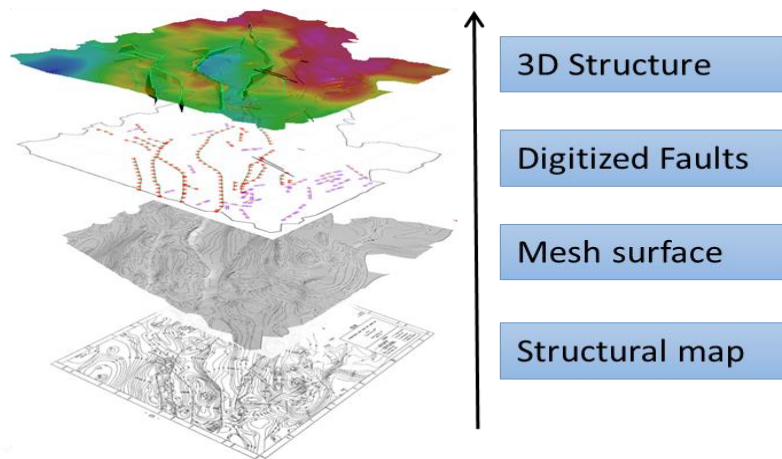


Figure 15: From structural scanned map to a 3D structure

3.3 Depth conversion

Velocity check-shot surveys from the study area were used to convert the sections from two-way traveltimes (twl) to depth. Time and depth were correlated using the interval velocity measurements for each layer. Then, the depth converted surveys were compared to lower resolution 3D seismic horizons interpolated across the study area (Druckman et al., 1994), as a validation step. For the full data refer to section 8.1 in the appendix.

3.3.1 Velocity surveys

Two velocity surveys were used in this work: Qeren_01 and Shizaf_01. These were check-shot surveys (Figure 16), in which a geophone is locked successively at different depth levels, and the vertical travel time to each level is measured directly from a source of energy at the surface (Schlumberger Oilfield Glossary).

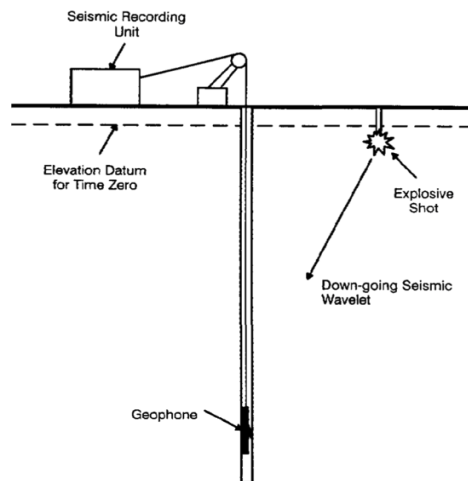


Figure 16: A simplified check-shot velocity survey (modified after Schlumberger Oilfield Glossary)

3.3.2 3D structure

The three-dimensional structure (Figure 17, Figure 18) was constructed based on the interpretation of some 2000 km of seismic lines, acquired over several generations of oil prospecting surveys.

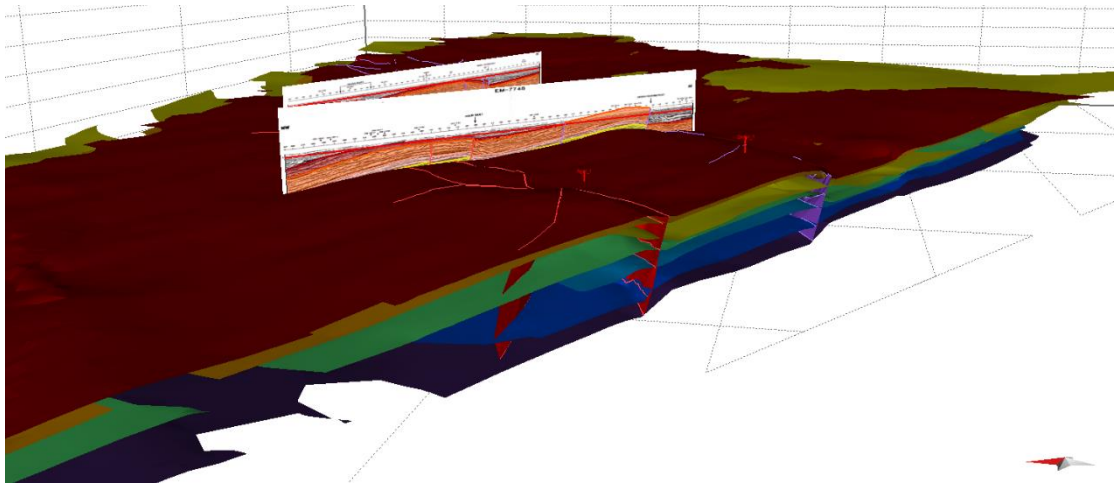


Figure 17: 3D structure of study area that is cut vertically by faults

The processed seismics were interpreted by E. Gelbermann (Gelbermann and Grossowicz, 1990; Fleischer et al., 1993; and Gelbermann, 1995) (refer to section 1.3). In this interpretation, seismic travel time was converted to depth by the "layer cake" method, using interval velocities from borehole information.

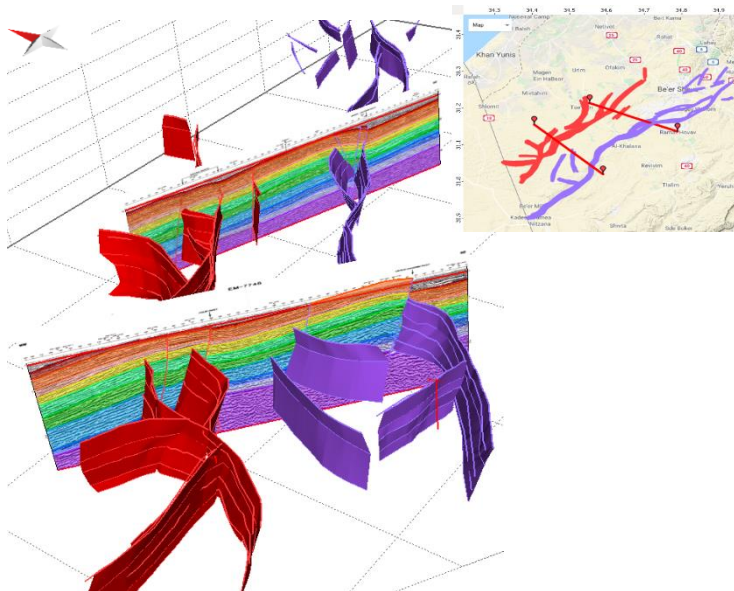


Figure 18: 3D fault structure of study area along with location map

3.4 The stratigraphic column

In order to build an accurate stratigraphic column (Figure 19) the geological ages of key unconformity surfaces were taken from the Stratigraphic Table of Israel, Outcrops and Subsurface (Fleischer, 2002).

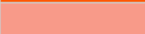
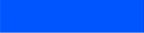
	Horizon	Colour	Age	Active
1	TopJudea		89.0 Ma	<input checked="" type="checkbox"/>
2	C4		99.0 Ma	<input checked="" type="checkbox"/>
3	LC3		112.0 Ma	<input checked="" type="checkbox"/>
4	TopJurassic		150.0 Ma	<input checked="" type="checkbox"/>
5	TopZohar		159.0 Ma	<input checked="" type="checkbox"/>
6	TopDaya		168.0 Ma	<input checked="" type="checkbox"/>
7	TopQeren		176.0 Ma	<input checked="" type="checkbox"/>
8	TopTriassic		220.0 Ma	<input checked="" type="checkbox"/>
9	TopRaaf		240.0 Ma	<input checked="" type="checkbox"/>
10	BaseTriassic		251.0 Ma	<input checked="" type="checkbox"/>

Figure 19: Stratigraphic column used in the restoration process

3.5 Restoration

3.5.1 Faulting

The present day 2D sections are 'unfaulted' in order to restore the slip between footwall and hanging wall. By selecting an appropriate restoration algorithm, a geologically viable geometry should result as the fault displacement is removed. The unfaulting step of the restoration is considered complete when the hanging wall and footwall cut-offs are joined.

3.5.1.1 Parallel flow unfaulting

The 'Fault Parallel Flow' algorithm is based on 'Particulate Laminar Flow' over a fault ramp (Egan et al., 1997; Ziesch et al., 2014) and is suitable to restore brittle rock deformation. It is a scale independent method that describes how material nodes (the nodes that are used, for example, to construct the geological surfaces of the hanging-wall) are displaced parallel to the fault plane, in the direction of fault movement (Figure 20).

Using the algorithm, the node points of beds are fixed such that they can only move along flow planes that are parallel to the fault surface and in the plane of the tectonic transport vector (Tanner et al. 2003). Bed length and thickness are not maintained as beds pass over angular changes in the fault surface.

For a first-pass restoration, vertical shear is appropriate. Then iterative steps determine the appropriate shear angle under the condition that the hanging wall is flattened during restoration (Move™ knowledge database).

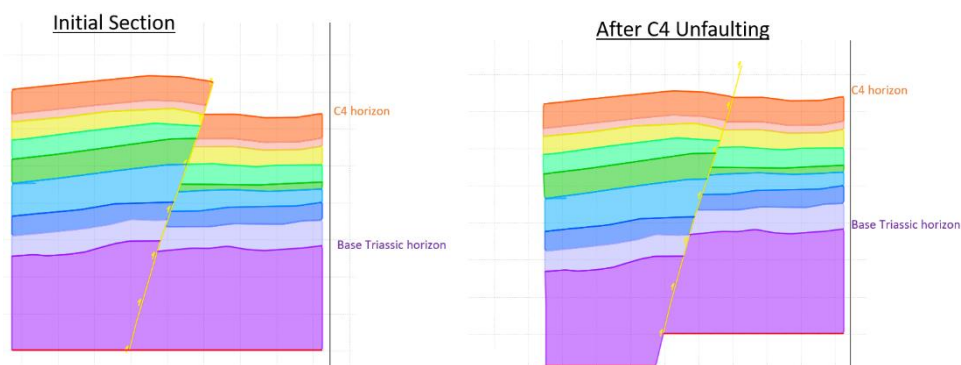


Figure 20: Before and after unfaulting of horizon C4

3.5.2 Folding

Seismic horizons are defined by geometry and age, and so flattening can reveal significant features present at a particular time. Unfolding algorithms allow geological (seismic)

horizons to be restored to a pre-deformation datum. Structural domains are restored by applying one or more kinematic algorithms. Each algorithm fulfills conditions based on an assumption of the folding mechanism, in order to restore the deformed-state structure to its pre-deformation configuration. The horizons in this study are unfolded using the Simple Shear mechanism.

3.5.2.1 *Oblique Simple shear*

Simple shear is the geometry produced by slip on closely spaced, parallel planes with neither length nor thickness changes, neither parallel nor perpendicular to the slip planes (Tobergte and Curtis, 2006). The 'Simple Shear' unfolding algorithm oblique to bedding is a kinematic tool that causes bed length and bed thickness changes. In this algorithm, line length in the unfolding direction varies between the deformed and undeformed states. (Move™ Help pages).

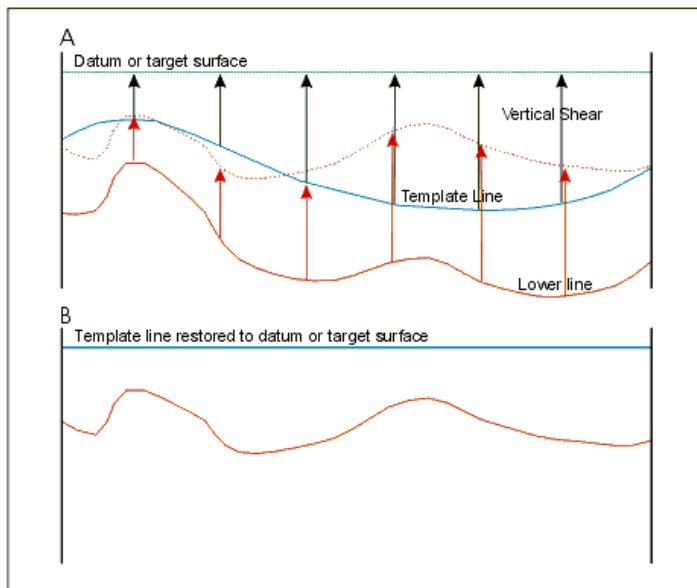


Figure 21: Folded horizon restoration using vertical simple shear unfolding tool (Move™ help pages)

An oblique simple shear restoration follows the same procedure as the vertical simple-shear restoration (Figure 21), except that the lines are inclined to the regional trend at an angle other than 90°. The oblique lengths measured on the deformed state cross section (Figure 22a) are restored by translation in the shear direction to return the reference horizon to the regional trend (Figure 22b).

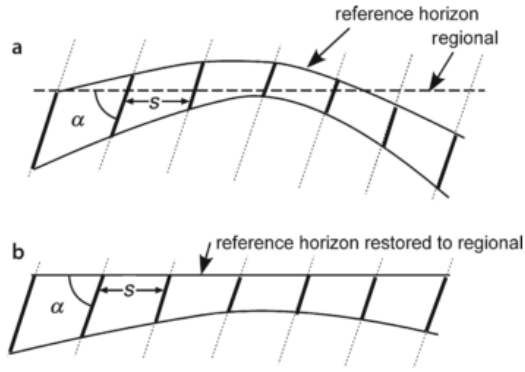


Figure 22: Restoration by oblique simple shear. a- Deformed state cross section; b- Restored cross section. Medium-weight solid lines are marker beds. Dotted lines represent the shear direction and are spaced in an arbitrary distance S apart. The shear angle is α (Tobergte and Curtis, 2006).

3.5.3 Compaction

In order to account for reduction of porosity and expulsion of fluid under pressure of burial, compaction was taken into account. Compaction can reduce the dip of buried surfaces such as fault planes. For example, a buried fault plane becomes shallower in dip (Haneberg, 1988). The variation of porosity with depth is commonly assumed to be constant through time for any particular lithology (Sclater and Christie, 1980).

In order to account for the compaction of the sedimentary section in the study area, two data sets were used. Borehole data was obtained from the updated version (Fleischer and Varshavsky, 2002) of the ATLAS subsurface database (Flexer et al., 1981). Porosity had been measured on the borehole plugs in the Geological Survey using Helium gas. For more data on the petrophysical analysis please refer to Calvo et al. (2014). In order to account for porosity of units not in the porosity surveys, a compaction function was used based on the work of Sclater and Christie (1980). For more details refer to appendix 8.2. A formula allowing prediction of compaction with depth of burial is $f = f_0 * e^{-cy}$, where f represents the present day porosity at depth, f_0 is the porosity at the surface, C is the porosity depth coefficient ($\frac{1}{km}$) and y is the depth (m).

3.5.4 Flexural Isostasy

As the lithosphere has an inherent strength and rigidity, local load changes due to contraction, extension or erosion are not isostatically compensated locally, but are supported regionally. The extent to which the support is spread is determined by the flexural properties of the lithosphere. Flexural isostasy exerts significant regional control

on sequence thickness and fault geometry. Hence, flexural isostatic adjustment has a significant effect on deformation when modeling regional cross sections in regions of extension or contraction (Move™ knowledge database).

Flexural isostasy is used when the length of the section is on the order of tens of kilometers or longer. The equations used to model the flexural response follow Watts (2001). The deflection w caused by a load $q(x)$ on a plate with dimensions $h \times L$

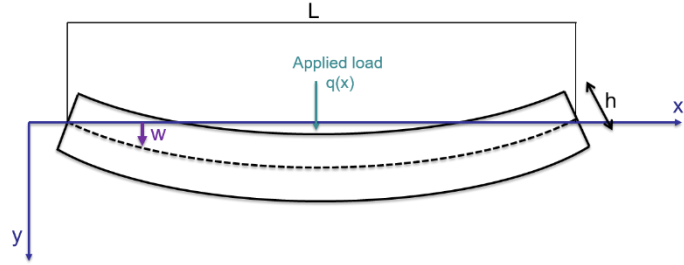


Figure 23: Schematic figure showing the deflection (w) applied on a plate with $h \times L$ dimensions (Modified after Watts, 2001)

(Figure 23) can be calculated using the general equation for the deflection of the plate,

$$(1) \quad D \frac{d^4 w}{dx^4} = q_a(x) - (\rho_m - \rho_w)gw - P \frac{d^2 w}{dx^2},$$

where ρ_m is the density of the asthenosphere, P is a constant representing the lateral support of the load in the lithosphere and D is the flexural rigidity defines the strength of the plate. D is defined as

$$(2) \quad D = \frac{E * T_e^3}{12(1 - \nu^2)},$$

where E is Young's modulus. This is the average Young's modulus for all of the rocks in the section. It is assumed to be constant throughout the section. In this work it is set to 70,000 mPa and ν is Poisson's ratio and is set to 0.25 in this work (Turcotte and Schubert, 2014).

T_e is the effective elastic thickness. It is defined as the thickness of a perfectly elastic layer with the same flexural strength as the lithosphere. It isn't a directly measurable quantity. T_e is a function of Young's modulus and the actual thickness of the crust and in this work is set to 18000m (Ebinger et al., 1989). The deflection w is calculated for each column of width x . The deflection of the lithosphere is then summed using a summation function to calculate the total isostatic response for the whole section. The Move™ workflow assumes that flexural response occurs synchronously with deposition, or shortly after. In view of the uncertainty in the flexural behavior, the effect of 40% change in elastic thickness (T_e) was explored, and found to be negligible.

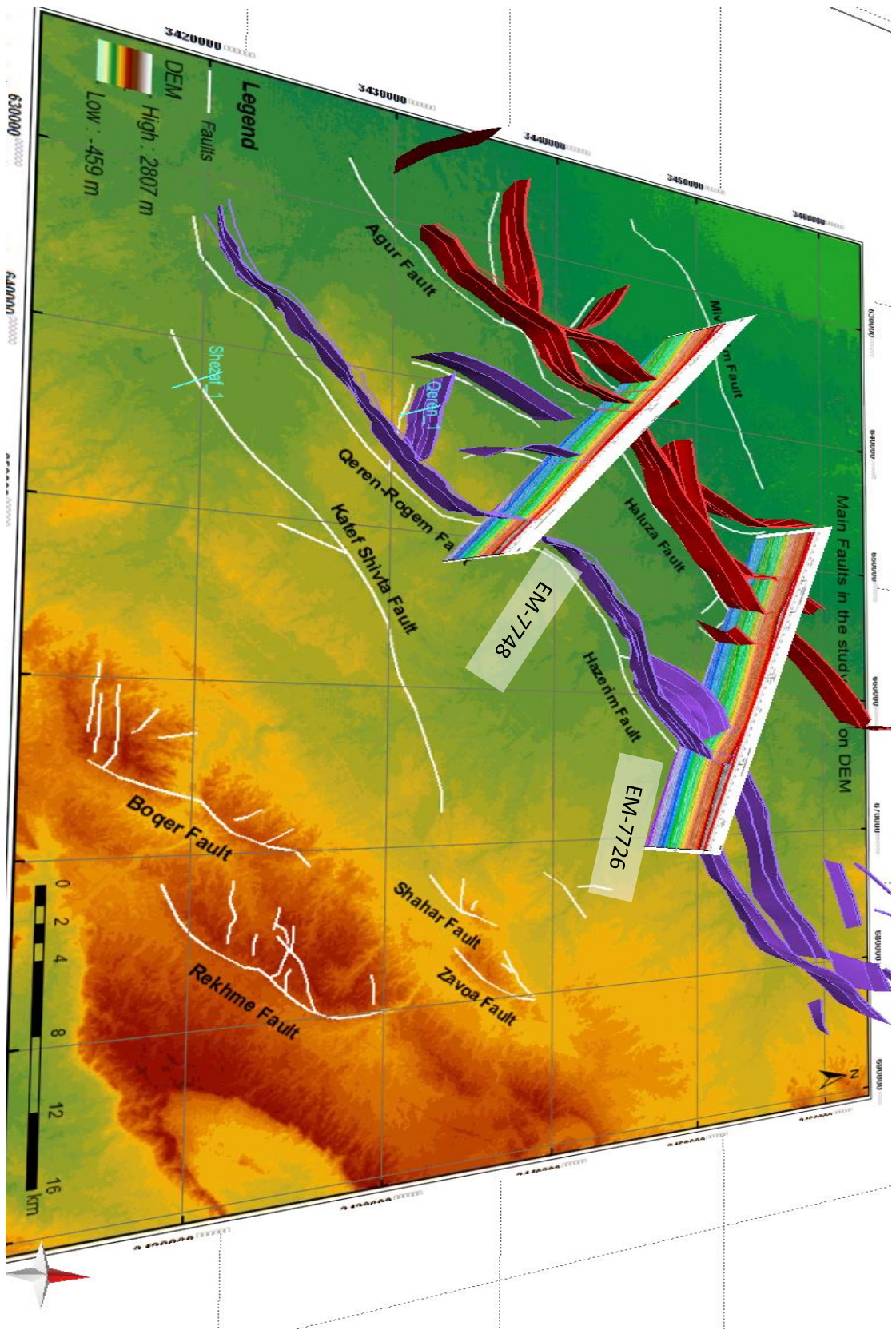
4 Results

In this study, we took a high resolution look at two buried anticlines, the Qeren-Rogem-Hazerim and the Agur-Haluza, removing folding and isostasy related thickness variations in order to examine the complex slip history that was revealed.

Locations of the seismic sections investigated, velocity surveys and the main faults in the study area are shown in Figure 24. Seismic section EM-7726 is 30.5 km long and crosses branches of the Agur-Haluza and Qeren-Rogem-Hazerim fault structures from the north in a WNW- ESE direction. The section straddles the northeastern plunge of the Haluza anticline in the northern part of the research area, the center of the Hazerim anticline, and the Qeren-Hazerim faults.

Seismic section EM-7748 is 24.1 km long and crosses branches of the Agur-Haluza and Qeren-Rogem-Hazerim faults as well, southeastwards in a NW-SE direction. EM-7748 passes through the center of the study area, across the north-eastern plunge of the Agur anticline and the center of Qeren structure. Two velocity surveys were conducted in the study area, Qeren_01 and Shezaf_01. The accurate locations of the velocity surveys are shown in Figure 24.

Figure 24: Locations of faults, seismic sections and velocity surveys across the study area over a structural map of top Judea horizon (modified after Druckman (1995)).



4.1 Section EM-7748

Figure 25 shows the interpreted section EM-7748 (Figure 25a), the section after depth conversion (Figure 25b) and after digitization (Figure 25c). For the full data regarding digitization process refer to section 8.3 in the appendix. Section EM-7748 was converted to depth using the time-depth correlation from velocity survey Qeren_01. The section was then sequentially restored using the ‘Fault parallel flow’ unfaulting algorithm, ‘oblique simple shear’ unfolding algorithm, along with decompaction.

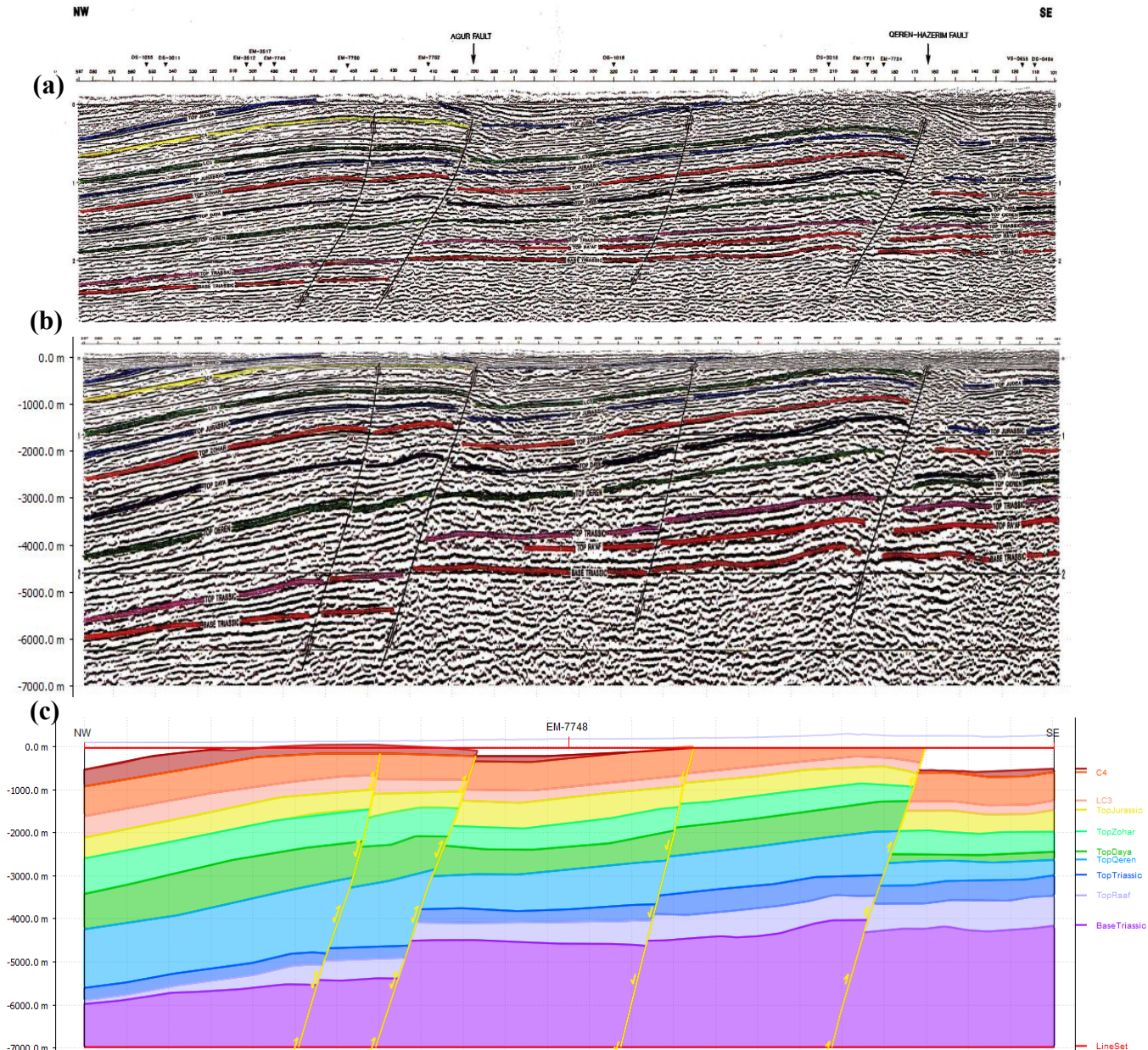


Figure 25: Seismic section EM-7748. (a) Original section (b) Section after depth conversion (c) Section after depth conversion and digitization.

4.2 Section EM-7726

Figure 26 shows the interpreted section EM-7726 (Figure 26a), the section after depth conversion (Figure 26b) and after digitization (Figure 26c). For the full data regarding digitization process refer to section 8.3 in the appendix. Section EM-7726 was converted to depth using the time-depth correlation from velocity survey Shezaf_01. The section was then sequentially restored using the ‘Fault parallel flow’ unroofing and ‘oblique simple shear’ unfolding algorithms, along with decompaction.

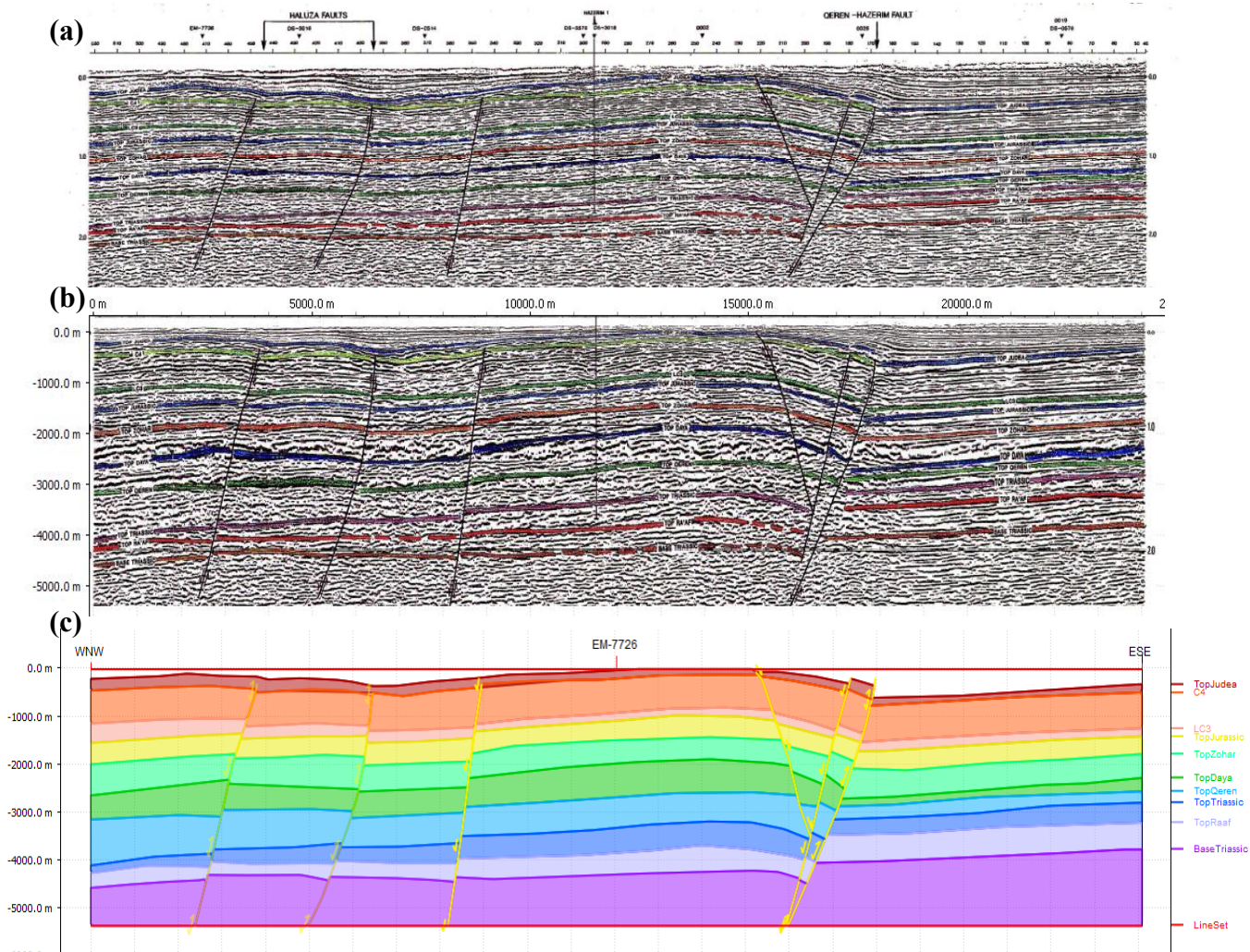


Figure 26: Seismic section EM-7726. (a) Original section (b) Section after depth conversion (c) Section after depth conversion and digitization.

4.3 Restoration results

4.3.1 Determination of detection limit

To correctly relate to the relatively poor quality of the analog seismic data records available, an estimation of error in the amount of slip is necessary. This is needed to filter out small slips on faults observed in the results that can be caused by poor seismic resolution that leads to interpretation errors. The average spacing between reflectors was chosen to represent this error is 80m (Figure 27). All slips below 80m aren't reviewed.

For the full step-by-step restoration process refer to section 8.4 in the appendix.

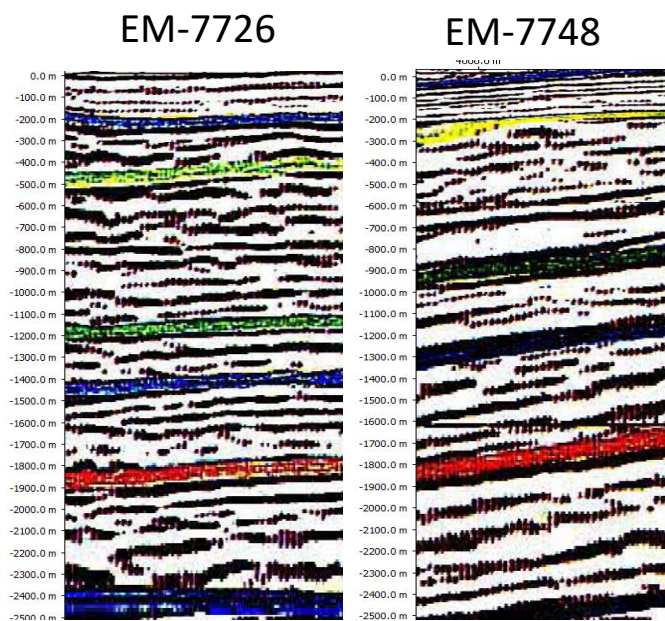


Figure 27: Detection limit determination based of reflector spacing

4.3.2 Lower to middle Triassic- after the deposition of base Triassic horizon (251-240 Myr):

A reverse slip on the Qeren-Rogem fault is observed in both the EM-7748 and EN-7726 sections (Figure 28). This reverse movement lowers the south-eastern flank of the sections compared to the north-western. The movement is characterized by steps of approximately 100m: one step in section EM-7748 and two steps in section EM-7726.

There is a gradual thickening towards the SE. The south-eastern flank of the section has more accommodation space, forming a morphological basin.

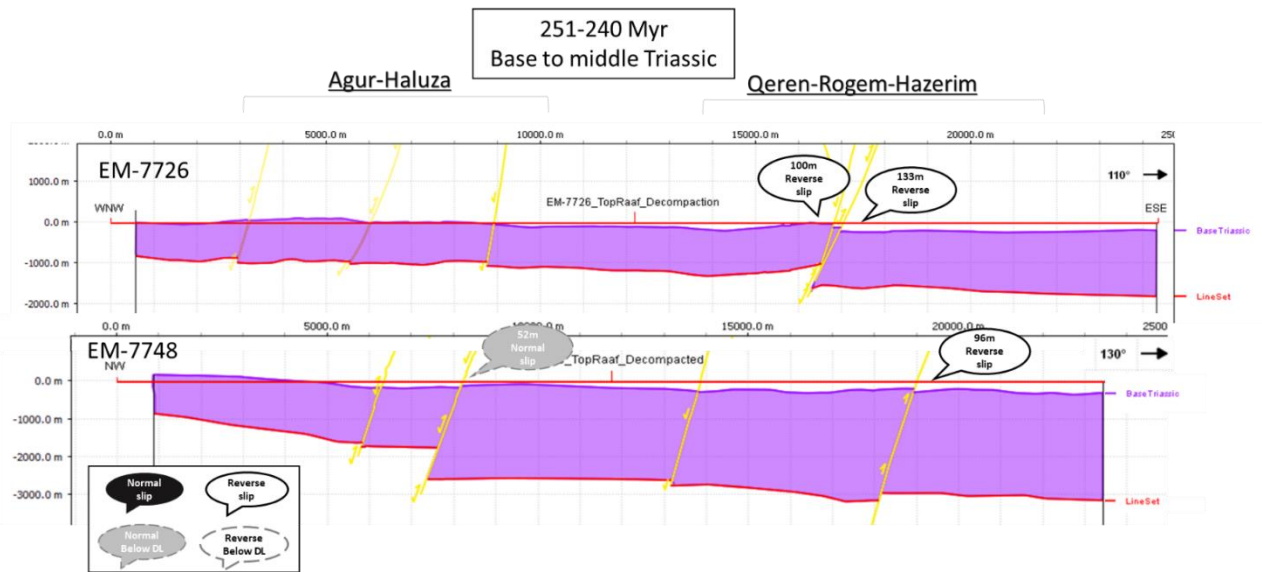


Figure 28: Restoration of lower to middle Triassic in sections EM-7726 and EM-7748

4.3.3 Middle to late Triassic- after the deposition of top Raaf horizon (240-220 Myr):

Normal slip is observed in section EM-7726 on the Agur-Haluza and Qeren-Rogem-Hazerim faults (Figure 29). On both faults, the north-western flank is lowered as compared to the south-eastern flank. The slip amount is relatively higher than that of base Triassic; 155m on Agur and 170m on Qeren. This is the earliest activity of the Agur fault noticed in this work. As a continuum to the lower Triassic, there is a gradual thickening towards the SE. The south-eastern flank of the section has more accommodation space, forming a morphological basin.

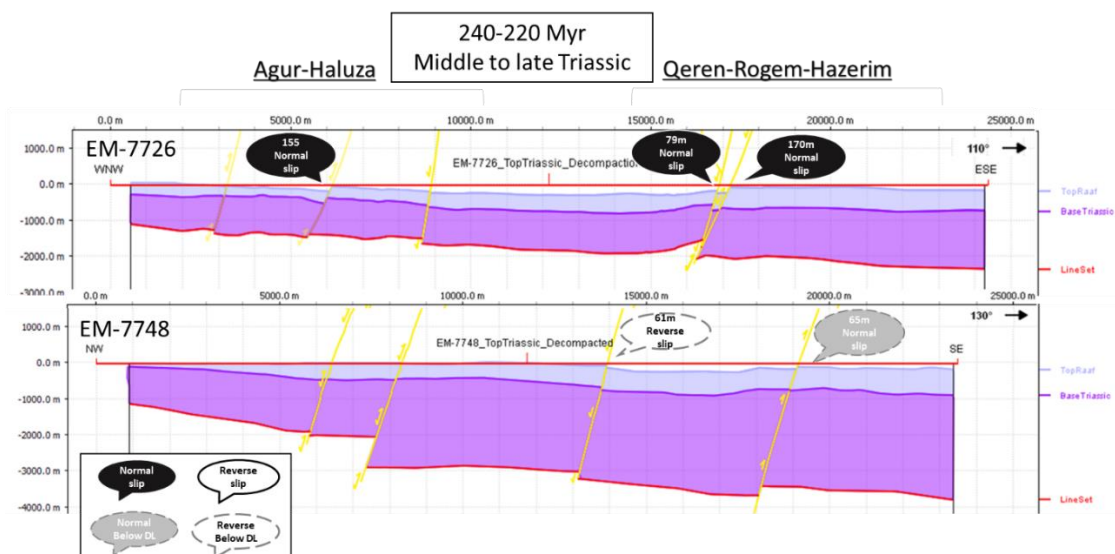


Figure 29: Restoration middle to late Triassic in sections EM-7726 and EM-7748

4.3.4 Late Triassic to early Jurassic- after the deposition of top Triassic horizon (220-176 Myr):

Normal slip continues on the Afur-Haluza and Qeren-Rogem-Hazerim faults in both seismic sections (Figure 30). The normal slip is observed on all the faults, as compared to the middle-late Triassic. The normal slips are lowering the north-western part of the section compared to the south-eastern. On the Qeren-Rogem-Hazerim fault, the slip is in two steps of 354m and 221m in the northern part (EM-7726) and in a big step of 529m in the southern part (EM-7748). On the Agur-Haluza fault, the northern flank (EM-7726) is slipping in an amount below the detection limit (60m, 25m), whereas the southern flank (EM-7748) slips 1030m and 366m. As a continuum to the middle and late Triassic, there is a gradual thickening towards the SE.

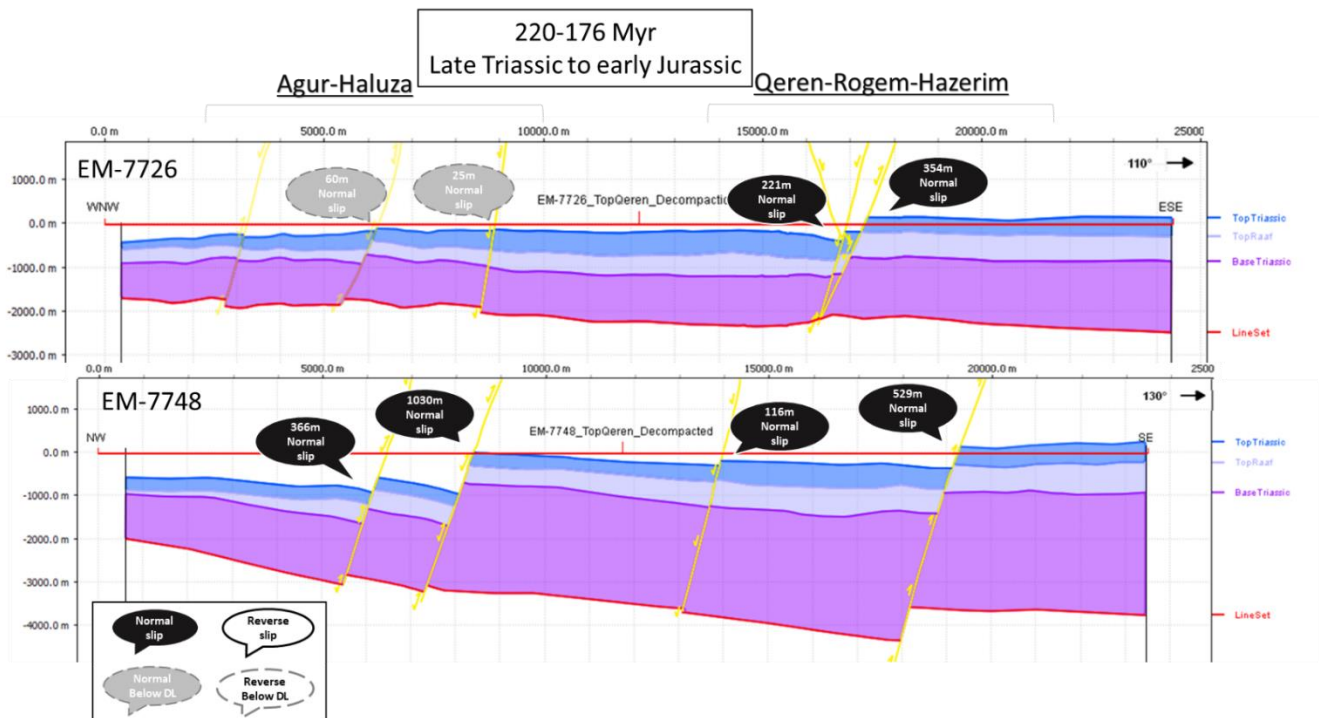


Figure 30: Restoration of late Triassic to early Jurassic in sections EM-7726 and EM-7748

4.3.5 Early to middle Jurassic- after the deposition of top Qeren horizon (176-168 Myr):

Both normal as well as reverse slips are observed in the beginning of the Jurassic period (Figure 31). On the Agur-Haluza fault, a normal slip of 232m and a reverse slip of 99m is observed on the northern flank (EM-7726), and a reverse slip of 117m is observed on

the southern flank (EM-7748). On the Qeren-Rogem-Hazerim fault, reverse and normal slips are observed on the northern flank (EM-7726), forming a small graben. A normal slip is observed on the southern flank (EM-7748) of the Qeren-Rogem-Hazerim fault. The fault structure of the Qeren fault in section EM-7726 is complex and normal and reverse slips are observed simultaneously. Reverse movement is confined, as compared to the normal slip, in the Triassic.

Thickness variations throughout both sections show a clear syn-depositional trend of thickening towards the NW, compared to the SE as before (Figure 29Figure 30). This can be observed from both sections.

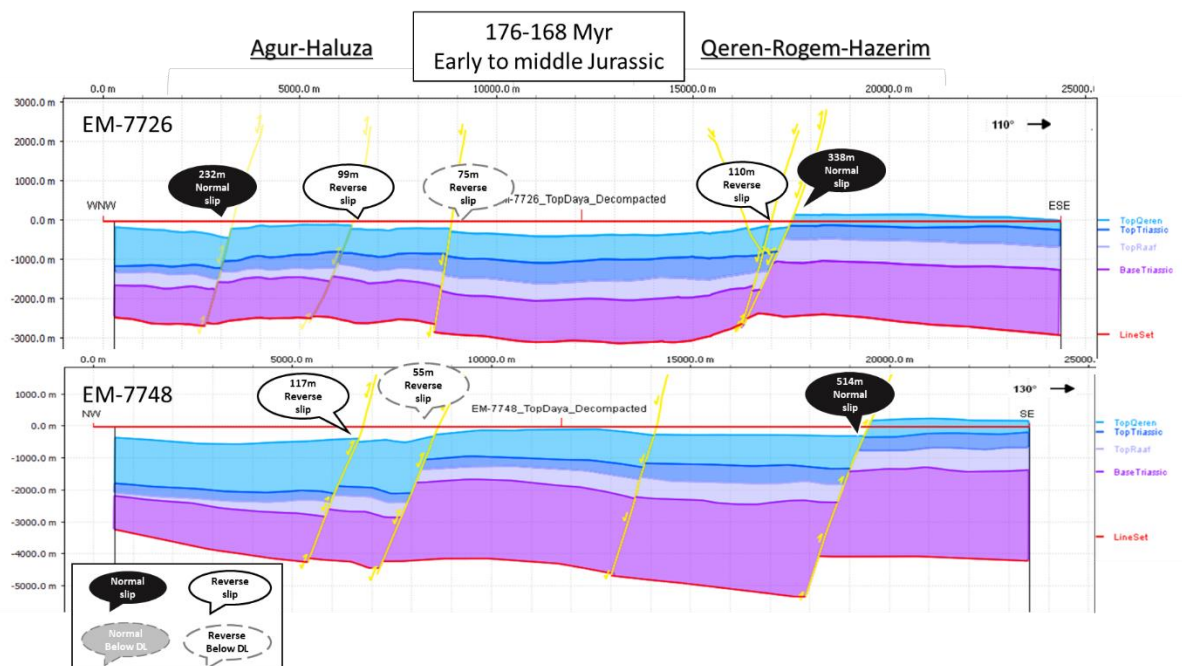


Figure 31: Restoration of early to middle Jurassic in sections EM-7726 and EM-7748

4.3.6 Middle to late Jurassic- after the deposition of top Daya horizon (168-159 Myr):

Normal slip continues and dominates the fault slips of Qeren-Rogem on the northern flank (EM-7726- 136m) as well as southern flank (EM-7748- 207m) (Figure 32). Normal faulting is also observed in the Qeren-Rogem-Hazerim fault in the northern flank (EM-7726-102m). A sharp sudden thickness change of the southeastern segment on both sections causes a reverse slip to be observed.

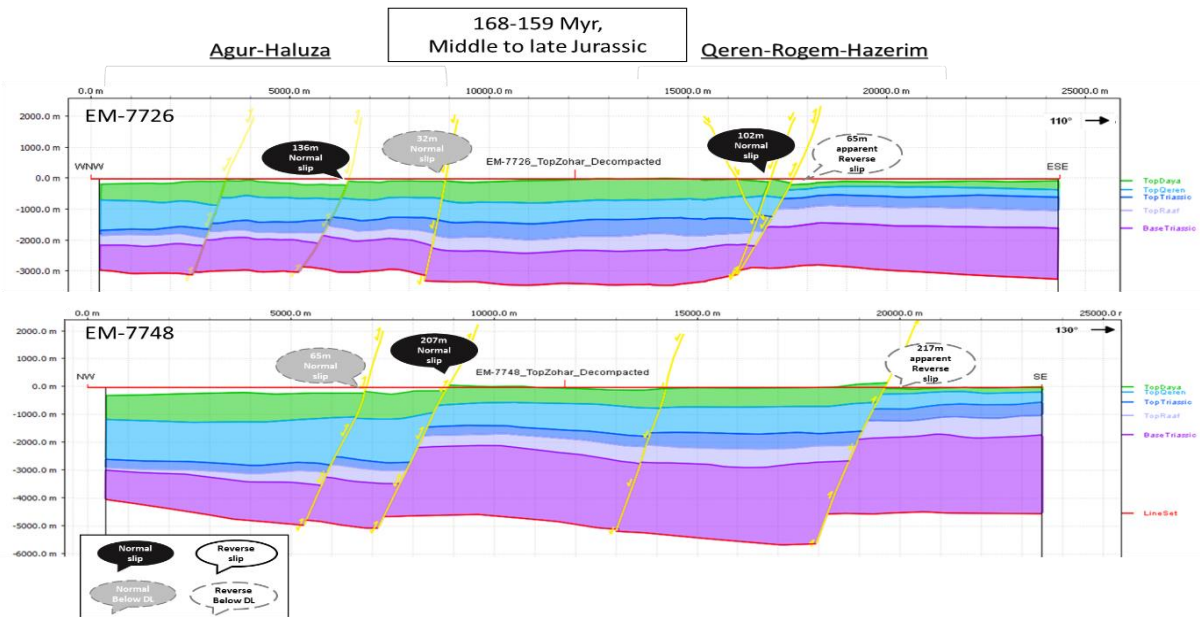


Figure 32: Restoration of middle to late Jurassic in sections EM-7726 and EM-7748

4.3.7 Oxfordian to Tithonian in the late Jurassic- after the deposition of top Zohar horizon (159-150 Myr):

Reverse slip is observed in section EM-7748, in the southern flank of the Agur-Haluza and Qeren-Rogem-Hazerim faults (Figure 33). The slips are lowering the south-eastern flank of the section compared to the north-western. The slip amount is relatively high; 89m and 205m on Agur-Haluza and 197m on Qeren-Rogem-Hazerim. This is the first regional evidence for reverse faulting in the study area.

A thickening trend to the NW is observed as part of a regional trend from the early Jurassic (Figure 31) from about 250m in the east, to about 375 m in the middle of the area. It is important to note that the upper boundary of this interval is defined by the regional base Cretaceous unconformity which has eroded deeper into the Late Jurassic formations towards the southeast (Druckman et al., 1994).

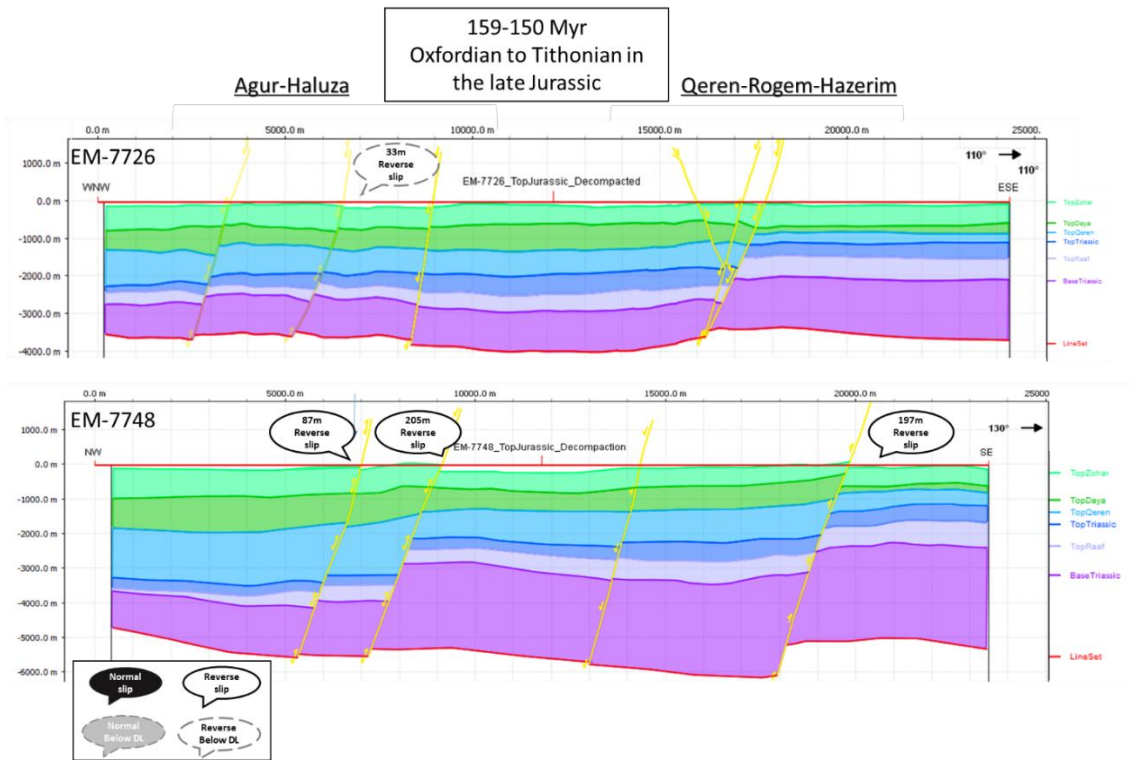


Figure 33: Restoration of late Jurassic in sections EM-7726 and EM-7748

4.3.8 Late Jurassic to Albian in lower cretaceous- after the deposition of Top Jurassic horizon (150-112 Myr):

A quiet tectonic period with no apparent slip on the Agur-Haluza or Qeren-Rogem-Hazerim faults (Figure 34). A gradual thickening towards the north-west is present, implying a NW depo-center.



Figure 34: Restoration of late Jurassic to lower Cretaceous in sections EM-7726 and EM-7748

4.3.9 Albian in lower Cretaceous to Cenomanian in Upper Cretaceous- after the deposition of LC3 horizon (112-99 Myr):

Reverse faulting of approximately 100m continues on the Agur-Haluza fault, in the northern (EM-7726) as well as the southern (EM-7748) segments (Figure 35).

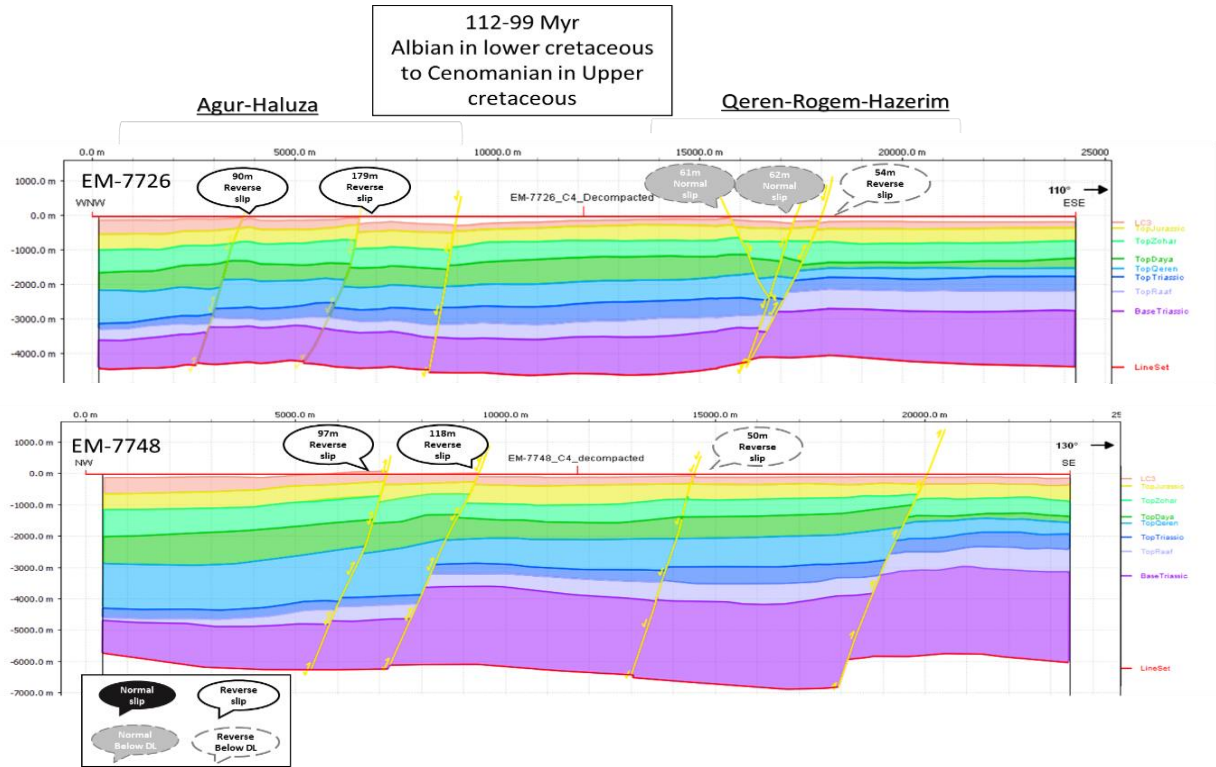


Figure 35: Restoration lower Cretaceous to upper Cretaceous in sections EM-7726 and EM-7748

4.3.10 Cenomanian to Coniacian in Upper Cretaceous- after the deposition of C4 horizon (99-89 Myr):

Reverse faulting continues on the Agur-Haluza fault in the northern (EM-7726) and southern (EM-7748) flanks (Figure 36). Reverse slip is also observed in the Qeren-Rogem-Hazerim fault on the southern flank, uplifting a part of Mt. Qeren, as seen in the DEM (Figure 4). Slight normal slips of 77m and 122m in section EM-7726.

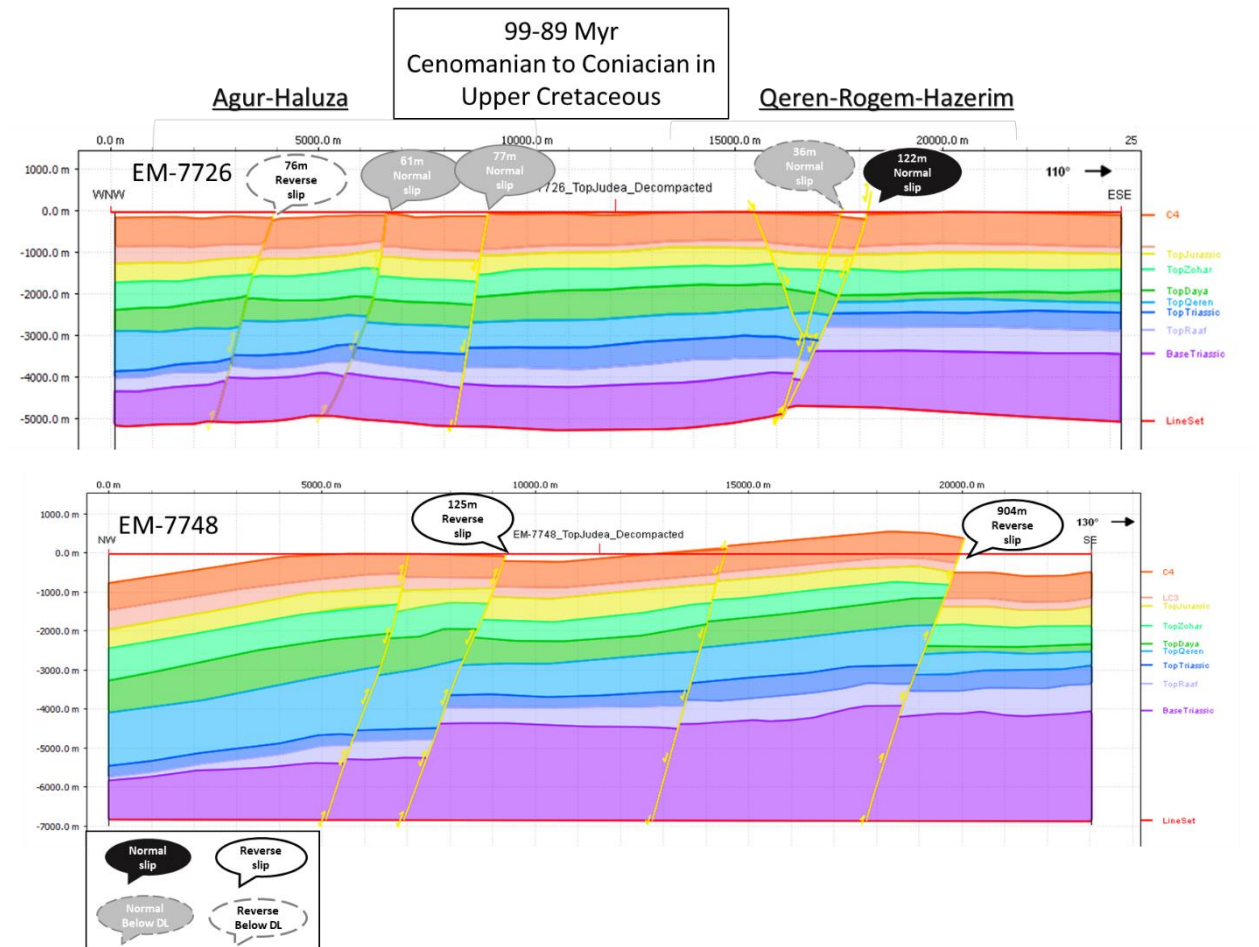


Figure 36: Restoration Cenomanian to Coniacian in upper Cretaceous in sections EM-7726 and EM-7748

4.4 Restoration synthesis

A synthesis of the restoration results on both seismic sections is presented in Figure 37 and Figure 38. Normal throws are presented as positive values and reverse throws are presented as negative values. A grey rectangle represents the detection limit below which throw amounts aren't reviewed, to account for the relatively low quality of the seismic data (please refer to section 4.1).

4.4.1 EM-7726

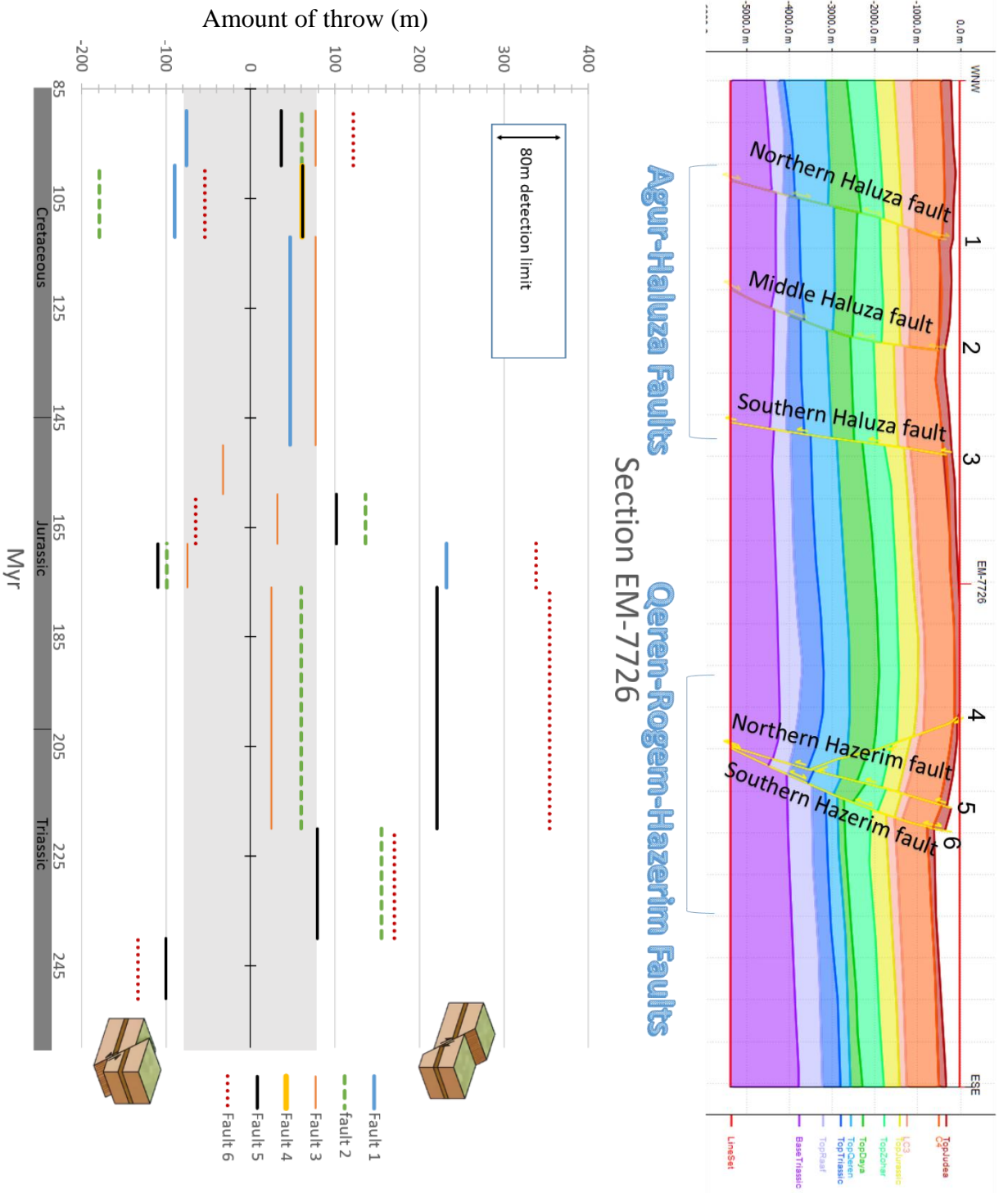


Figure 37: Restoration synthesis of section EM-7726. Y axis represents the amount of throw on a numbered fault. Negative values are reverse throws and positive are normal throws. A grey rectangle represents the detection limit of the amount of throw, -80m to 80m.

4.4.2 EM-7748

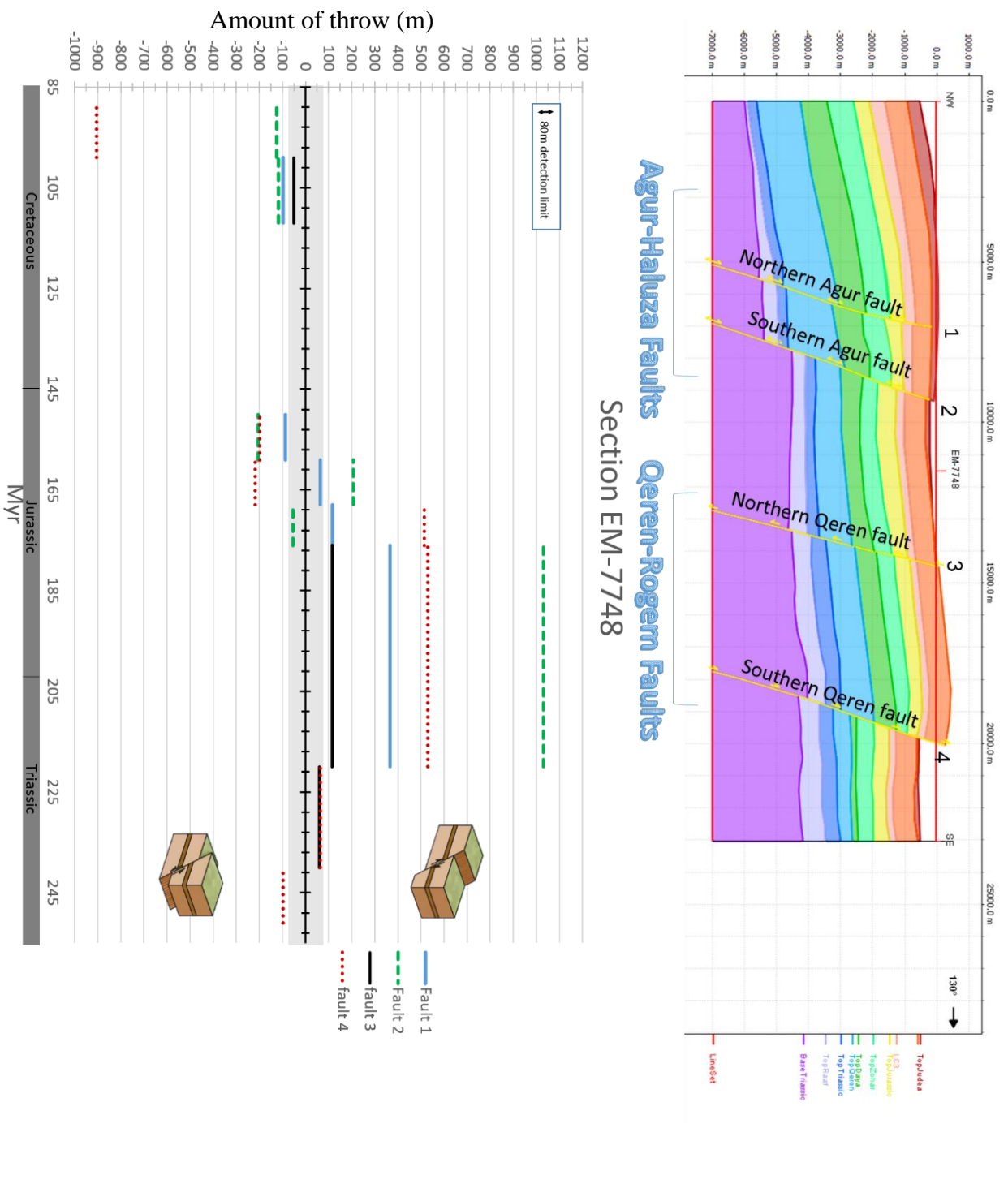


Figure 38: Restoration synthesis of section EM-7748. Y axis represents the amount of throw on a numbered fault. Negative values are reverse throws and positive are normal throws. A grey rectangle represents the detection limit of the amount of throw, -80m to 80m.

5 Discussion

The tectonic development of the northern Negev anticlines and other related structures was recounted by Freund et al. (1975). According to his concept, the present-day high angle reverse faults that underlie monoclines in places (Druckman et al., 1994) were normal faults in the early Mesozoic. This followed from thickness and facies analyses of the Late Triassic and Early Jurassic formations in the northern Negev. The model that was suggested for the structural development of the Syrian Arc monoclines was a 'structure inversion model' (Freund et al., 1975; Druckman et al., 1994). Since then, spatial variations were observed in the timing of the folding process on various monoclines (Freund and Zak, 1973), shifting from the post-Judea group in the Negev monoclines to Eocene in the Hebron and Ramallah cases. Others stated that there is no reason to believe that the folding in the Negev, the Sinai and the Judean hills was strictly contemporaneous (Begin, 1981). As the folding process is associated with the faulting underneath, one can assume spatial variations of the faulting process as well.

According to Freund's model (1975), the faults that underlie the monoclines of Israel were re-activated once. Begin's (1981) work on the Qeren area did not clarify whether Qeren is a reverse or a normal fault. As the present work showed, it intermittently flipped between both types of faulting. From the Qeren and Agur deformation history since the Mesozoic, several re-activations of the Qeren and Agur faults can be discerned. The amount of displacement (slip) in these structures varies on nearly all the stratigraphic markers throughout the entire sedimentary sequence, indicating that several deformation events took place.

5.1 Timing the shortening periods in the Qeren-Agur area

According to widely held concepts, the Triassic was a period of extension. It is contemporaneous with orogenic deformation and magmatism in Turkey and Iran (Freund et al., 1975). Whether starting in the Late Permian and continuing to middle Triassic (Granot, 2016) or starting in the early Triassic and continuing to the Jurassic (Garfunkel and Derin, 1984; Gardosh and Druckman, 2006), it is related to the rifting of the Neo-Tethys ocean (e.g Hardy et al., 2010; Stampfli, 2000; Freund et al., 1975; Gardosh and Druckman, 2006; Garfunkel, 2004). Normal faults trending NE–SW, detected onshore and offshore by geophysical studies and borehole data (Freund et al., 1975; Gardosh and

Druckman, 2006), are also clearly seen in the results of this study. Normal slip of over 100m on the Agur and Qeren structures was observed for the middle Triassic (220 Myr), and continued to the late Jurassic (150 Myr). This normal slip activity is seen both in the northern (EM-7726) and southern (EM-7748) segments of the Qeren and Agur structures (Figure 28). According to Freund et al. (1975), the structure in the northern Negev would have consisted of blocks tilted to the south-east and separated by normal faults dipping to the northwest. Each of the present anticlines would have been, according to this interpretation, a separate tilted block basin. This structure is clearly seen in the results as well (Figure 29, Figure 30, 37, 38).

According to Freund et al. (1975) and Stampfli (2000), from the Turonian (Upper Cretaceous) and onto the Cenozoic, a shortening regime was established in the region, in correlation with the Alpine orogeny in the north-east. As part of this shortening regime, there was a reactivation of the normal Triassic faults to a reverse slip (Garfunkel, 2004; Gardosh and Druckman, 2006), and formation of the S-shaped Syrian arc monoclines (Moustafa, 2013; Shahar, 1994). This is well established in the present study, although the timing of the reverse slip is somewhat earlier than what was known from surface studies inland (Eran, 1982) and Seismics from the Mediterranean: Sagy et al. (2015), Gardosh and Druckman (2006), and Gardosh et al. (2010).

According to the present results, reverse slip in the SE-NW direction was observed from the Cenomanian to Coniacian (99-89 Myr) (Upper Cretaceous) (Figure 26, 37, 38) but also earlier; the Albian to Cenomanian (112-99 Myr) in the Agur structure (Figure 35, 37, 38) and Oxfordian to Tithonian (late Jurassic) (150-159 Myr) in both Agur and Qeren structures (Figure 33, 37, 38). The reverse slip phase in the top Jurassic is observed only on the southern flank of both the Qeren and Agur structures (EM-7748), and is separated from the lower Cretaceous by 40 Myr (150-112 Myr) tectonically quiet period (Figure 34), along both structures.

Two scenarios can explain the results. According to the first scenario, the shortening related to the Syrian arc mechanism was activated early on the Agur and Qeren structures in the northern Negev. Due to limited outcrops of Paleozoic, Triassic and Jurassic rock units in Israel, data about the Early Mesozoic tectonic history of the southern Levant is rare. The evidence, however rare, support a regime of extension. In the Ramon structure NNE–SSW extension ruled during the Lower Jurassic (Hardy et al., 2010). In addition,

tectonic and magmatic activity of Liassic to Bajocian age (Early to middle Jurassic) was very prominent next to the southern Levant Basin (Gardosh and Druckman, 2006). There is also evidence for tectonic activity in the Tauride block which produced widespread clastics and unconformities at the base of the Jurassic section (Gutnic et al., 1979; Monod and Akay, 1984; Demirtasli, 1984) which may be interpreted as block faulting related to extension (Garfunkel, 1998). Also, the earliest period of Alpine related deformation is timed to the upper Cretaceous/early Tertiary (Ring, 1992; Butler et al., 2006). Combined with the lack of published evidence for reverse faulting in Israel earlier than Cretaceous, these make the first scenario less probable.

The second scenario involves slip partitioning (Bowman et al., 2010). According to this, the reverse slip detected is part of a complex oblique fault system in the subsurface, which is partially expressed in this area by a reverse slip. This can be supported by the fragmentation of Qeren and Agur structures, as observed from the 3D model (Figure 24). These reverse faults can then be viewed as a local expression of distributed deformation of the crust (Devès et al., 2011). When modelled as a strain weakening elasto-plastic material, the crust deforms in a combination of localized and distributed deformation. The geometric and kinematic evolution has import on the deformation style, causing some deformation to localize and some to remain distributed in process zones. In such zones, geometric complexities prevent localization (Devès et al., 2011). This produces small faults with various orientations. Such a scenario can explain the co-existence of early Jurassic reverse as well as normal throws (Figure 31). The variety of faulting directions modelled for distributed deformation is supported by highly variable focal mechanisms for small earthquakes, along the Dead Sea (Hofstetter et al., 2007), the Carmel fault (Hofstetter et al., 1996) and the entire Sinai sub-plate (Salamon et al., 2003), just to give local examples.

5.2 Evidence for strike-slip in the Cenomanian

A normal slip of 158m is detected in the Cenomanian to Coniacian in Upper Cretaceous (99-89 Myr) (Figure 36) in section EM-7726 at the south-eastern fault of the Qeren structure. In the same period 20km to the south (EM-7748), a reverse slip of 904m is observed. Although the quality of the seismic data is low, the slip is detected in the upper part of the seismic section, thus supporting the interpretation. From the 3D structure of

the northern part of Qeren, a flower structure comes to mind (Figure 39). This structure is strongly correlated to possible strike-slip activity (Woodcock and Fischer, 1986). Oblique motion along tectonic boundaries is commonly partitioned into slip on faults with pure senses of motion (dip- and strike-slip). Partitioning can be explained by the upward propagation of oblique slip from a fault or shear zone at depth. The strain field ahead of the propagating fault separates into zones of predominantly normal, reverse, and strike-slip faulting (Bowman et al., 2010). The faults of strike-slip duplexes may converge downwards and appear in vertical sections as flower structures (Woodcock and Fischer, 1986).

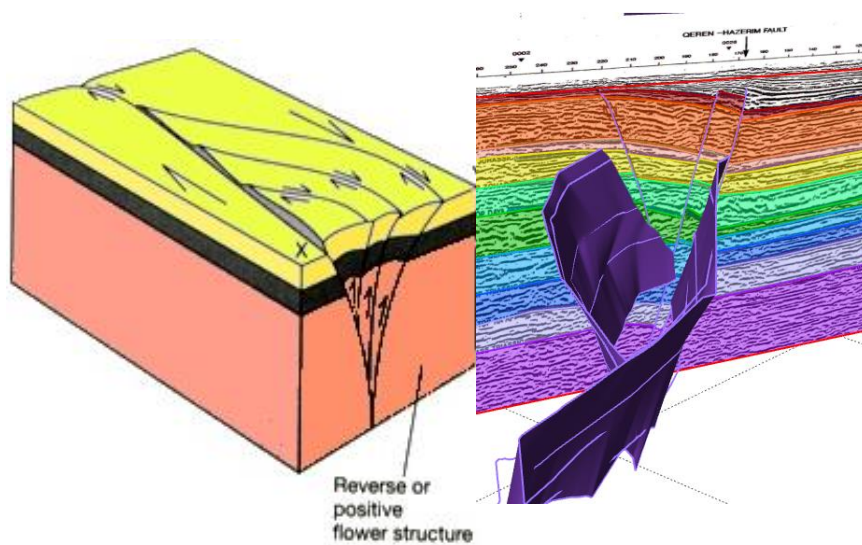


Figure 39: Left- Flower structure scheme (Woodcock and Fischer, 1986), Right- possible flower structure from 3D model

Evidence for strike slip activity is observed in the Ramon (Becker, 1994) and Hebron (Reches et al., 1981) anticlines. These are associated with reverse faults, and are showing a right-lateral displacement (Hardy et al., 2010). The development of both extensional and compressional (strike-slip and reverse) structures during the Late Cretaceous to Early Cenozoic period can be explained in the general context of the Late Cretaceous to Paleogene continuous inversion (Eyal and Reches, 1983; Eyal, 1996). The normal faults described may reflect local transitions of the principal stresses, causing changes in the stress regimes. Transitions between strike-slip and normal regimes (e.g. Angelier et al., 2000), and between strike-slip and reverse regimes (e.g. Homberg et al., 2002) have been previously described. Their occurrence implies that two of the principal stresses are similar in magnitude (Hardy et al., 2010).

5.3 Thickness variations in the middle Jurassic

An apparent reverse fault is detected in the middle to late Jurassic (168-159 Myr), in the south eastern faults of the Qeren structure, in both the northern (EM-7748) and southern (EM-7748) parts (Figure 32). Also, a sudden change in thickness of the Daya layer is observed, limited only to the southeastern flank in both seismic sections. The thickness of Daya layer was significantly reduced from 650m to 150m.

From looking at Daya horizon in the 3D maps, a topographic 'low' in the NE-SW direction stretches 75km along the Qeren-Agur area (Figure 40). The topographic 'low' seems to be bounded by a fault from the south, dipping to the north and forming steep slopes on the Daya horizon, forming a basin.

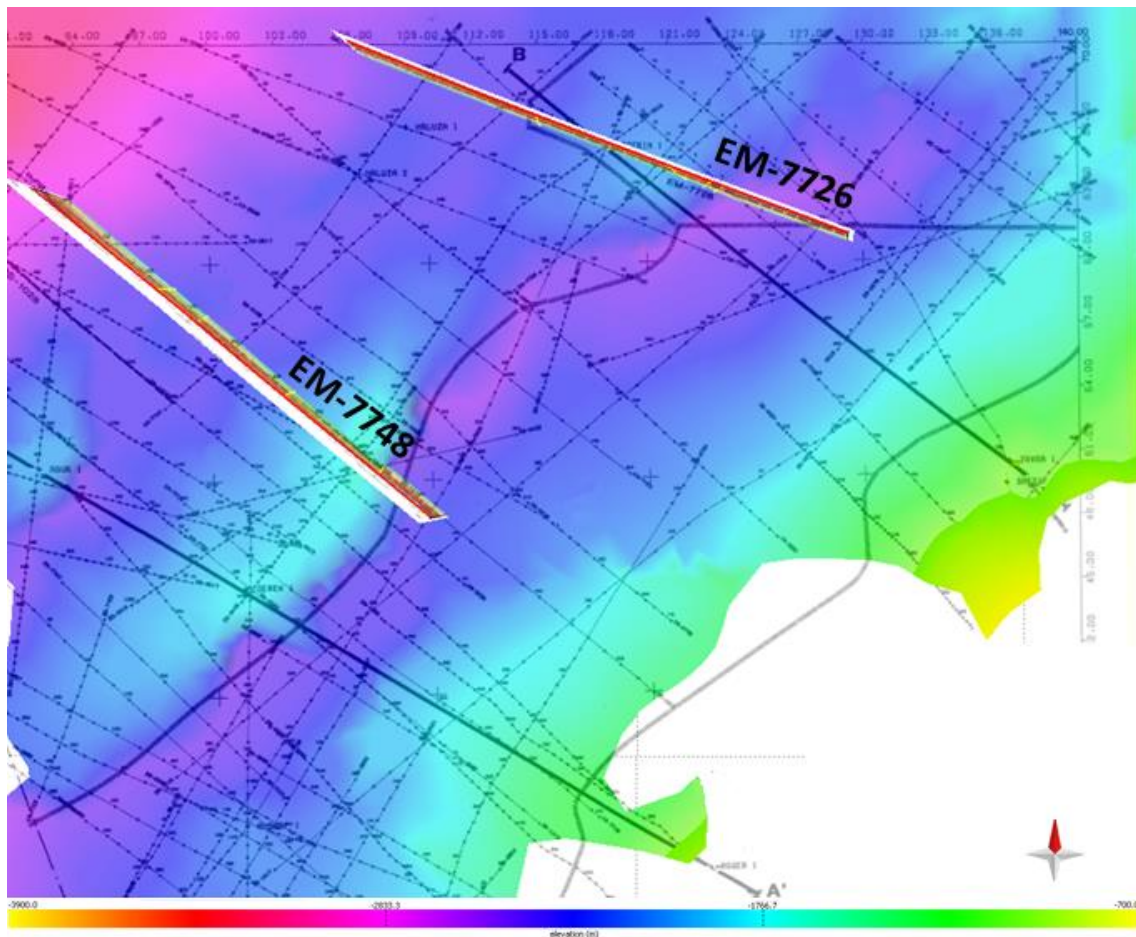


Figure 40: Top Daya horizon surface (168 Myr) along with locations of seismic sections and surveys, showing a topographic 'low' on the south-eastern side of both seismic sections. Survey locations are taken from Druckman (1994).

This basin is a part of the Qeren-Haluza depression referred to by Freund et al. (1975) as part of a regional extension, indicated by normal faults in the Jurassic period (Freund et

al., 1975). Another way to interpret the thickness variation of the south-eastern segment of both sections lies in the uplift of the area after normal faulting of the Qeren structure in the late Triassic to early Jurassic (176-168 Myr) (Figure 31). Thickness variations in the following period, middle to late Jurassic (168-159 Myr) (Figure 32) can then be explained by erosion, as there was less deposition on the uplifted part than on other segments, or was eroded afterwards.

From lithological observations, the Jurassic Daya layer as defined in this study (Top Qeren to Top Daya horizons) consists of the Inmar and Daya Formations. These consist of fluvial and fluvio-deltaic sandstones, siltstones and mudstones. Regression took place during the deposition of the Upper member of the Inmar Formation. This regression was the most extensive in the Jurassic in Israel. The section continues with the shallow marine shelf and tidal carbonates and sandstones of the Daya Formation, representing transgression (Goldberg and Friedman, 1974, Druckman et al., 1995). Non-marine sedimentary deposits can vary laterally and generate thickness variations during or after deposition. Both proposed scenarios can be envisioned to interpret the thickness variations observed, as they do not contradict one another.

5.4 From SE regional trend in the Triassic to NW in following periods

Thickness variations appear across the section, as observed from the unfolded seismic horizons. The thickness of the Triassic units (Figure 41) changes from 1410m NW to 4059m SE in section EM-7748 and from 1376m NW to 2631 SE in section EM-7726. This shows a clear trend of thickening towards the SE. In the Jurassic and Cretaceous horizons (Figure 36Figure 32) the thickness changes more gradually, showing a regional gradient towards the NW. The regional gradient has thus changed from the SE in the Triassic to the NW in later periods.

In the southern section (EM-7748), sediment thickness of the late Triassic to middle Jurassic (176-168 Myr) interval varies laterally from 1417m in NW to 400m in SE. In the northern section (EM-7726), sediment thickness varies laterally from 955m in NW to 338m in SE. In the period interval of middle to late Jurassic (168-159), section EM-7726 shows a lateral variation of 551m NW and 510m SE and section EN-7748 shows lateral variation of 930m NW to 700m SE, a change of ~200m.

The lateral variation in the late Triassic to middle Jurassic (176-168 Myr) was higher than in the following period. It can be thus inferred, that the change in regional gradient was

limited to a short period in the middle Jurassic, where a local syn-depositional syn-sedimentary event took place. In the Triassic, there was an uplift of southern Israel, as inferred from the thickness variation of Triassic strata (Hall et al., 2005). This change in regional trend in early Jurassic can be related to the rapid subsidence and accumulation of thick marine sequences in the Mediterranean (Freund, 1975; Druckman, 1995), following the thin Paleozoic platform sediments. The subsidence made room for accumulation of a few kilometers thick sedimentary wedge. As the direction of the sections is perpendicular (EM-7748) and sub-perpendicular (EM-7726) to the strike of the Agur and Qeren structures (parallel and sub-parallel to the dip), and the sections are restored in 2D, there is more than one option to the location of the depo-center in each of these periods.

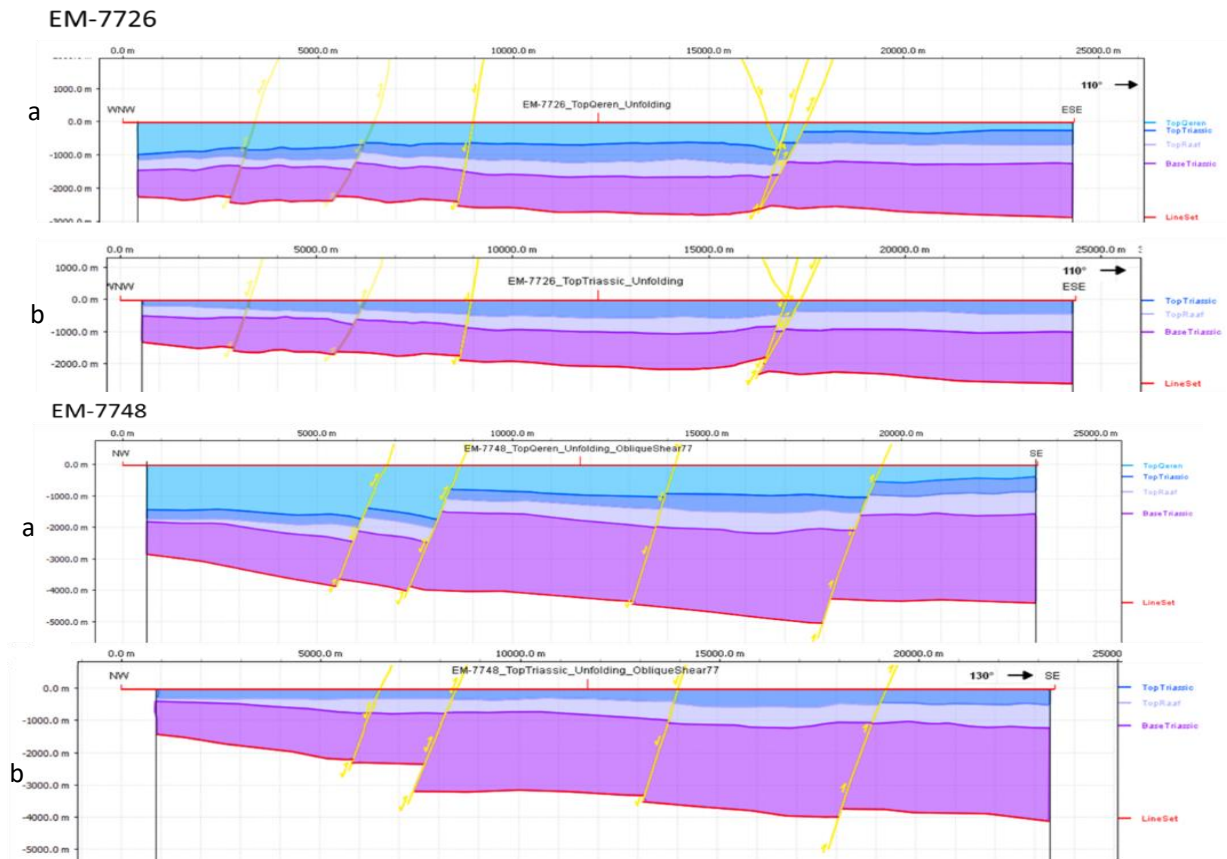


Figure 41: Thickness variations in both sections EM-7726 and EM-7748 after top Triassic (a) and after top Qeren horizon (b) deposition

The results show a reverse slip of ~100m on the northern as well as on the southern segments of the Qeren fault (Figure 28). The depth of the base Triassic horizon on the original seismic section is 4-5km in EM-7726 and 5-6km in EM-7748 (4-6 km) (Figure

25, Figure 26). This result should be taken with a grain of salt: The seismic data investigated, collected 1986, is of a relatively low quality. Moreover, there is no supporting evidence for an early Triassic reverse movement. To the contrary, plenty of evidence is available for rifting and normal faulting around the entire Levant (Guiraud, 1998; Garfunkel, 2004; Gardosh et al., 2010; Hardy et al., 2010). In view of these arguments, the reverse slip discerned is erroneous.

6 Conclusions

Sequential restoration carried out on two seismic sections cutting the Qeren and Agur fault structures in the northern Negev yielded useful insights on the structural evolution of both structures. The seismic sections cut the Qeren and Agur fault structures, EM-7726 from north and EM-7748 from south. Also, both sections are in the direction (EM-7748 NW-SE) or close to the direction (EM-7726 WNW-ESE) of the true dip, thus providing a suitable setting for evaluation of both structures' structural evolution. The process included removal of the effects of sediment compaction, isostatic adjustment, fault-related folding and fault-slip in order to restore each seismic section to the time of deposition of ten horizons, from base Triassic to Coniacian in upper Cretaceous.

Relating to the research objectives, temporal structural evolution of the Agur and Qeren structures was tested against known constrained tectonic regimes. Normal slip is resolved both in the northern and southern segments of the Agur and Qeren structures, in what is correlated to the Neo-Tethyan rifting in the early Mesozoic (Figure 29,30). Reverse slip is resolved both in the northern and southern segments of the Agur and Qeren structures, in what is correlated to the Alpine-related shortening during the Cretaceous (Figure 35, Figure 36). Nonetheless, there were clear differences between the northern and southern flanks of the Agur and Qeren, and between the Qeren and Agur structures as a whole.

Hidden tectonic phases of deformation were clearly observed in both structures. Reverse slip was detected in the Agur structure (north and south) during early to middle Jurassic (Figure 31). Reverse slip was also detected on the southern flanks of Agur and Qeren during the late Jurassic (Figure 33). This can be the earliest evidence of shortening in our region. These faults may also represent a local, rather than a regional, stress field. The use of structural restoration in an area with tectonic constraints proved to be effective in

shedding light on various phases of deformation on complex faults. The results highlight the complexity of tectonic inversion and the early onset of shortening in the Levant (Figures 37,38). Nonetheless, the low quality of seismic data used for restoration can highly influence the results. Taking this into consideration, this technique can now be used as a validation technique in poorly constrained geological structures elsewhere.

7 **References**

- Baur, F., Di Benedetto, M., Fuchs, T., Lampe, C., and Sciamanna, S., 2009, Integrating structural geology and petroleum systems modeling - A pilot project from Bolivia's fold and thrust belt: *Marine and Petroleum Geology*, v. 26, p. 573–579, doi: 10.1016/j.marpetgeo.2009.01.004.
- Beauchamp, W., Allmendinger, W., Barazangi, M., Demnati, A., Alji, E., and Dahmani, M., 1999, Inversion tectonics and the evolution of the High Atlas Mountains, Morocco, based on a geological-geophysical transect: *Tectonics*, v. 18, p. 163–184.
- Begin, B., 1981, The nature and age of the Qeren fault.:
- Ben-Avraham, Z., 1989, Multiple opening and closing of the Eastern Mediterranean and South China Basins: *Tectonics*, v. 8, p. 351–362, doi: 10.1029/TC008i002p00351.
- Bosworth, W., Guiraud, R., and Kessler, L.G., 1999, Late Cretaceous (ca. 84 Ma) compressive deformation of the stable platform of northeast Africa (Egypt): Far-field stress effects of the “Santonian event” and origin of the Syrian arc deformation belt: *Geology*, v. 27, p. 633–636, doi: 10.1130/0091-7613(1999)027<0633:LCCMCD>2.3.CO;2.
- Bowman, D., King, G., and Tapponnier, P., 2010, Partitioning by Elastoplastic Slip Propagation of Oblique Depth: *Advancement Of Science*, v. 300, p. 1121–1123, doi: 10.1126/science.1082180.
- Brede, R., Hauptmann, M., and Herbig, H.G., 1992, Plate tectonics and intracratonic mountain ranges in Morocco - The mesozoic-cenozoic development of the Central High Atlas and the Middle Atlas: *Geologische Rundschau*, v. 81, p. 127–141, doi: 10.1007/BF01764544.
- Bruner, I., 1991, Investigation of the subsurface in the northern negev using seismic reflection techniques: TAU.
- Bulnes, M., and McClay, K., 1999, Benefits and limitations of different 2D algorithms used in cross-section restoration of inverted extensional faults: Application to physical experiments: *Tectonophysics*, v. 312, p. 175–189, doi: 10.1016/S0040-1951(99)00161-4.
- Butler, R.W.H., Tavarnelli, E., and Grasso, M., 2006, Structural inheritance in mountain belts: An Alpine-Apennine perspective: *Journal of Structural Geology*, v. 28, p. 1893–1908, doi: 10.1016/j.jsg.2006.09.006.

- Calvo, R., Knafo, R., and Rosenzweig, R., 2014, A comparative study for potential CO₂ storage units in the subsurface Paleozoic-Mesozoic section in Southern Israel: Petrological and petrophysical dataset: v. 16.
- Cukur, D., Horozal, S., Lee, G.H., Kim, D.C., Han, H.C., and Kang, M.H., 2011, Structural evolution of the northern East China Sea Shelf Basin interpreted from cross-section restoration: *Marine Geophysical Research*, v. 32, p. 363–381, doi: 10.1007/s11001-011-9114-4.
- Dahlstrom, C.D.A., 1969, Balanced cross sections: *Canadian Journal of Earth Sciences*, v. 6, p. 743–757, doi: 10.1139/e69-069.
- Delaunay, B., 1934, Sur la sphere vide: *Bull. Acad. Science USSR VII*, p. 793–800.
- Devès, M., King, G.C.P., Klinger, Y., and Agnon, A., 2011, Localised and distributed deformation in the lithosphere: Modelling the Dead Sea region in 3 dimensions: *Earth and Planetary Science Letters*, v. 308, p. 172–184, doi: 10.1016/j.epsl.2011.05.044.
- Druckman, Y., Gill, D., Fleischer, L., Gelbermann, E., and Wolff, O., 1995, Subsurface geology and structural evolution of the northwestern Negev, southern Israel: *Israel Journal of Earth Sciences*, v. 44, p. 115–135.
- Druckman, Y., Gill, D., Fleischer, L., Gelbermann, E., and Wolff, O., 1994, Subsurface Geology and Structural Evolution of the northwestern negev, southern israel.:
- Durand-Riard, P., Guiofski, C., Caumon, G., and Titeux, M.O., 2013, Handling natural complexity in three-dimensional geomechanical restoration, with application to the recent evolution of the outer fold and thrust belt, deep-water Niger Delta: *AAPG Bulletin*, v. 97, p. 87–102, doi: 10.1306/06121211136.
- Durand-Riard, P., Shaw, J.H., Plesch, A., and Lufadeju, G., 2013, Enabling 3D geomechanical restoration of strike- and oblique-slip faults using geological constraints, with applications to the deep-water Niger Delta: *Journal of Structural Geology*, v. 48, p. 33–44, doi: 10.1016/j.jsg.2012.12.009.
- Ebinger, C.J., Bechtel, T.D., Forsyth, D.W., and Bowin, C.O., 1989, Effective elastic plate thickness beneath the East African and Afar plateaus and dynamic compensation of the uplifts: *Journal of Geophysical Research: Solid Earth*, v. 94, p. 2883–2901.
- Egan, S.S., Buddin, T.S., Kane, S., and Williams, G.D., 1997, Three-dimensional

- modelling and visualisation in structural geology: New techniques for the restoration and balancing of volumes: The 1996 Geoscience Information Group Conference On Geological Visualisation, *Electron Geology*, p. 67–82, <http://www.electronicjournals.co.uk/eg/pdf/EG1-7.pdf>.
- Eyal, Y., 1996, Stress field fluctuations along the Dead Sea rift since the middle Miocene: *Tectonics*, v. 15, p. 157, doi: 10.1029/95TC02619.
- Eyal, Y., and Reches, Z., 1983, Tectonic analysis of the dead sea rift region since the late-Cretaceous based on mesostructures: v. 2, p. 167–185.
- Fleischer, L., Gelbermann, E., and Wolff, O., 1993, A geological–geophysical reassessment of the Judea Group (Yarkon-Taninim Aquifer):, doi: 244/147/92.
- Freund, R., 1979, Progressive strain in beds of monoclinial flexures: *Geology*, v. 7, p. 269–271, doi: 10.1130/0091-7613(1979)7<269:PSIBOM>2.0.CO;2.
- Freund, R., 1970, The geometry of faulting in the Galilee: *Israel Journal of Earth Sciences*, v. 19, p. 117–140.
- Freund, R., Goldberg, M., Weissbrod, T., Druckman, Y., and Derin, B., 1975a, The Triassic-Jurassic structure of Israel and its relation to the origin of the eastern Mediterranean: *Geological Survey of Israel Bulletin*,.
- Freund, R., Goldberg, M., Weissbrod, T., Druckman, Y., and Derin, B., 1975b, The Triassic-Jurassic Structure of Israel and its Relation to the Origin of the Eastern Mediterranean.:
- Freund, R., and Zak, I., 1973, Shifting of folding and faulting along geological structures: “Teva ve’aretz” Hebrew, v. 6, p. 264–270.
- Gardosh, M.A., Garfunkel, Z., Druckman, Y., and Buchbinder, B., 2010, Tethyan rifting in the Levant Region and its role in Early Mesozoic crustal evolution: *Geological Society of London Special Publications*, v. 341, p. 9–36, doi: 10.1144/SP341.2.
- Garfunkel, Z., 1998, Constrains on the origin and history of the Eastern Mediterranean basin: *Tectonophysics*, v. 298, p. 5–35, doi: 10.1016/S0040-1951(98)00176-0.
- Garfunkel, Z., 2004, Origin of the Eastern Mediterranean basin: A reevaluation: *Tectonophysics*, v. 391, p. 11–34, doi: 10.1016/j.tecto.2004.07.006.
- Garfunkel, Z., and Derin, B., 1984, Permian-early Mesozoic tectonism and continental margin formation in Israel and its implications for the history of the Eastern Mediterranean: *Geological Society, London, Special Publications*, v. 17, p. 187–201,

- doi: 10.1144/GSL.SP.1984.017.01.12.
- Gelbermann, E., 1995, Revised seismic structural and isopach maps, central and southern Israel:, doi: 201/22/88-94.
- Gelbermann, E., and Gossovicz, Y., 1990, Seismic structural and isopach maps, central, southern, and offshore Israel:, doi: 201/89-90.
- Granot, R., 2016, Palaeozoic-aged oceanic crust preserved beneath the eastern Mediterranean: *Nature Geoscience*, v. in press, p. 1–6, doi: 10.1038/ngeo2784.
- Griffiths, P., Jones, S., Salter, N., Schaefer, F., Osfield, R., and Reiser, H., 2002, A new technique for 3-D flexural-slip restoration: *Journal of Structural Geology*, v. 24, p. 773–782, doi: 10.1016/S0191-8141(01)00124-9.
- Guiraud, R., 1998, Mesozoic rifting and basin inversion along the northern African Tethyan margin: an overview: *Geological Society, London, Special Publications*, v. 132, p. 217–229, doi: 10.1144/GSL.SP.1998.132.01.13.
- Guiraud, R., and Bosworth, W., 1997, Senonian basin inversion and rejuvenation of rifting in Africa and Arabia: Synthesis and implications to plate-scale tectonics: *Tectonophysics*, v. 282, p. 39–82, doi: 10.1016/S0040-1951(97)00212-6.
- Guiraud, R., Bosworth, W., Thierry, J., and Delplanque, a., 2005, Phanerozoic geological evolution of Northern and Central Africa: An overview: *Journal of African Earth Sciences*, v. 43, p. 83–143, doi: 10.1016/j.jafrearsci.2005.07.017.
- Gvirtzman, Z., and Steinberg, J., 2012, Inland jump of the Arabian northwest plate boundary from the Levant continental margin to the Dead Sea Transform: *Tectonics*, v. 31, p. 1–13, doi: 10.1029/2011TC002994.
- Hall, J., Krasheninnikov, V., Hirsch, F., Benjamini, C., Flexer, A., and Hall, J., 2005, *Geological Framework of the Levant: v. II*, 836 p., doi: 10.1016/j.gloenvcha.2011.08.005.
- Haneberg, W.C., 1988, Some possible effects of consolidation on growth fault geometry: *Tectonophysics*, v. 148, p. 309–316, doi: 10.1016/0040-1951(88)90137-0.
- Hardy, C., Homberg, C., Eyal, Y., Barrier, É., and Müller, C., 2010, Tectonic evolution of the southern Levant margin since Mesozoic: *Tectonophysics*, v. 494, p. 211–225, doi: 10.1016/j.tecto.2010.09.007.
- Hofstetter, A., Van Eck, T., and Shapira, A., 1996, Seismic activity along fault branches of the Dead Sea-Jordan transform system: The Carmel-Tirtza fault system:

- Tectonophysics, v. 267, p. 317–330, doi: 10.1016/S0040-1951(96)00108-4.
- Hofstetter, R., Klinger, Y., Amrat, A.Q., Rivera, L., and Dorbath, L., 2007, Stress tensor and focal mechanisms along the Dead Sea fault and related structural elements based on seismological data: Tectonophysics, v. 429, p. 165–181, doi: 10.1016/j.tecto.2006.03.010.
- Jolivet, L., and Faccenna, C., 2000, Mediterranean extension and the Africa-Eurasia collision: Tectonics, v. 19, p. 1095–1106, doi: 10.1029/2000TC900018.
- Kempler, D., and Garfunkel, Z., 1994, Structures and kinematics in the northeastern Mediterranean: A study of an irregular plate boundary: Tectonophysics, v. 234, p. 19–32, doi: 10.1016/0040-1951(94)90202-X.
- Krenkel, E., 1924, Der Syrische Bogen: Zentralblatt Mineralogie, v. 9, p. 9, 274–281 and 10, 301–313.
- Lee, D.T., and Schachter, B.J., 1980, Two algorithms for constructing a Delaunay triangulation: International Journal of Computer & Information Sciences, v. 9, p. 219–242, doi: 10.1007/BF00977785.
- Lowell, J.D., 1995, Mechanics of basin inversion from worldwide examples: Geological Society, London, Special Publications, v. 88, p. 39–57, doi: 10.1144/GSL.SP.1995.088.01.04.
- Picard, L.E.O., 1943, Structure and evolution of Palestine with comparative notes on neighbouring countries: The geological department, Hebrew University.
- Le Pichon, X., 1982, Land-locked oceanic basins and continental collision: the Eastern Mediterranean as a case example: Mountain building processes, p. 201–211.
- Reches, Z., Hoexter, D.F., and Hirsch, F., 1981, the Structure of a Monocline in the Syrian Arc System, Middle East-Surface and Subsurface Analysis: Journal of Petroleum Geology, v. 3, p. 413–426, doi: 10.1111/j.1747-5457.1981.tb00939.x.
- Ring, U., 1992, The Alpine geodynamic evolution of Penninic nappes in the eastern Central Alps: geothermobarometric and kinematic data: Journal of Metamorphic Geology, v. 10, p. 33–53, doi: 10.1111/j.1525-1314.1992.tb00070.x.
- Ron, H., and Eyal, Y., 1985, Intraplate deformation by block rotation and mesostructures along the dead sea transform, northern Israel: Tectonics, v. 4, p. 85–105.
- Rouby, D., Raillard, S., Guillocheau, F., Bouroulllec, R., and Nalpas, T., 2002, Kinematics of a growth fault/raft system on the West African margin using 3-D restoration:

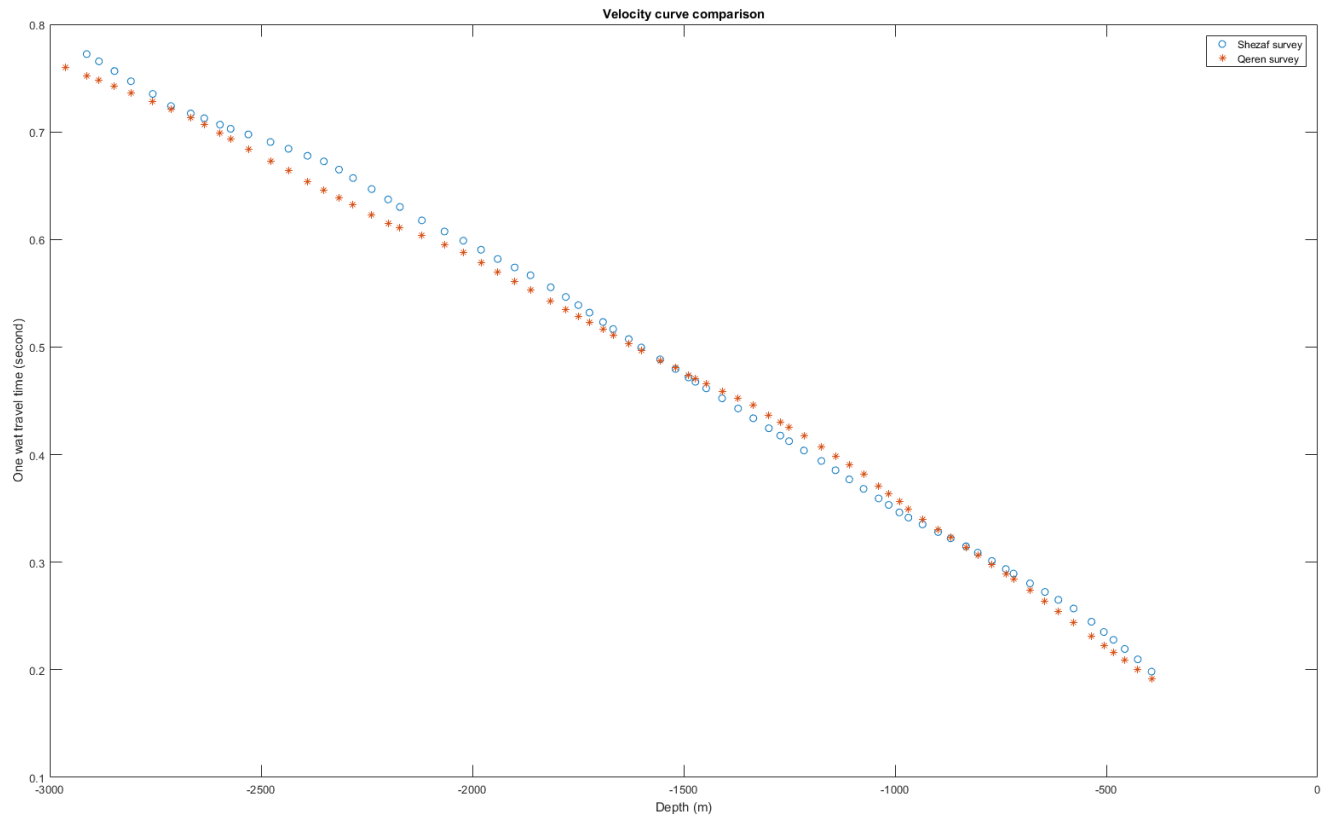
- Journal of Structural Geology, v. 24, p. 783–796, doi: 10.1016/S0191-8141(01)00108-0.
- Salamon, A., Hofstetter, A., Garfunkel, Z., and Ron, H., 2003, Seismotectonics of the Sinai subplate-the eastern Mediterranean region: *Geophysical Journal International*, v. 155, p. 149–173, <http://adsabs.harvard.edu/full/2003GeoJI.155..149S>.
- Santi, M.R. De, Luiz, J., Campos, E., Martha, L.F., and Brazil, T.P., 2002, 3D Geological Restoration using a Finite Element Approach 1 Introduction 2 The Restoration Process 3D Geological Restoration using a FE Approach: , p. 1–12.
- Slater, J.G., and Christie, P.A.F., 1980, Continental stretching: An explanation of the Post-Mid-Cretaceous subsidence of the central North Sea Basin: *Journal of Geophysical Research: Solid Earth*, v. 85, p. 3711–3739, doi: 10.1029/JB085iB07p03711.
- Sengor, A.M.C., Yilmaz, Y., and Sungurlu, O., 1984, Tectonics of the Mediterranean Cimmerides: nature and evolution of the western termination of Palaeo-Tethys: Geological Society, London, Special Publications, v. 17, p. 77–112, doi: 10.1144/GSL.SP.1984.017.01.04.
- Shahar, J., 1994, The Syrian arc system: an overview: *Palaeogeography, Palaeoclimatology, Palaeoecology*, v. 112, p. 125–142, doi: 10.1016/0031-0182(94)90137-6.
- Shamir, G., and Eyal, Y., 1995, Elastic modeling of fault-driven monoclinical fold patterns: *Tectonophysics*, v. 245, p. 13–24, doi: 10.1016/0040-1951(94)00250-D.
- Stampfli, G.M., 2000, Tethyan oceans: Geological society, london, special publications, v. 173, p. 1–23.
- Stampfli, G.M., Hochard, C., Vérard, C., Wilhem, C., and vonRaumer, J., 2013, The formation of Pangea: *Tectonophysics*, v. 593, p. 1–19, doi: 10.1016/j.tecto.2013.02.037.
- Steinberg, J., Gvirtzman, Z., Gvirtzman, H., and Ben-Gai, Y., 2008, Late Tertiary faulting along the coastal plain of Israel: *Tectonics*, v. 27, p. 1–22, doi: 10.1029/2007TC002151.
- Tanner, D.C., Behrmann, J.H., and Dresmann, H., 2003, Three-dimensional retro-deformation of the Lechtal Nappe, Northern Calcareous Alps: *Journal of Structural Geology*, v. 25, p. 737–748, doi: 10.1016/S0191-8141(02)00057-3.

- Tobergte, D.R., and Curtis, S., 2006, 3-D Structural Geology, *in* 3-D Structural Geology, v. 53, p. 1689–1699, doi: 10.1017/CBO9781107415324.004.
- Turcotte, D., and Schubert, G., 2014, Geodynamics:
- Walley, C.D., 1998, Some outstanding issues in the geology of Lebanon and their importance in the tectonic evolution of the Levantine region: *Tectonophysics*, v. 298, p. 37–62, doi: 10.1016/S0040-1951(98)00177-2.
- Watts, A.B., 2001, *Isostasy and Flexure of the Lithosphere*: Cambridge University Press.
- Williams, G.D., Powell, C.M., and Cooper, M.A., 1989, Geometry and kinematics of inversion tectonics: *Geological Society, London, Special Publications*, v. 44, p. 3–15, doi: 10.1144/GSL.SP.1989.044.01.02.
- Wilson, J.T., 1963, A possible origin of the Hawaiian Islands: *Canadian Journal of Physics*, v. 41, p. 863–870, doi: 10.1139/p63-094.
- Ziegler, P.A., 1990, Collision related intra-plate compression deformations in Western and Central Europe: *Journal of Geodynamics*, v. 11, p. 357–388, doi: 10.1016/0264-3707(90)90017-O.
- Ziesch, J., Tanner, D.C., and Krawczyk, C.M., 2014, Strain Associated with the Fault-Parallel Flow Algorithm During Kinematic Fault Displacement: *Mathematical Geosciences*, v. 46, p. 59–73, doi: 10.1007/s11004-013-9464-3.
- Zilberman, E., 1980, A geo-engineering survey for construction in the Shivta-Qeziioth area.:

8 Appendix

8.1 *Depth conversion*

A comparison was made between both velocity check-shot surveys, to validate the use of both in the depth conversion of the study area. To do so, Shezaf time values were subtracted from Qeren time values. The maximum difference was 0.027 s, an error of 5%.



8.2 Compaction calculation

טבלה 4: סיכום תוצאות האנליזות הפטרופיזיות (נקבוביות וחדירות) במאגר המידע לפי חבורות ותצורות גיאולוגיות.

Group	Total analyses (and %), by groups	Formation	Total analyses (and %), by formation	Porosity [%]					Permeability [md, as log K]				
				Median	Average	SD	Kurtosis	Skweness	Median	Average	SD	Kurtosis	Skweness
Judea Gr.	91 (2%)	Avnon	12 (13%)	2.15	2.26	0.71	-0.55	0.69	-1.16	-0.72	0.85	1.86	1.51
		Dalyya	12 (13%)	15.10	17.96	11.71	-1.48	0.36	1.54	1.12	0.93	0.23	-1.29
		Derorim	12 (13%)	0.50	2.39	4.05	6.21	2.50	-0.82	-0.57	0.71	6.10	2.45
		Hevyon	20 (21%)	20.60	19.63	4.94	0.10	-0.90	1.04	1.30	0.98	-1.15	0.43
		Negba	10 (10%)	0.70	1.14	1.05	2.92	1.77	-1.78	-1.72	0.41	4.84	2.08
		Yagur	11 (12%)	9.10	12.23	10.39	0.80	1.32	0.18	0.40	1.27	-0.53	-0.06
		Yakhim	11 (12%)	20.70	21.12	10.24	-0.86	-0.25	2.11	1.91	0.98	1.04	-1.23
		Zaft	3 (3%)	16.50	17.10	1.37		1.40	0.23	0.20	0.15		-0.79
Kurnub Gr.	203 (5%)	Heletz	111 (54%)	11.20	13.56	9.33	-0.53	0.60	-0.07	0.32	1.66	-1.23	0.23
		Kurnub?	4 (1%)	11.15	11.28	4.49	-5.11	0.05	-0.98	-0.99	0.25	-4.24	-0.12
		Telamim	22 (10%)	7.49	8.96	5.09	0.61	0.98	0.62	0.28	1.40	-0.91	-0.35
		Uza	2 (0%)	18.45	18.45	3.85			2.49	2.49	0.39		
		Yaquim	20 (9%)	0.87	1.10	0.91	-1.24	0.54	-0.88	-0.71	1.20	-0.77	0.66
		Zeweira	44 (21%)	12.20	12.98	8.17	-0.92	0.26	0.65	0.64	1.68	-0.84	0.22
Arad Gr.	2385 (69%)	Nir-Am	7 (0%)	3.07	5.06	4.24	-0.56	1.11	-1.22	-0.87	0.44	-1.11	0.89
		Haluza	50 (2%)	1.90	2.71	2.98	12.08	3.39	-0.92	-0.88	0.48	7.68	2.22
		Beer Sheva	45 (19%)	3.00	4.13	2.58	-0.06	1.01	-1.52	-1.22	0.81	0.80	1.13
		Kidod	67 (2%)	7.14	6.38	2.97	-0.14	-0.12	-2.00	-1.58	0.77	1.92	1.77
		Zohar	1119 (46%)	7.00	7.91	5.63	1.53	1.04	-1.40	-1.21	0.85	4.74	1.64
		Sherif	436 (18%)	4.65	6.66	6.23	0.36	1.14	-1.52	-0.87	1.42	-0.03	1.08
		Dava	244 (10%)	5.35	7.42	5.97	-0.49	0.79	-0.59	-0.03	1.77	-1.35	0.41
		Karmon	19 (0%)	13.80	12.03	4.93	-0.71	-0.64	0.02	-0.10	0.78	-1.34	0.03
		Shederot	36 (1%)	10.41	10.12	5.34	-1.23	-0.13	-0.51	-0.70	0.57	0.63	-0.57
		Upper Inmar	124 (5%)	10.65	11.51	7.51	-0.33	0.61	1.00	0.80	1.56	-0.93	-0.30
		Qeren	57 (2%)	3.88	5.74	4.84	-0.76	0.81	-0.44	-0.33	1.18	-1.02	0.19
		Lower Inmar	126 (5%)	11.00	12.38	7.15	-1.04	0.29	1.79	1.49	1.57	0.44	-1.05
		Ardon	55 (2%)	4.21	5.10	3.64	1.99	1.55	-2.00	-1.38	0.82	1.20	1.34
		Ramon Gr.	225 (6%)	Saharonim	28 (12%)	2.15	3.43	2.85	3.66	1.84	-1.11	-0.82	0.95
Gevanim	108 (48%)			12.66	13.23	4.86	-0.17	-0.01	0.09	-0.10	0.96	-0.96	-0.38
Raaf	89 (39%)			3.56	4.63	3.16	-0.33	0.84	-0.92	-0.62	1.10	1.89	1.29
Negev Gr.	476 (13%)	Zafir	29 (6%)	12.94	11.81	6.16	-1.21	-0.12	-1.00	-1.07	0.81	1.42	1.15
		Yamin	7 (1%)	2.50	2.69	0.98	4.04	1.86	-1.52	-1.49	0.20	-1.99	0.36
		Shezaf	28 (5%)	14.90	13.42	3.97	0.24	-1.06	1.83	1.56	0.75	0.65	-1.40
		Arqov	18 (3%)	5.10	7.42	6.35	-1.20	0.62	-0.59	-0.15	1.23	-1.35	0.59
		Saad	394 (82%)	4.49	6.12	4.58	-0.45	0.81	-0.37	-0.08	1.40	-1.09	0.43
		Zenifim	61 (100%)	2.20	3.10	2.58	3.59	2.02	-1.00	-0.96	0.75	0.28	0.61

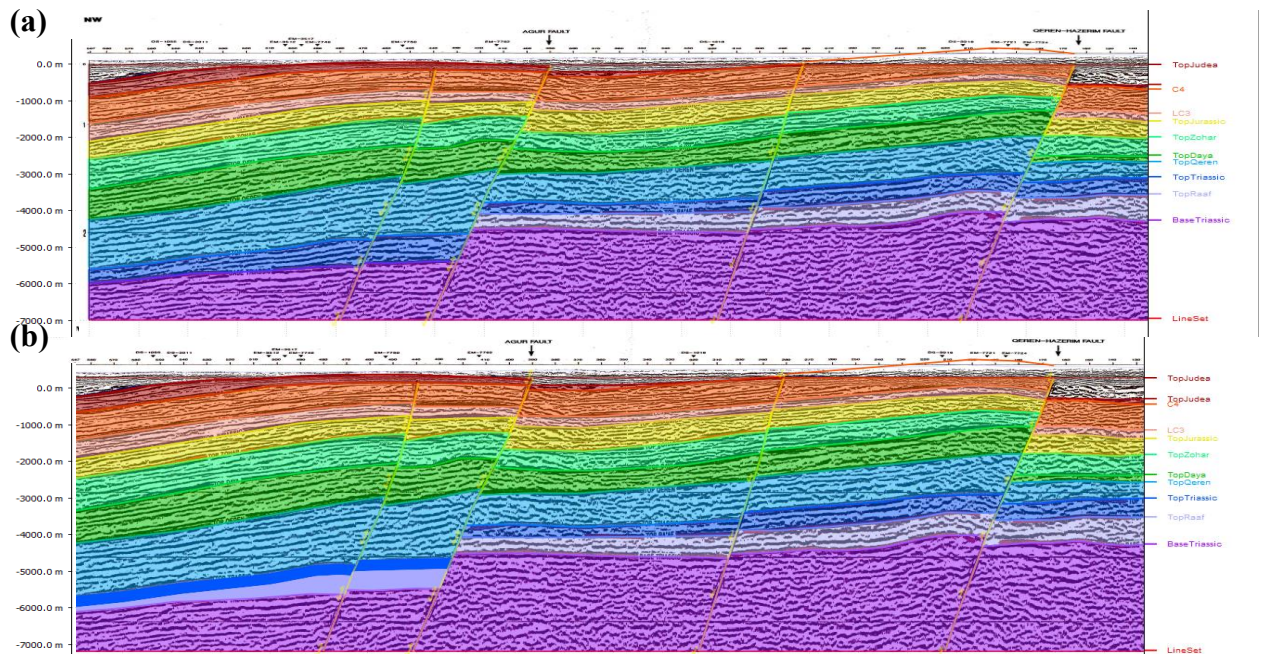
Group	Formation	Median	average	SD	thickness(m)	Horizons from structural maps	Horizons from Vertical sections	Regular Average of % porosity of seismic horizons in vertical sections	Geometric mean of % porosity of seismic horizons in vertical sections	נומרו לר כי להכניס לנוב	נומרו לר של החתכים הרי הלבנים לנב
Judea Group	Avnon	2.15	2.26	0.71		Top Judea	Top Judea				
	Dalyya	15.1	17.96	11.7				7.53666667	0.075366667	4.594845265	0.045948
	Derorim	0.5	2.39	4.05							
	Hevyon	20.6	19.63	4.94							
	Negba	0.7	1.14	1.05							
	Yagur	9.1	12.23	10.39				13.72285714	0.137228571	10.60826465	0.106083
	Yakhini	20.7	21.12	10.24							
	Zaft	16.5	17.1	1.37							
Kurnub Group	Heletz	11.2	13.56	9.33		Top LC3					
	Kurnub?	11.15	11.28	4.49							
	Telamim	7.49	8.96	5.09							
	Uza	18.45	18.45	3.85 60-80							
	Yaquim	0.87	1.1	0.91				9.31	0.0931	6.537691976	0.065377
	Zeweira	12.2	12.98	8.17 90-240		Base Cretaceous					
Arad Group	Nir-Am	3.07	5.06	4.24							
	Haluza	1.9	2.71	2.98 40-300							
	Beer Sheva	3	4.13	2.58 100-230				4.40666667	0.044066667	4.148712505	0.041487
	Kidod	7.14	6.38	2.97 0-120		Top Zohar					
	Zohar	7	7.91	5.63 108-182							
	Sherif	4.65	6.66	6.23 238-338		Top Dava		7.285	0.07285	7.258140258	0.072581
	Dava	5.35	7.42	5.97 38-308							
	Karmon	13.8	12.03	4.93							
	Shederot	10.41	10.12	5.34							
	Upper Inmar	10.65	11.51	7.51		Top Qeren		10.27	0.1027	10.09790643	0.100979
	Qeren	3.88	5.74	4.84							
	Lower Inmar	11	12.38	7.15 181-576							
	Ardon	4.21	5.1	3.64 12-541		Top Ramon		7.74	0.0774	7.129639502	0.071296
	Ramon Group	Saharonim	2.15	3.43	2.85 172-290						
Gevanim		12.66	13.23	4.86 55-287		Top Raaf		8.33	0.0833	6.736386272	0.067364
Raaf		3.56	4.63	3.16 96-128							
Zafir		12.94	11.81	6.16 174-357		Base Triassic		8.22	0.0822	7.394612904	0.073946

8.3 Stratigraphic interpretation

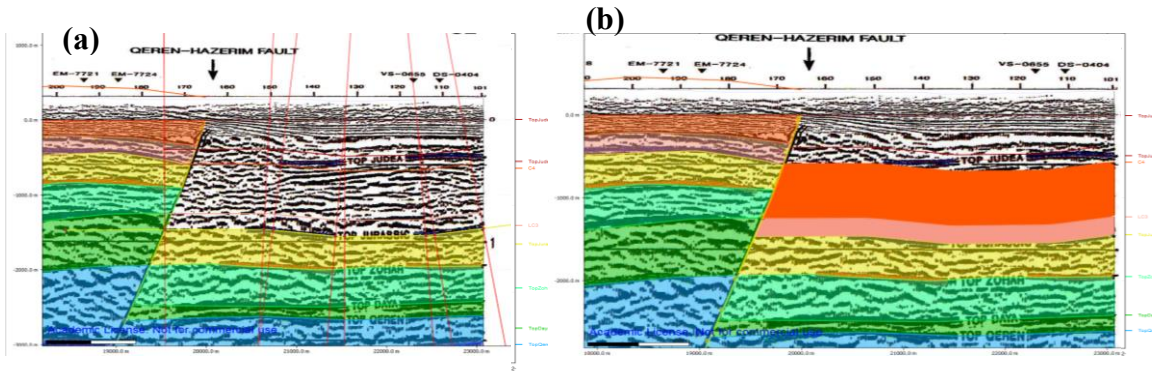
8.3.1 EM-7748

In order to sequentially restore an interpreted seismic section, all stratigraphic horizons should be continuous along the section. However, in section EM-7748, three horizons were absent in various parts across the section. Those were reconstructed following geological assumptions.

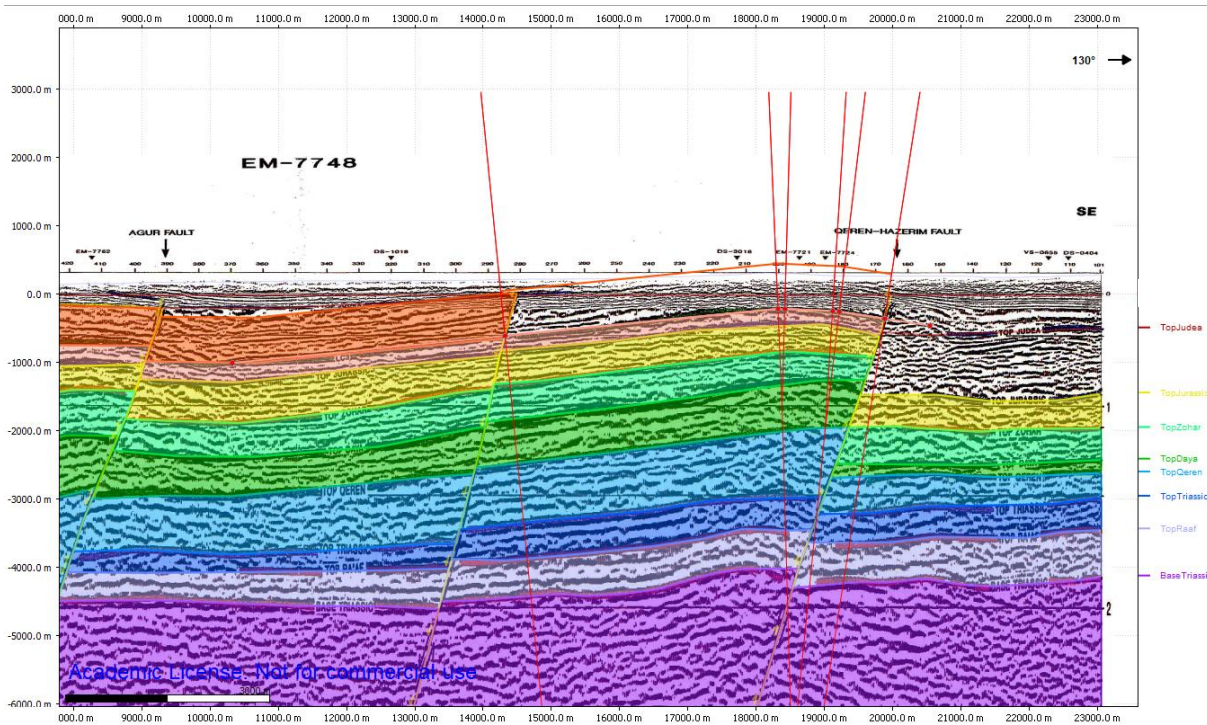
1. 'Top Raaf' horizon is missing from the northwestern part of the section, probably not mapped. 'Top Raaf' horizon was constructed according to an assumption of constant thickness between the horizons 'Top Triassic' and 'Top Raaf'



2. In order to keep the continuity of 'C4' and 'LC3' horizons across the section, same thickness between horizons 'C4', 'LC3' and 'Top Judea' was estimated on the footwall and hanging wall of the most northern fault in the section. Figure below shows the section before (a) and after (b) horizon construction.



3. From thickness considerations, horizon 'C4' was constructed along the entire section. The construction process is shown in the figure below.



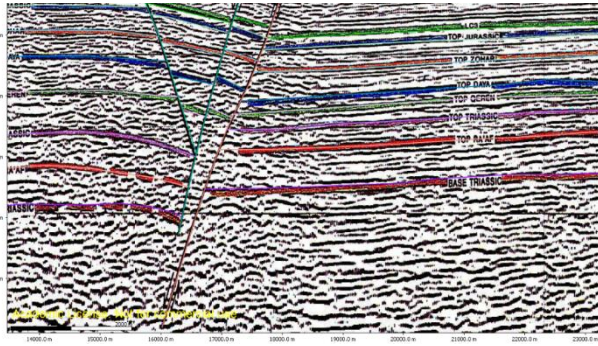
8.3.2 EM-7726

In order to perform sequential restoration on an interpreted seismic section, all stratigraphic horizons should be continuous along the section. However, in section EM-7726, two horizons were absent in various parts across the section. Those were reconstructed following geological assumptions.

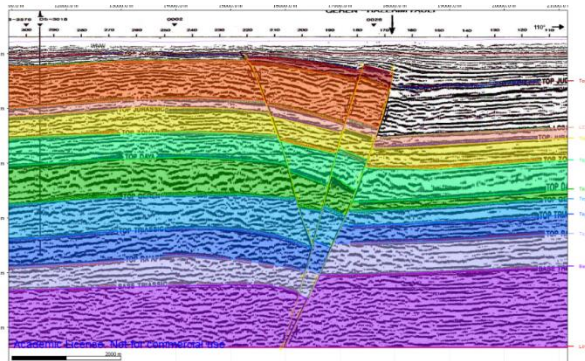
1. The thickness of the stratigraphic units inside the fault wedge was estimated from the average thickness between the horizons on both sides of the wedge.

Figure below shows the initial interpreted section (a) and the section after horizon construction (b).

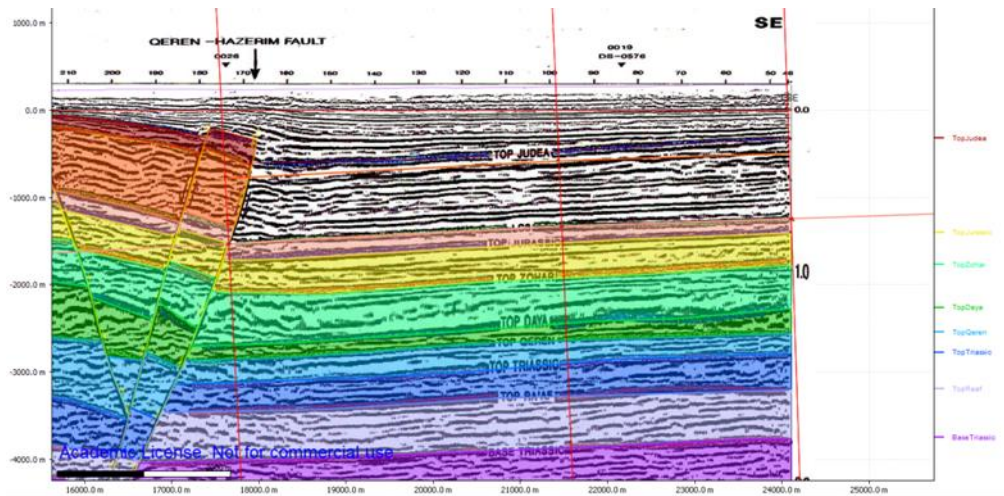
(a)



(b)

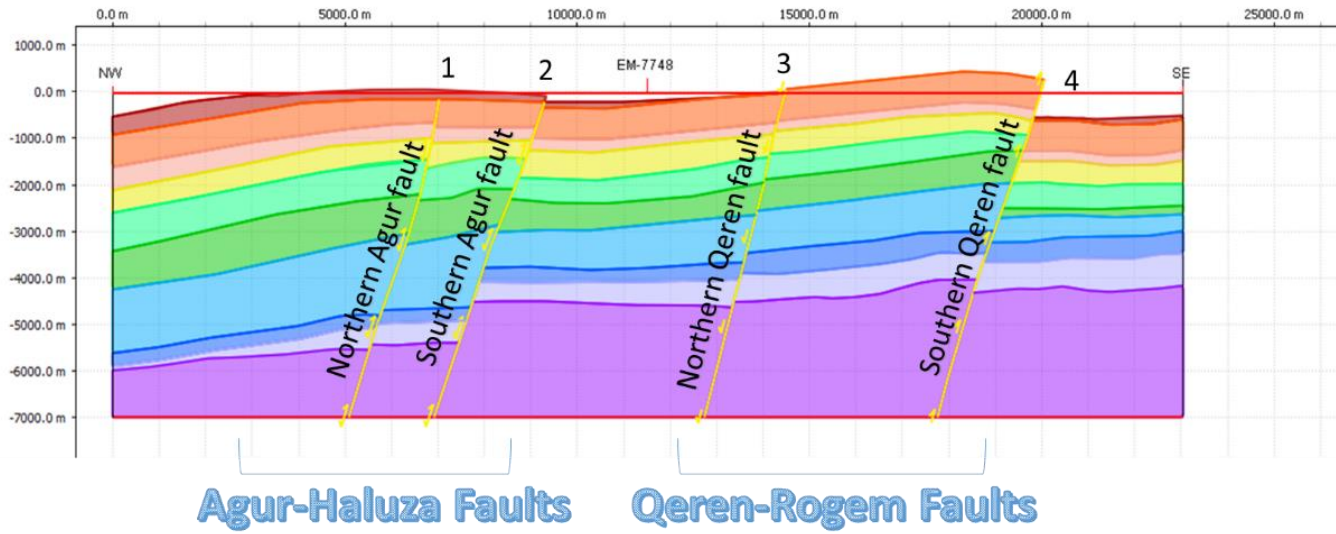


- Thickness between horizon 'C4' and 'Top Judea' was calculated along the northern side of the section from the thickness between those horizons on the southern side of the fault. Figure below shows the process of horizon construction.



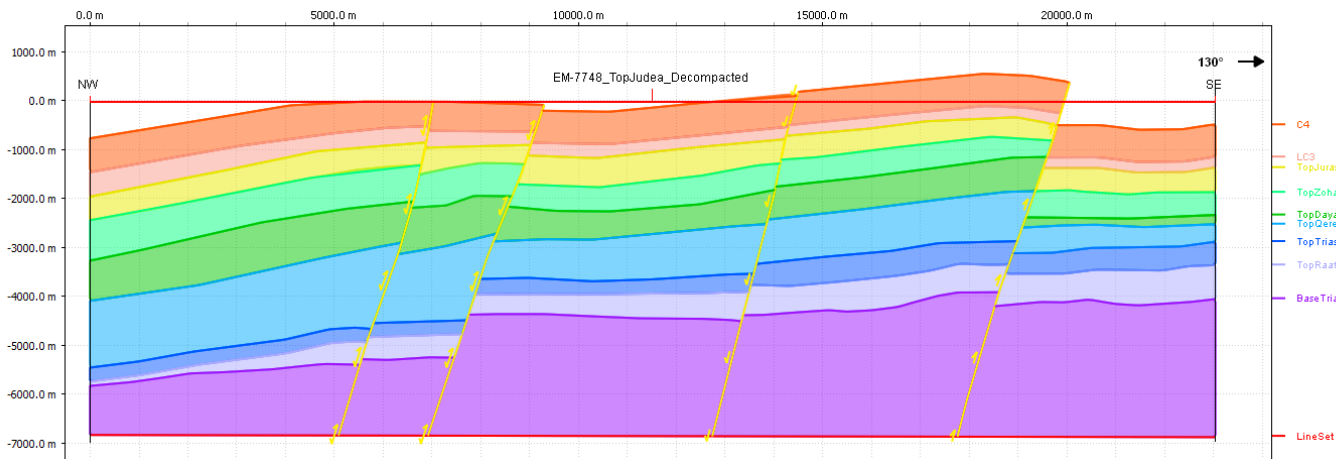
8.4 Restoration procedure

8.4.1 EM-7748



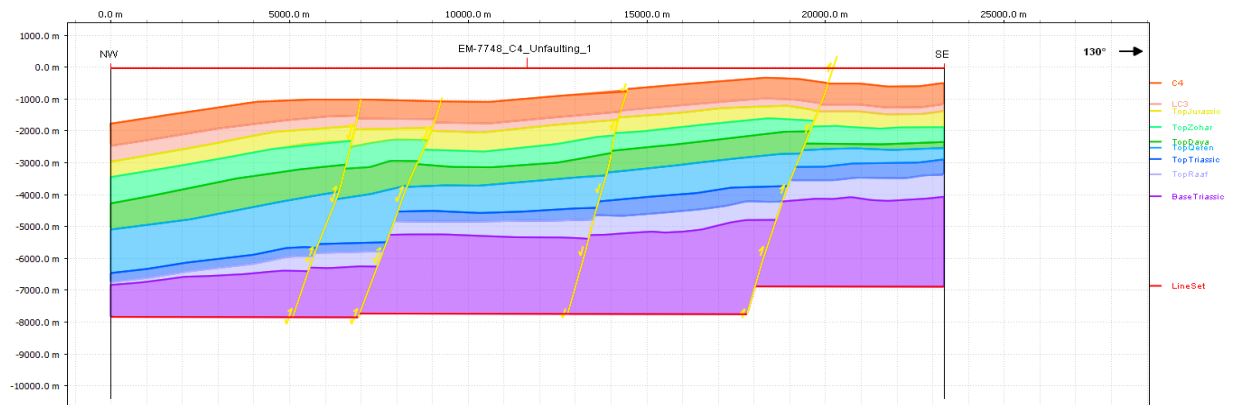
Initial section

Top Judea horizon decompaction



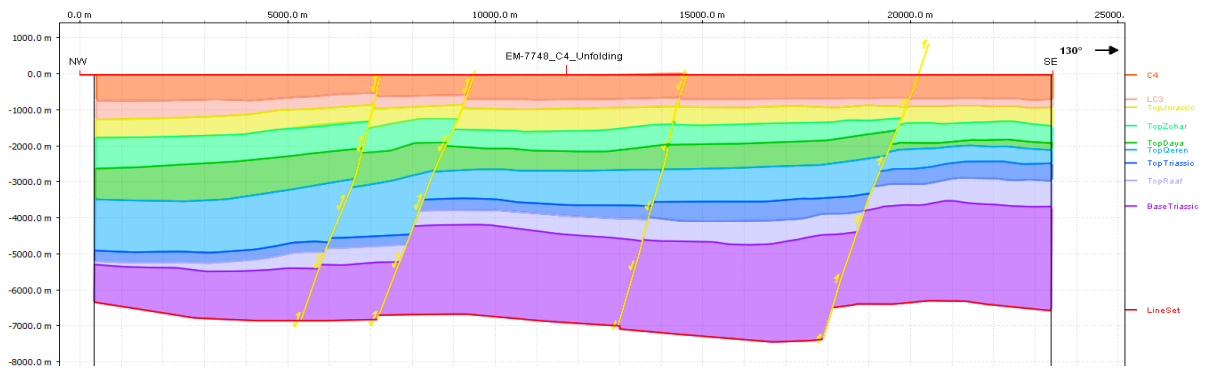
Post Judean reverse faulting on the southern Agur fault (2) with a slip of 125.3 m and southern Qeren fault (4) with a slip of 903.7 m

C4 horizon unfauling



C4 horizon unfolding

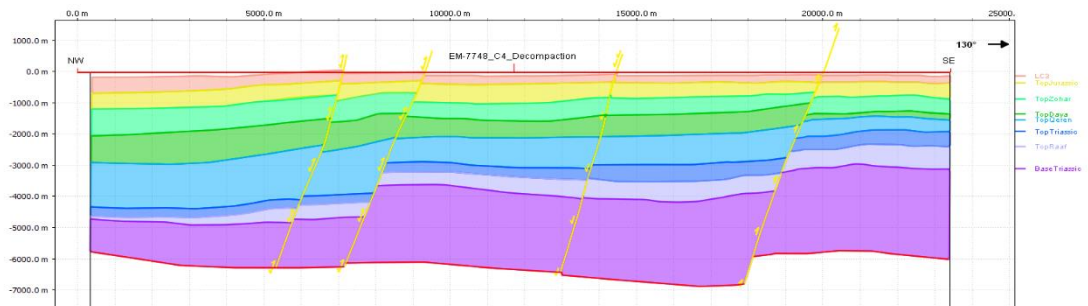
Thickening to the NW of the C4 layer, from 664 m in the SE to 726 m in the NW.



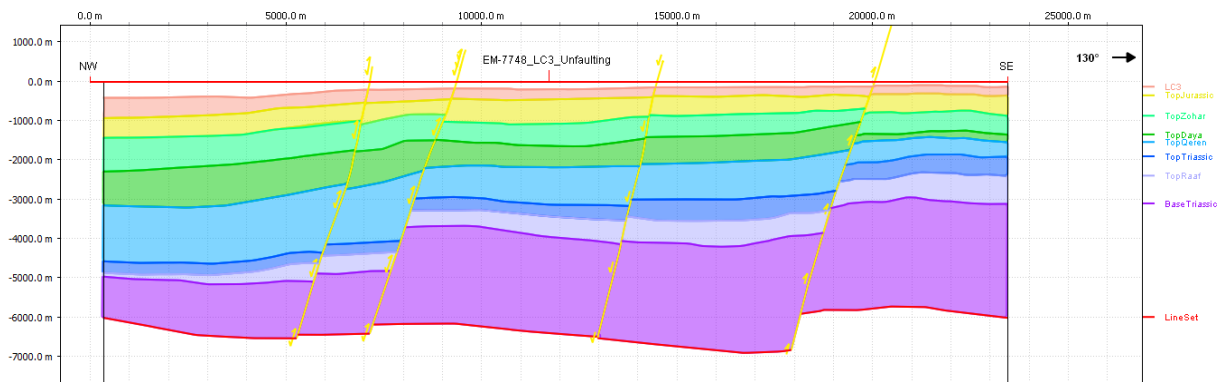
C4 horizon decompaction

Post C4 horizon reverse slip on the Agur faults (1 and 2) of 97.1 m and 117.9 m.

Reverse slip the northern Qeren fault (3) of 49.8 m

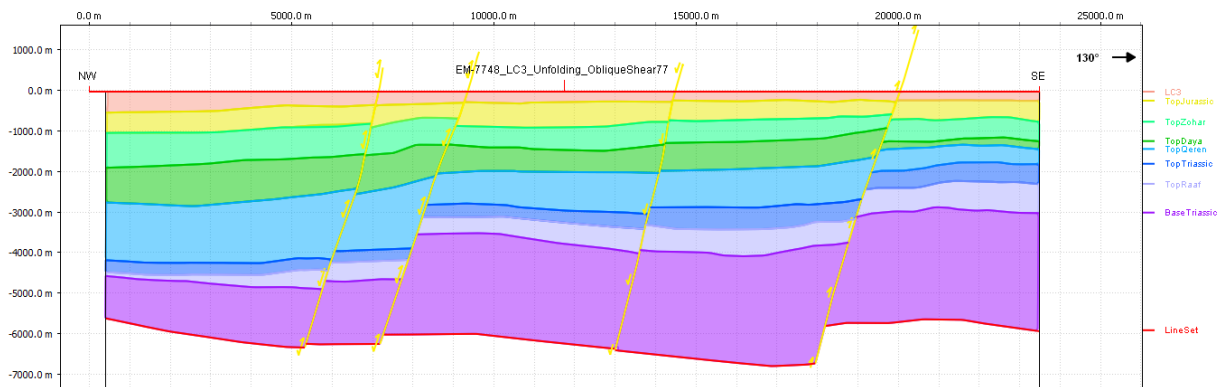


LC3 horizon unfauling

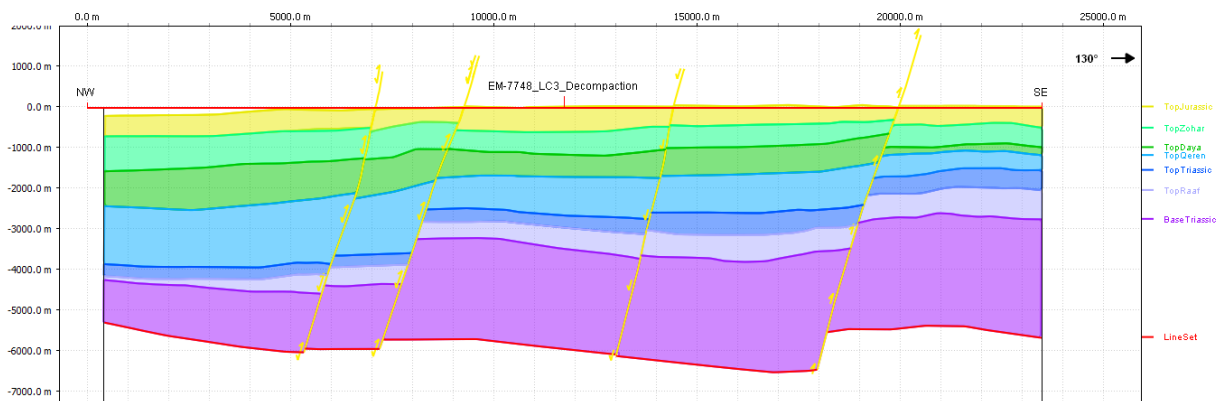


LC3 horizon unfolding

A gradual thickening towards the NW, from 225.7 m on the SE corner to 517.1 m on the NW corner

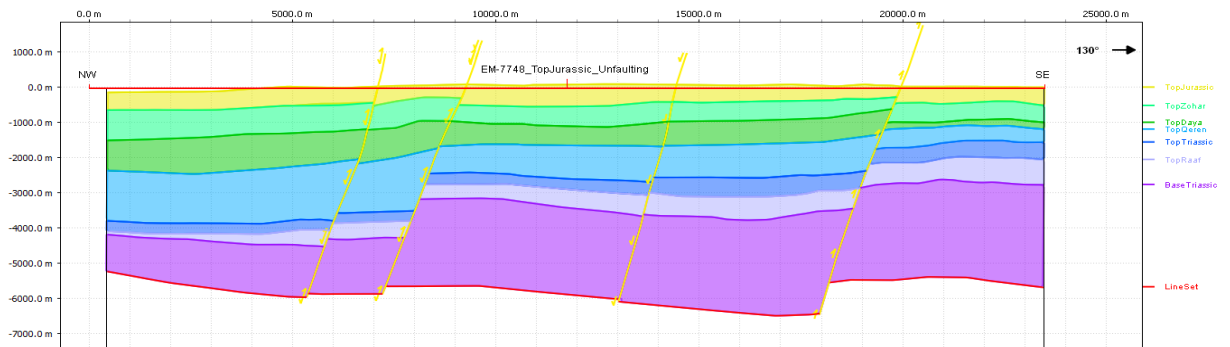


LC3 horizon decompaction



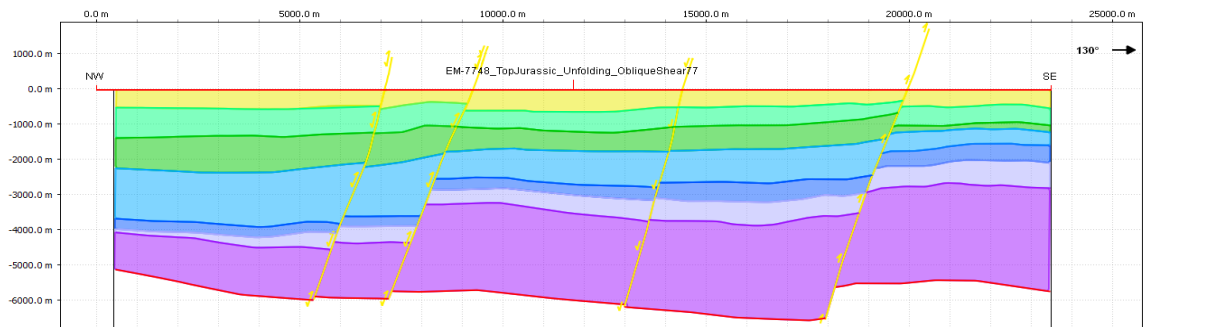
A quiet tectonic period with no apparent slip on the faults

Top Jurassic horizon unfaulting

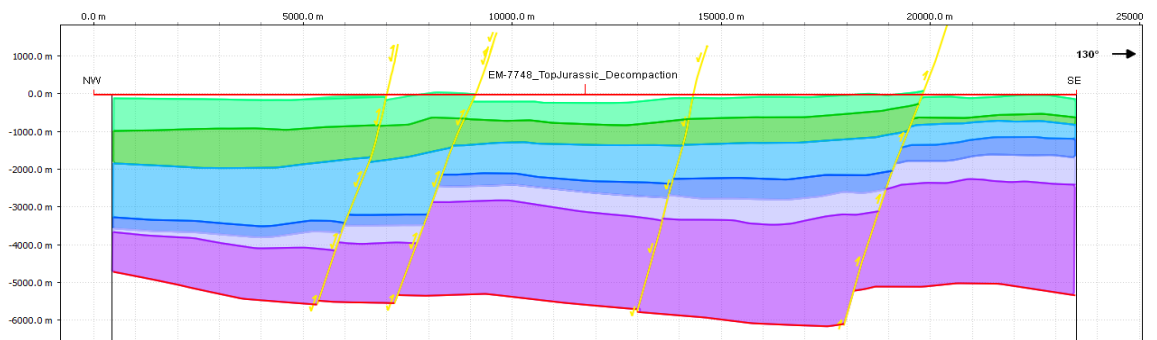


Top Jurassic horizon unfolding

A slight thickening to the centre of the section- from 490 m (average) to 622 m in the center

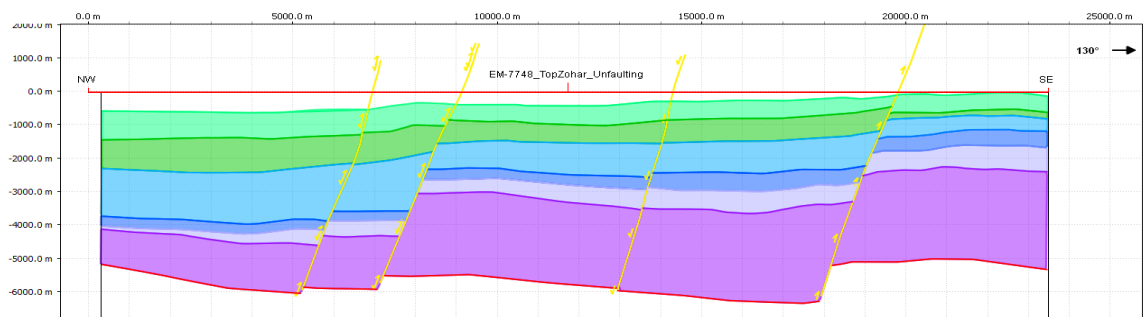


Top Jurassic horizon decompaction



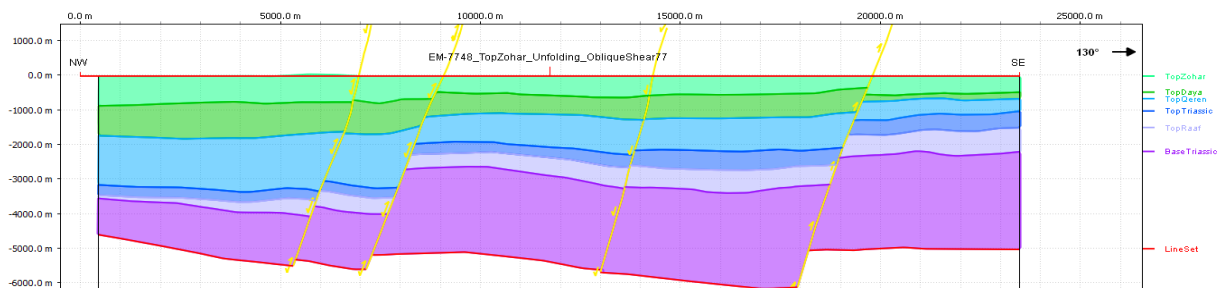
Reverse slip on the Agur faults (1 & 2) of 86.5m and 205.3 m. Reverse slip on the southern Qeren fault (4) of 197.1 m.

Top Zohar horizon unfauling



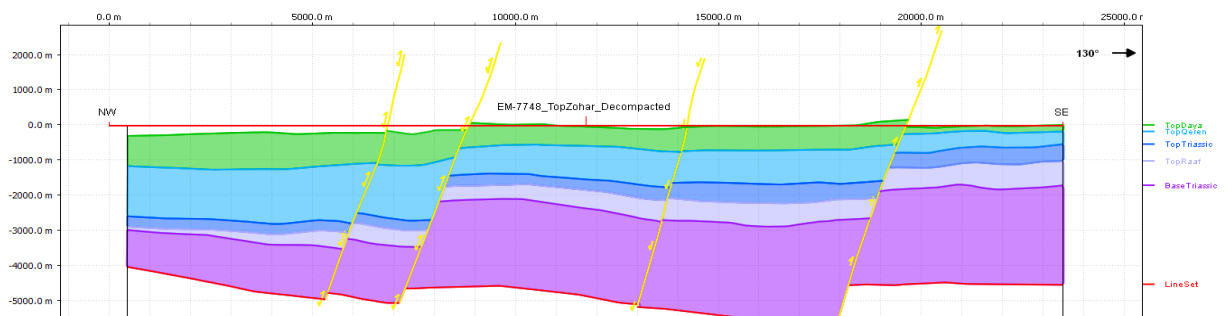
Top Zohar horizon unfolding

Thickening towards the NW, from 536 on the SE side to 860 m in the NW

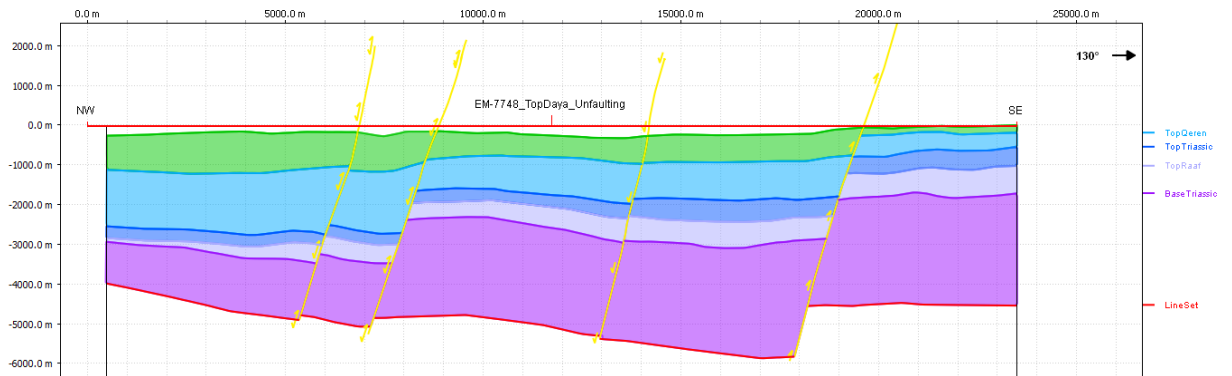


Top Zohar horizon decompaction

Post Zohar normal slip on the Agur faults (1 & 2) of 65.4 m and 206.5 m. Reverse slip on the southern Qeren fault (4) of 216.8 m.



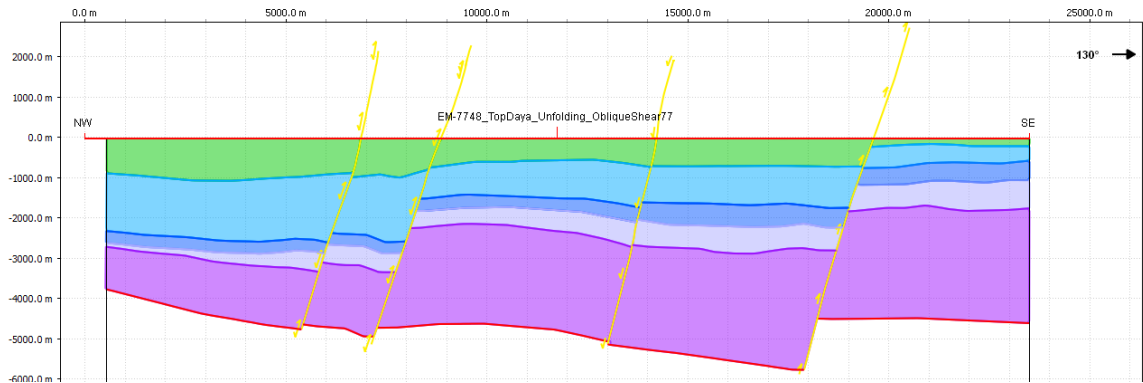
Top Daya horizon unfauling



Top Daya horizon unfolding

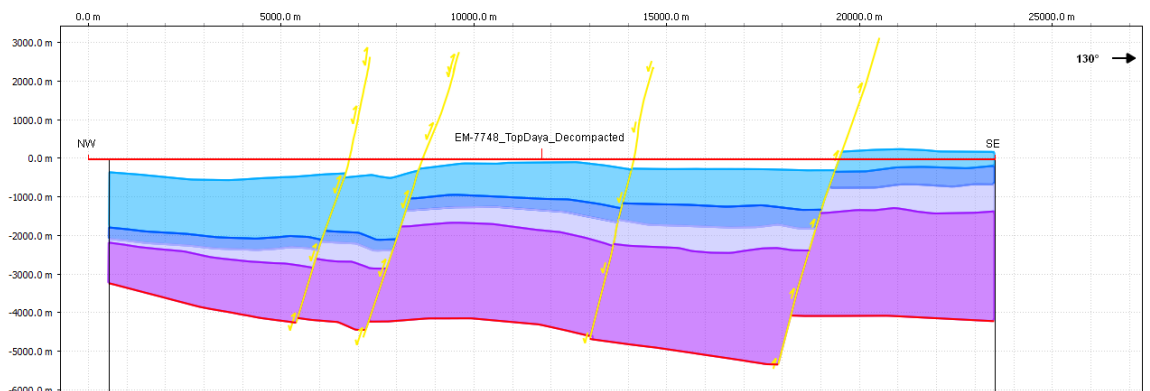
Thickening towards the NW, from 680 m on the SE side to 1059 m in the NW

Sudden thickness change at SE, thickness reduces to 150-180 m.

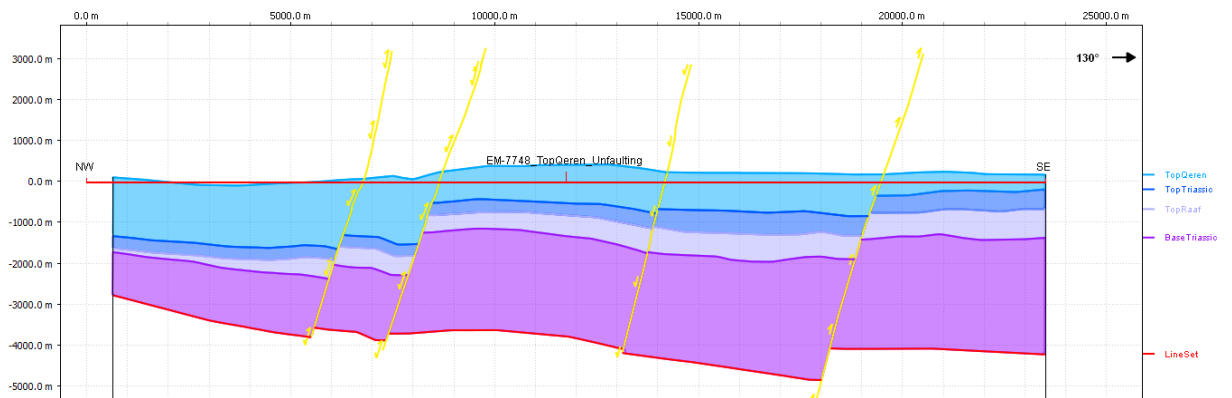


Top Daya horizon decompaction

Post Daya reverse slip on the Agur faults (1 & 2) of 117 m and 55 m. Normal slip on the southern Qeren fault (4) of 513.5 m.

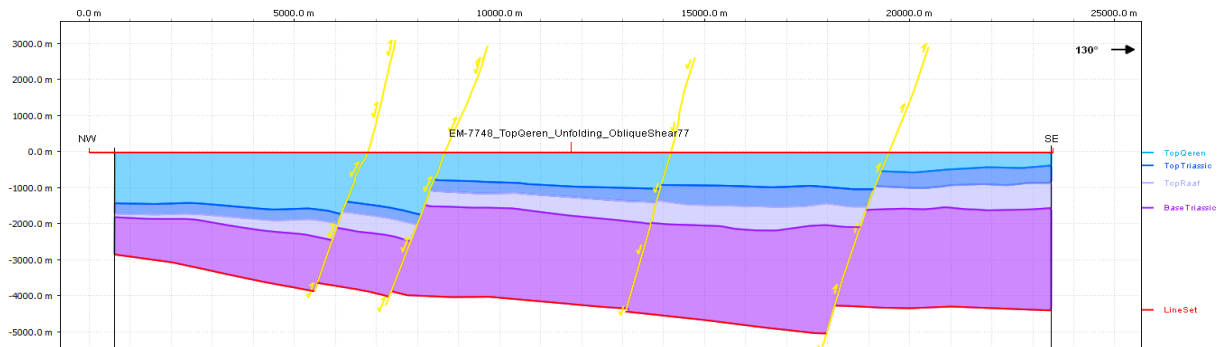


Top Qeren horizon unfauling



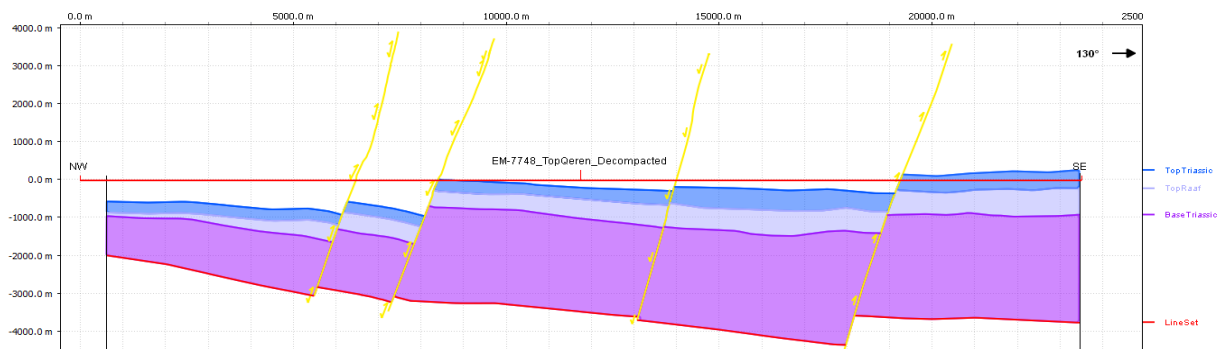
Top Qeren horizon unfolding

Abrupt thickness changes, but a trend of thickening to the NW. Thickness changes from 400 m on the SE corner to 1417 m on the NW corner of the section

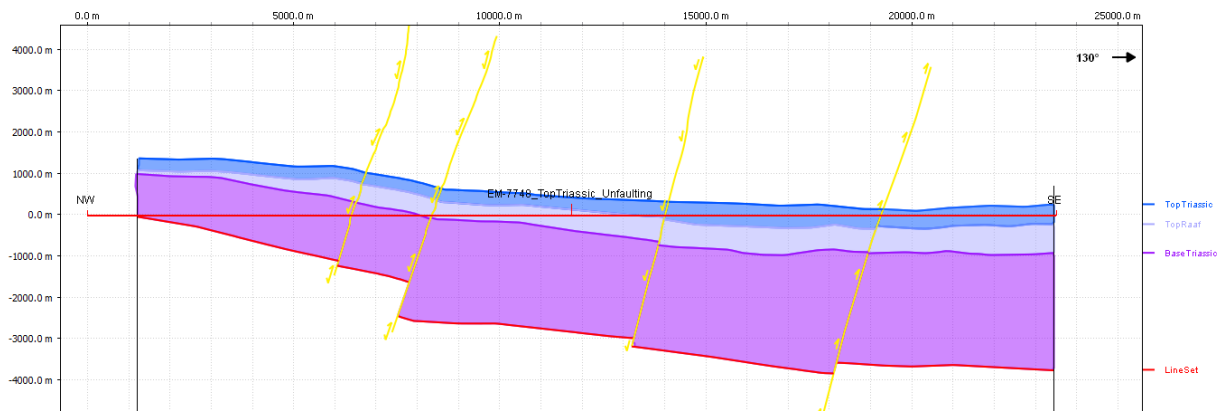


Top Qeren horizon decompaction

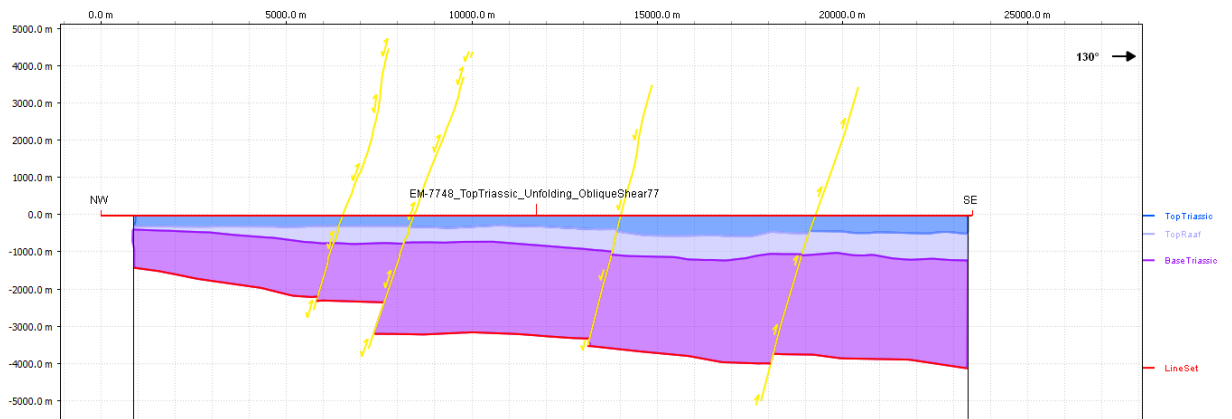
Normal slip on all four faults, which is post Qeren formation deposition. A slip of 366.3m, 1030.5m, 1115.6 m and 528.7 m.



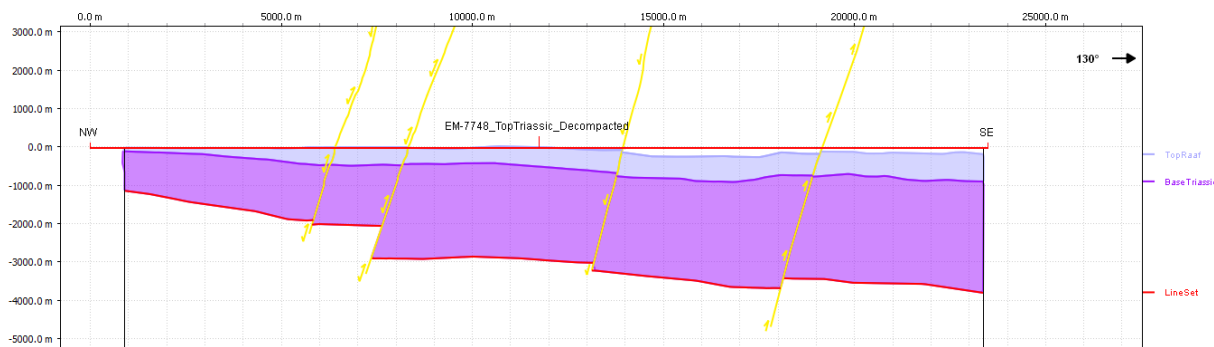
Top Triassic horizon unfauling



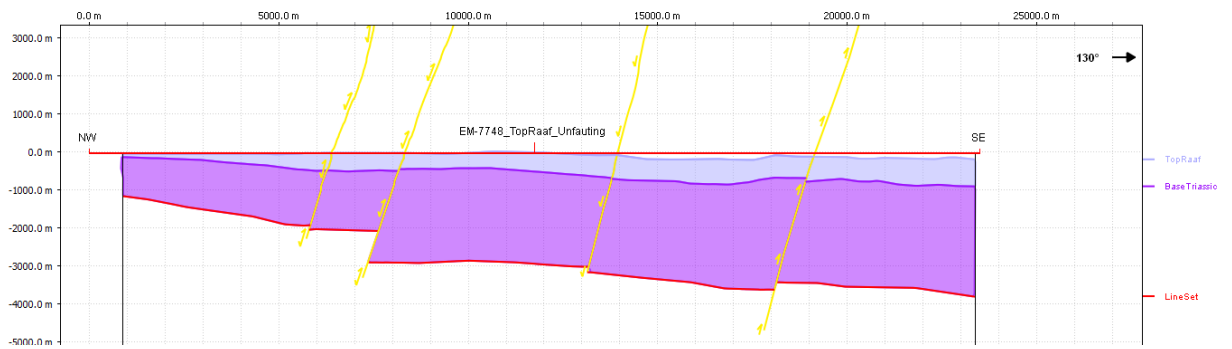
Top Triassic horizon unfolding



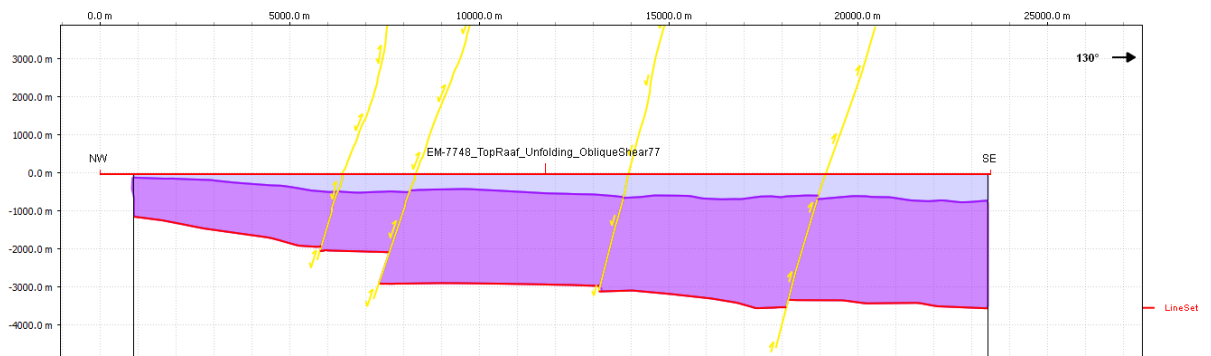
Top Triassic horizon decompaction



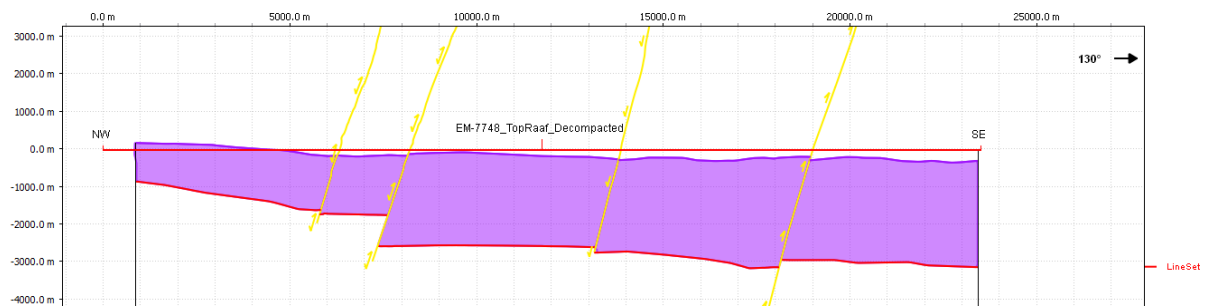
Top Raaf horizon unfauling



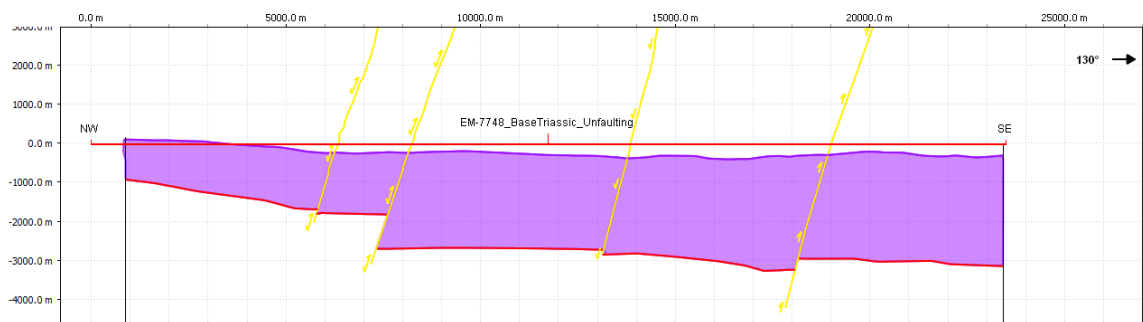
Top Raaf horizon unfolding



Top Raaf horizon decompaction



Base Triassic horizon unfauling

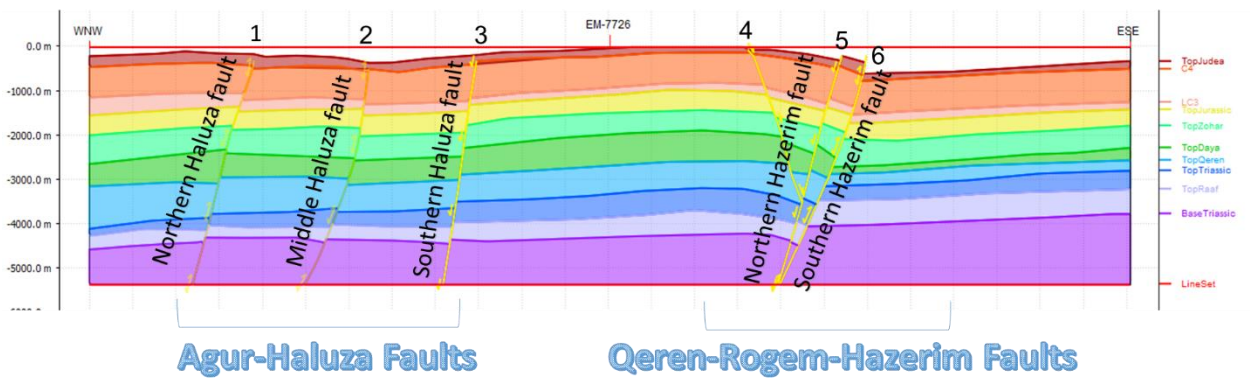


Base Triassic horizon unfolding



8.4.2 EM-7726

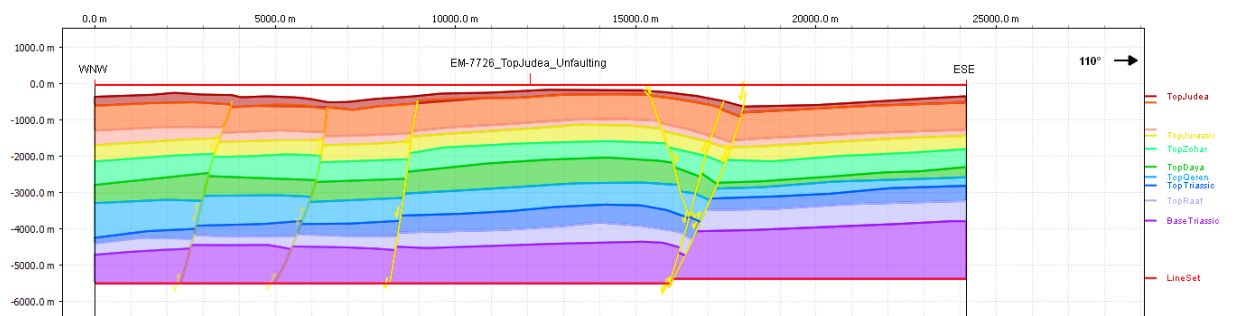
8.4.3 Sequential restoration results



Initial section

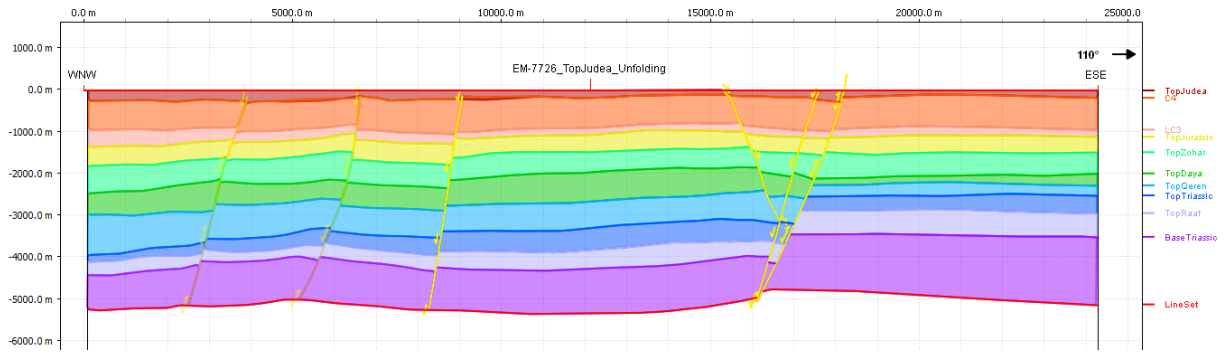
Top Judea horizon unfaulinging

Post-Judean reverse slip on the southern Hazerim fault (5 & 6) of 111m and 157.5 m



Top Judea horizon unfolding

A slight thickening towards the NW, from 167 m on the SE to 240m on the NW

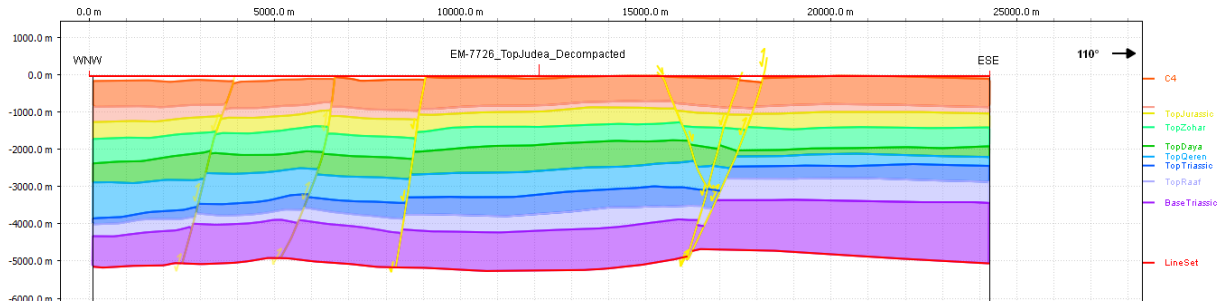


Top Judea horizon decompaction

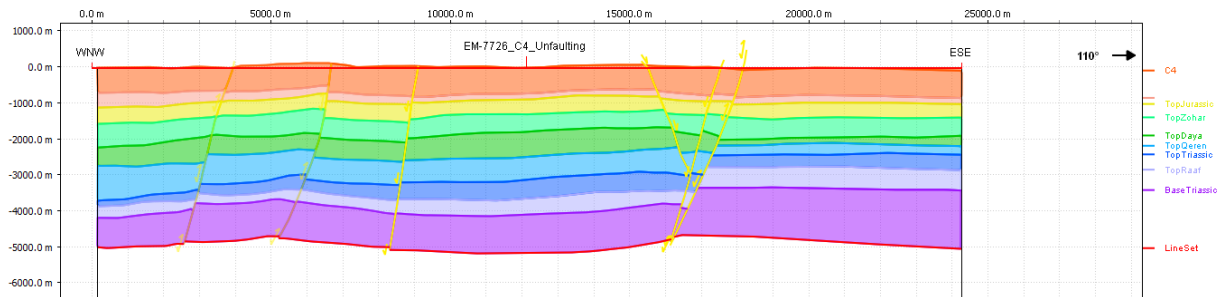
Post C4 horizon reverse slip on fault (1) of 76 m.

Normal slip of 61 m on fault (2) and 77m on fault (3),

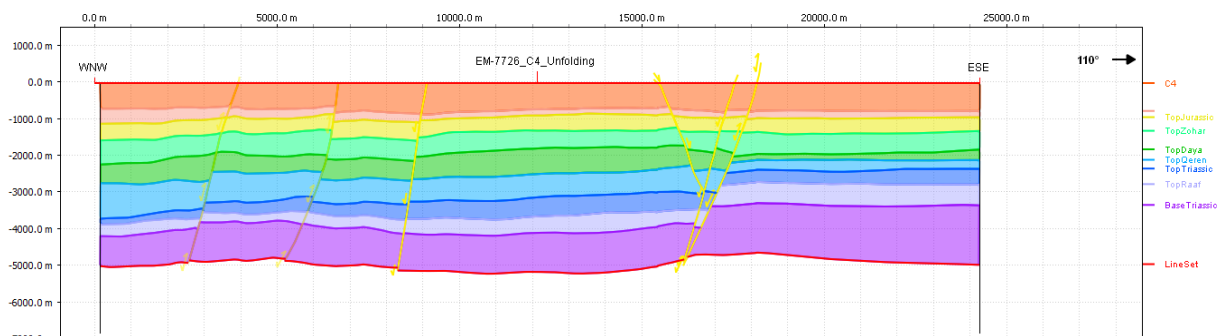
Normal slip of 36m on fault (5) and 122m on fault (6)



C4 horizon unfauling

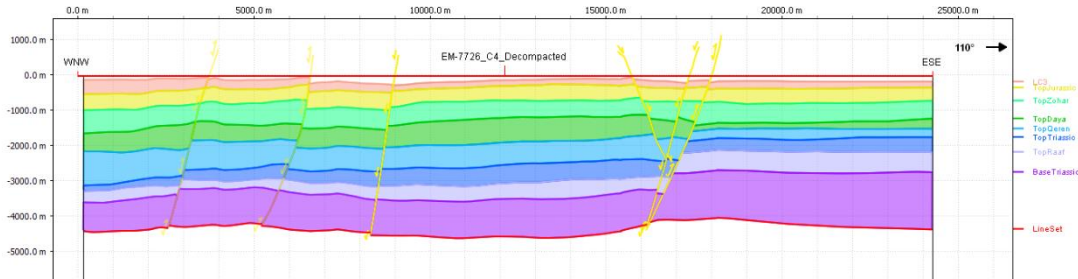


C4 horizon unfolding

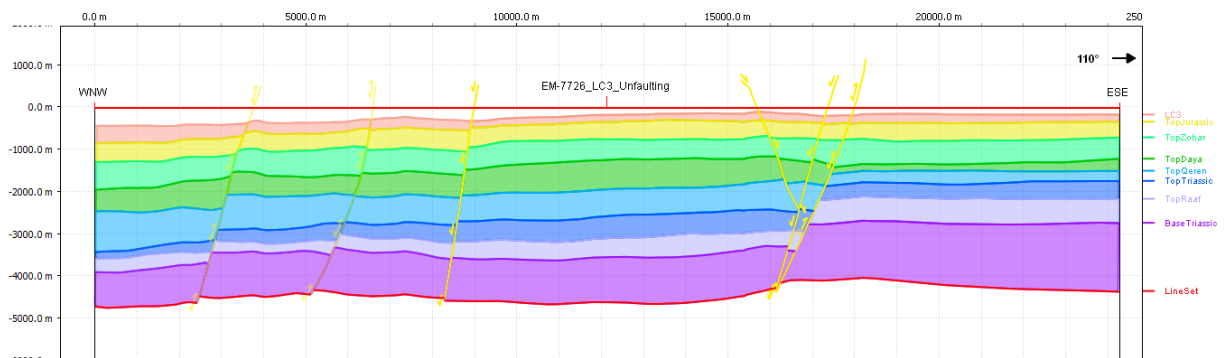


C4 horizon decompaction

Post LC3 horizon reverse slip on fault 1 of 89.8 m and 2 of 179.3m. Normal slip creating a graben on faults 4 (61 m slip) and 5 (62 m slip), Reverse slip on 6 of 54 m

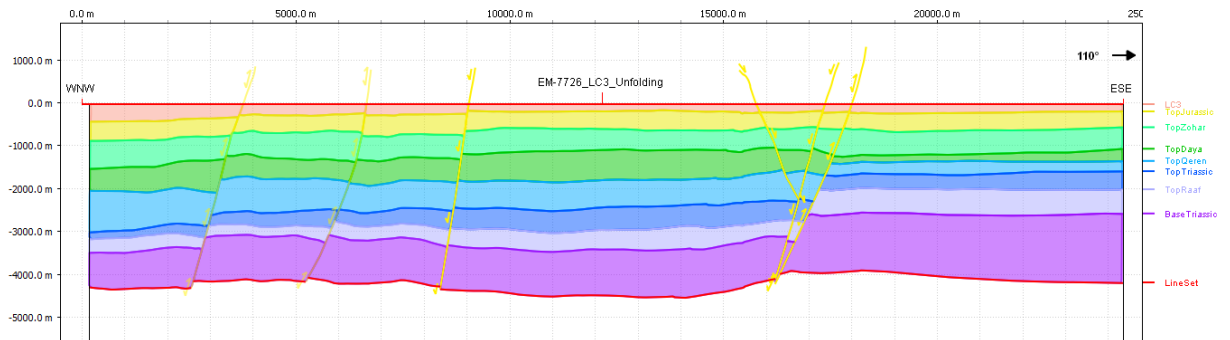


LC3 horizon unfauling



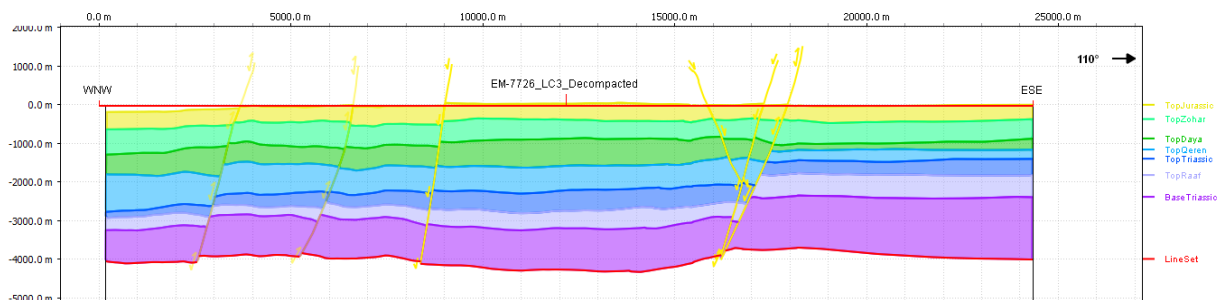
LC3 horizon unfolding

Thickening towards the NW, Thickness grows from 177 m in SE to 412 m in NW

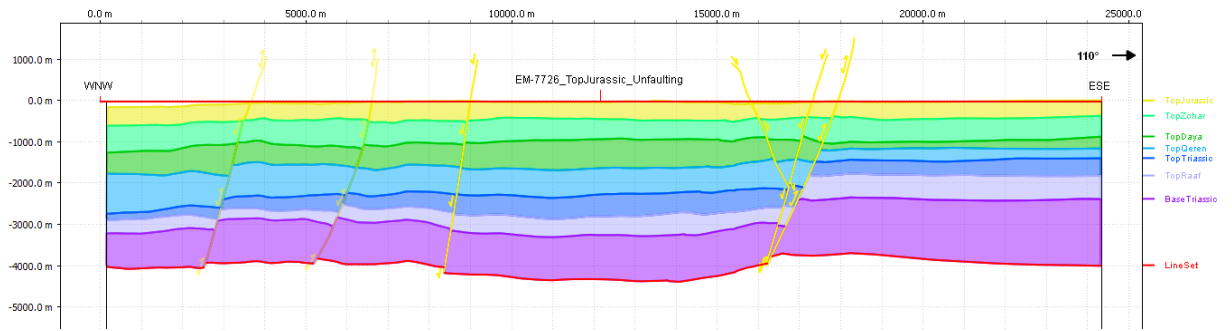


LC3 horizon decompaction

Slight normal slip on faults 1 (47 m) and 3 (77 m).

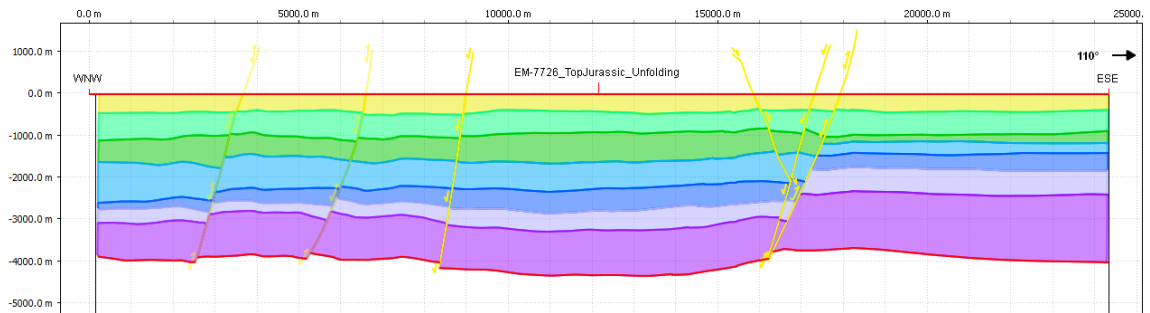


Top Jurassic horizon unfaulting



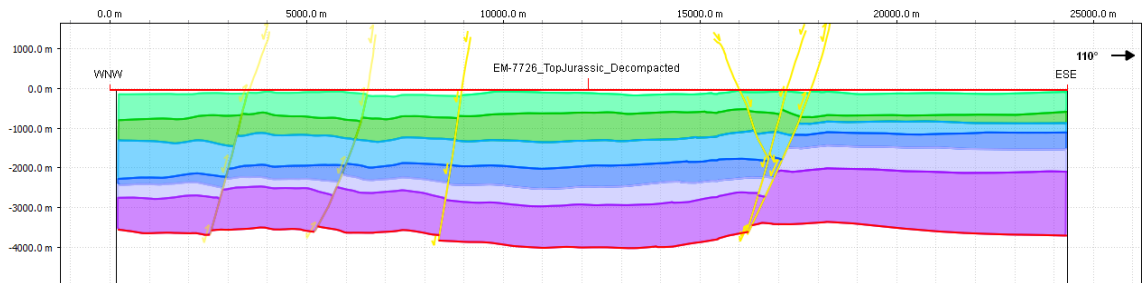
Top Jurassic horizon unfolding

No apparent thickness change

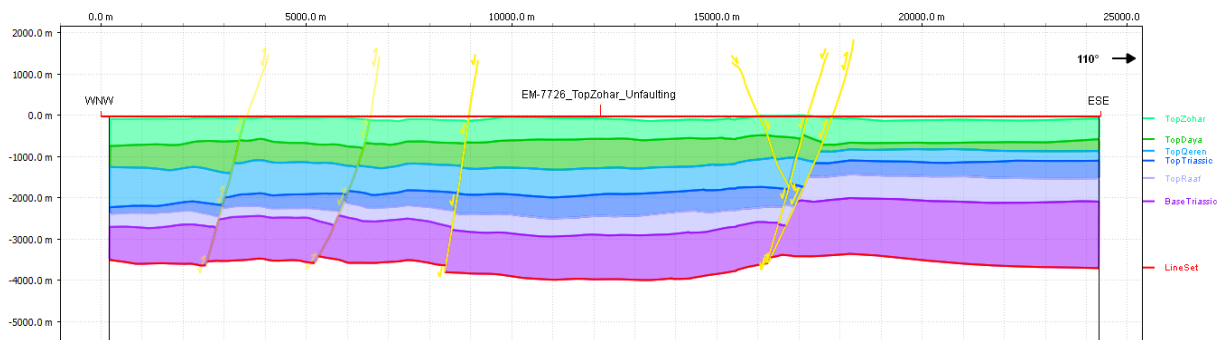


Top Jurassic horizon decompaction

A slight reverse slip on fault 2 (33.2 m)

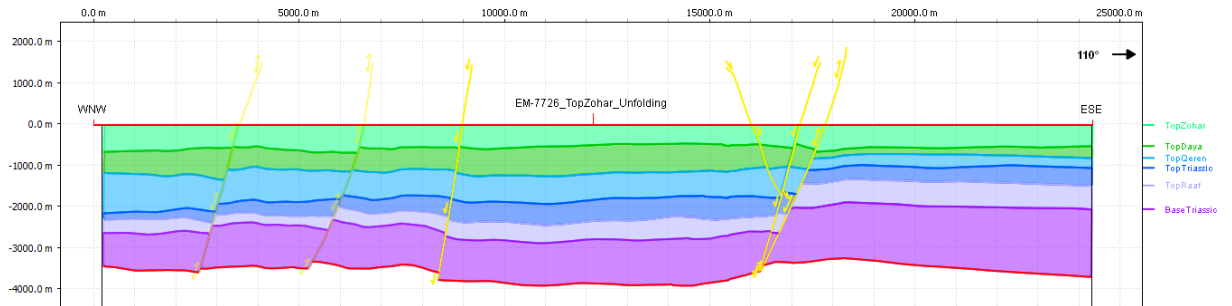


Top Zohar horizon unfaulting



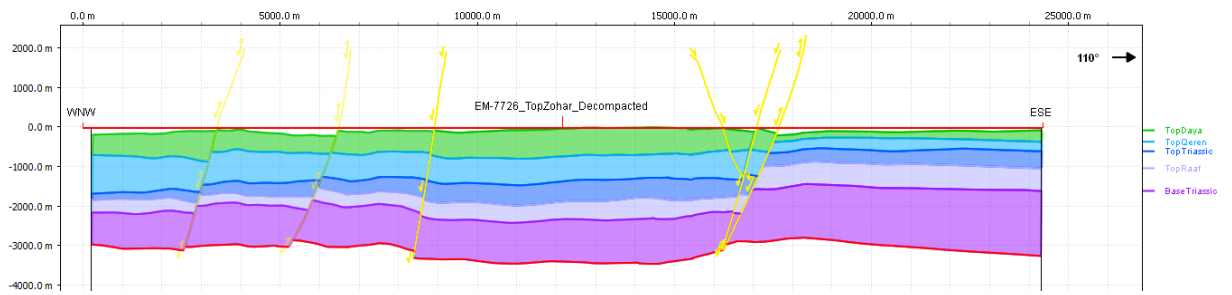
Top Zohar horizon unfolding

No apparent thickness variations

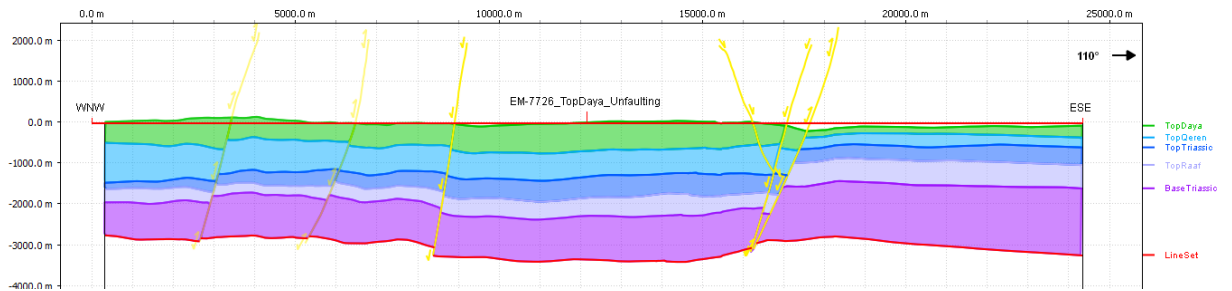


Top Zohar horizon decompaction

Normal slip on 2 of 136 m, 3 of 31.5 m. Normal slip on 5 of 102 m. Reverse slip on fault 6 of 64.7m.



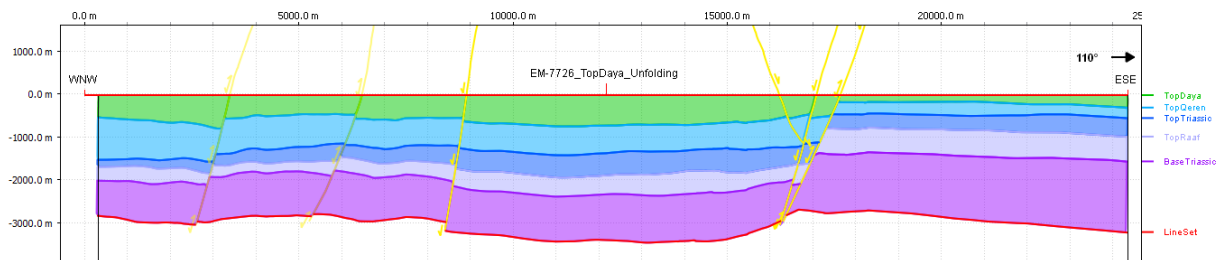
Top Daya horizon unfauling



Top Daya horizon unfolding

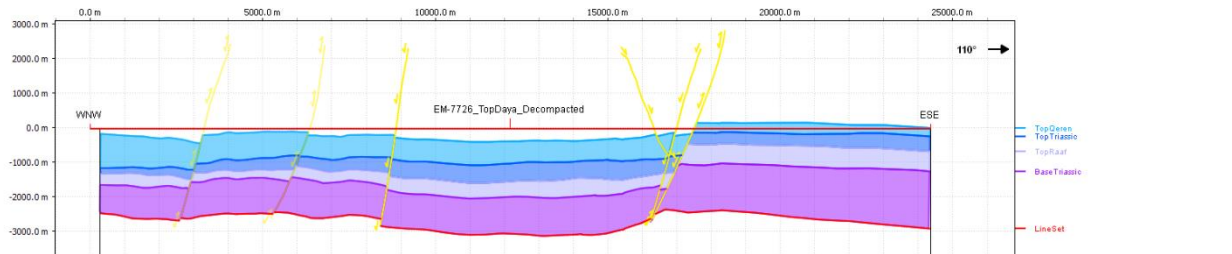
A sudden thickness change at SE corner to 165-200 m

Thickening towards the center of 734 m max, 550 m in NW side.

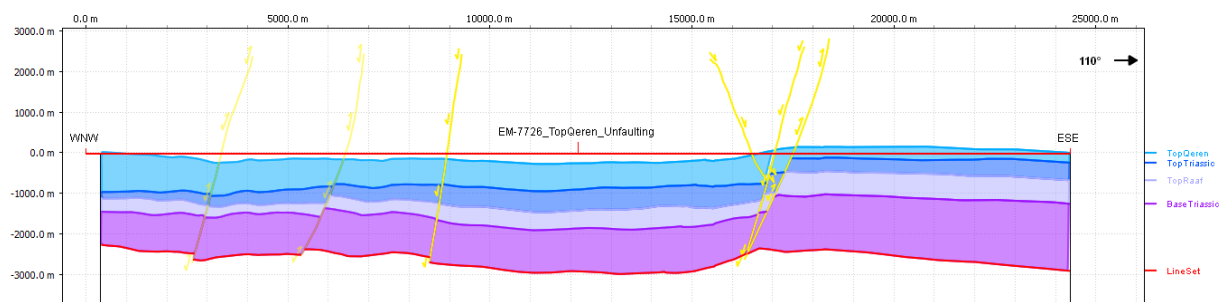


Top Daya horizon decompaction

Normal slip on 1 of 232 m. Reverse on 2 of 98.8 m, 3 of 75.3 m. Normal slip of 338 m on 6. Reverse of 110 on 5.

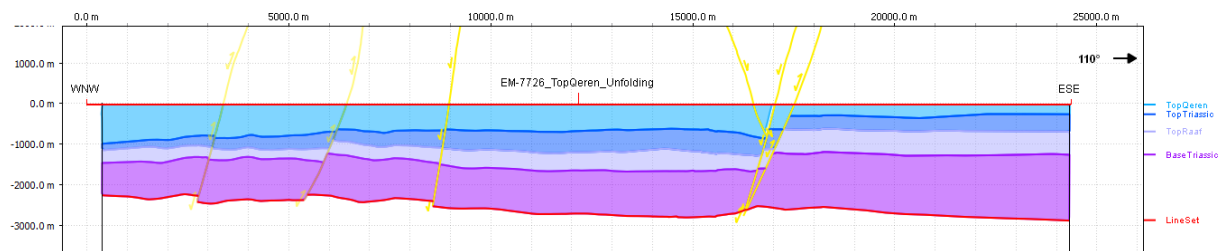


Top Qeren horizon unfauling



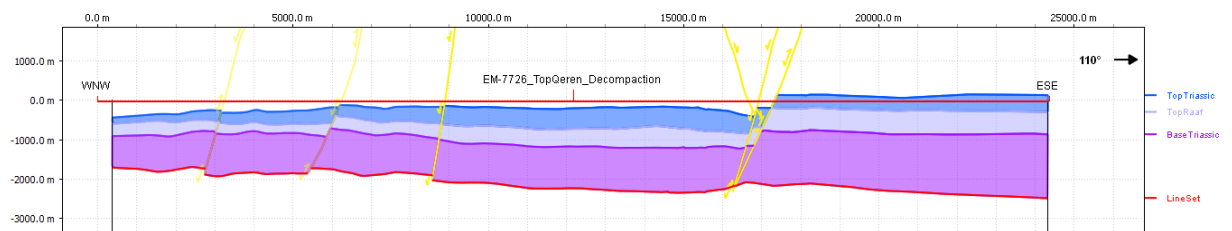
Top Qeren horizon unfolding

Abrupt thickness change to the SE of 280-320 m on SE.

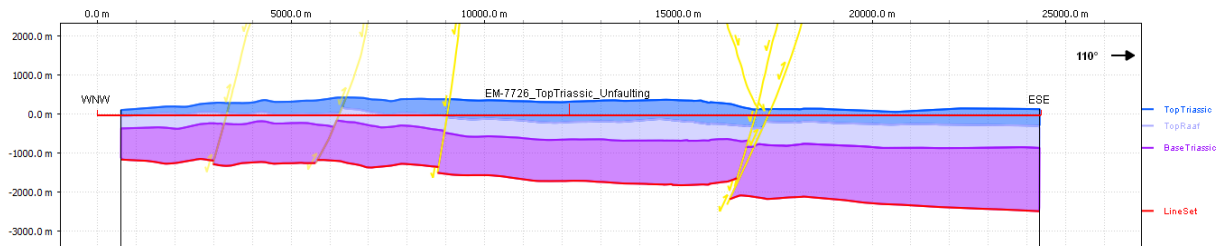


Top Qeren horizon decompaction

Normal on 2 of 60.4 m , normal on3 of 25 m . Normal on 5 of 221 m and 6 of 354 m

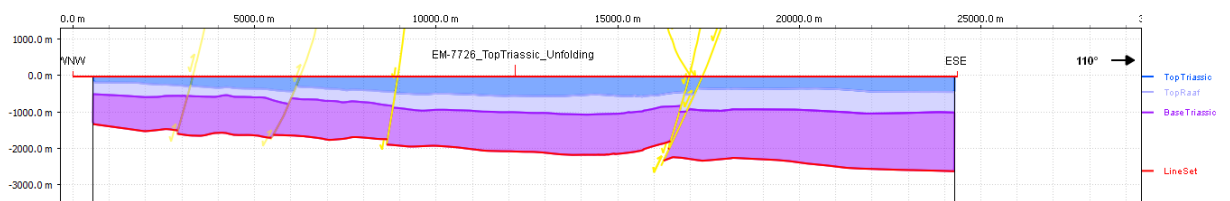


Top Triassic horizon unfauling



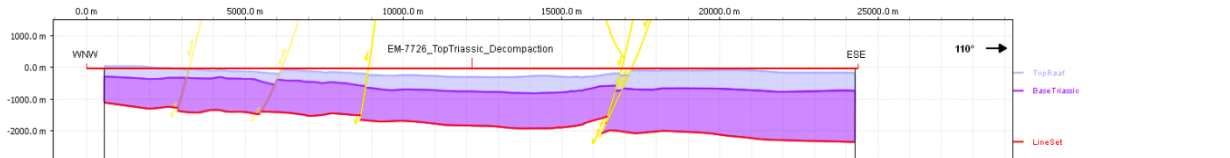
Top Triassic horizon unfolding

Gradual thickening to the SE, from 170 m on the NW to 430 m to the SE

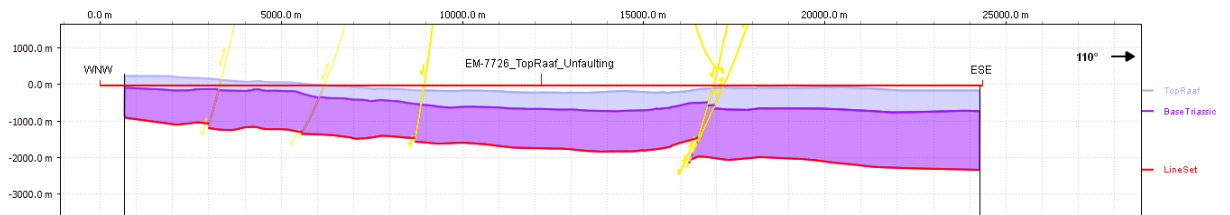


Top Triassic horizon decompaction

Normal slip on 2 of 155 m. Normal slip on 6 of 170 m

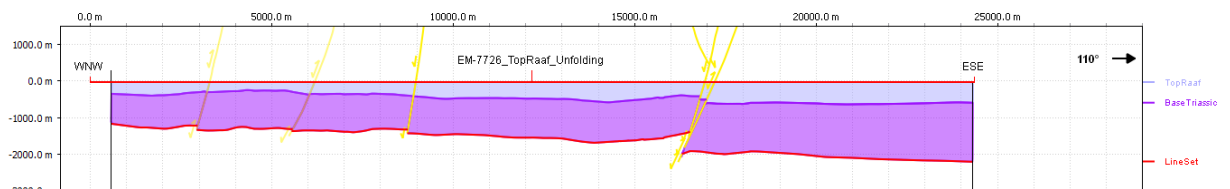


Top Raaf horizon unfauling



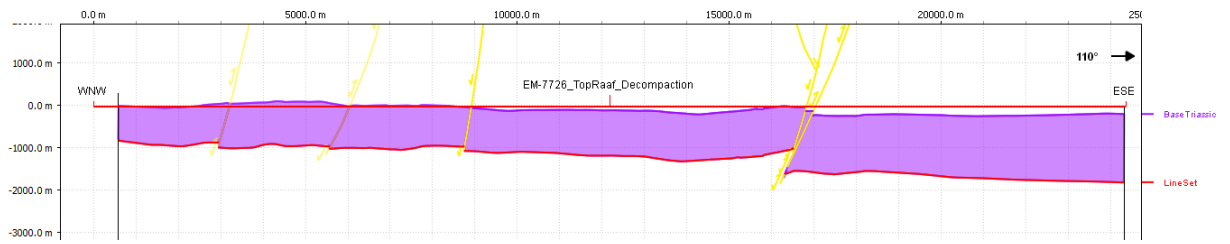
Top Raaf horizon unfolding

Thickening to the SE. From 370 m to the NW to 597 m on the SE

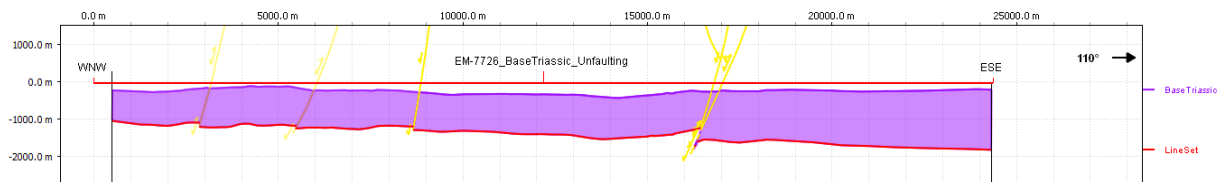


Top Raaf horizon decompaction

Reverse slip on 6 of 133 m and 5 of 99.4 m



Base Triassic horizon unfauling



Base Triassic horizon unfolding

Thickening to the SE, from 836 m on the NW to 1604m to the SE.



תקציר

בנגב הצפוני מתועדים אירועי דפורמציה מהמזוזואיקון המוקדם ולכן אפשר להיעזר בו כמודל להתפתחות אגן הלבנט. התאוריה המקובלת של התפתחות אגן הלבנט מבוססת על מנגנון של היפוך מבנים, כאשר משטר המאמצים השתנה מהתארכות בטריאס המוקדם להתקצרות בקרטיקון העליון. אולם, אנליזה סייסמית של מספר מבנים בנגב הצפוני שללה מנגנון היווצרות זהה לכולם, ותזמון המעבר מהתארכות להתקצרות משתנה מרחבית. רשת צפופה של קווים סייסמיים דו מימדיים וקידוחי מהירויות באזור קרן ועגור בנגב הצפוני מציעים הזדמנות לשחזור הדפורמציה בזמן השקעת החתך הסדימנטרי מהטריאס המוקדם ועד לקוניאק בקרטיקון העליון. מחקר זה השתמש בשני חתכים סייסמיים ושני קידוחים ובפענוח שלהם אשר כלל עשרה אופקים. בתהליך השחזור הסטרוקטורלי נלקחו בחשבון תהליכים של קומפקציה, איזוסטזיה פלקסורלית, העתקה וקימוט שהשפיעו על התפתחות המבנים של קרן ועגור. המחקר מאשש הטייה אזורית מדרום-מזרח לצפון-מערב ביורה המוקדם, שמעידה על תהליך של השתפלות אזורית בשולי אגן הים התיכון המזרחי (נאותטיס). תוצאות המחקר גם תומכות בקונצפט היפוך המבנים. המחקר מקדים באופן מובהק את תחילת תהליכי ההתקצרות באזור: כבר ביורה התיכון מופיעה זריקה הפוכה בשני המבנים. תוצאות השחזור העלו גם עדויות להעתקה צידית בקרטיקון העליון. שחזור סטרוקטורלי מפורט הוכח כיעיל בזיהוי פאזות טקטוניות מקומיות בתוך מבנה מורכב של העתקים וקמטים, למרות מגבלת האיכות של הנתונים. כעת ניתן להשתמש בשיטה זו במקומות שהידע עליהם פחות נרחב לתיקוף השערות טקטוניות ומידול התפתחות המבנים בזמן.

ממתיחה בנאו-תטיס עד התקצרות אלפינית בשחזור סייסמי דו

מימדי: צפון מערב הנגב, אגן הלבנט

עבודת גמר לתואר מוסמך במדעי הטבע

מוגשת על ידי:

אינגה בויאנז'ו

בהדרכת:

פרופ' אמוץ עגנון

אוגוסט 2018

אב תשע"ח

החוג לגיאולוגיה

המכון למדעי כדור הארץ

הפקולטה למדעי הטבע

האוניברסיטה העברית בירושלים